Techniques for Imaging the Endoplasm and Vacuole of Characean Algae

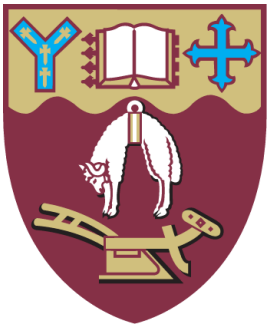

A THESIS

SUBMITTED IN PARTIAL FULFILMENT

OF THE REQUIREMENTS FOR THE DEGREE OF

Master of Science

in Cell Biology

at the

University of Canterbury

New Zealand

Robert W. Perry

2016

Contents

List of Figures

List of Tables

List of Movies

Acknowledgments

I would like to thank the following for all of their support throughout the duration of my studies. Thank you so much!

- My family, particularly my mother, Jennifer Franks, and her wonderful husband, Alan Franks, for providing me a home full of love and plants, which are also love!
- Dr. David Collings and Dr. Ashley Garrill, as my ever-dutiful supervisors who wrangled me into something resembling a scientist.
- The numerous academics throughout the world who have contributed greatly to the field of Characean biology, including but hardly limited to Mary Bisson, Mary Beilby, Michelle Casanova, Geoff Wasteneys, Ilse Foissner, Andreas Sievers, Dieter Hodick, Masashi Tazawa, Teruo Shimmen, and Eiji Kamitsubo.
- Stephanie McRae and Ayelen Tayagui, my office colleagues, for putting up with my Vulcan insanity in no short measure.
- David Conder, Alan Woods, Nicki Judson, Penny Moore, Dr. Paul Broady, Dr. Sharyn Goldstein, Dr. Tammy Steeves, Dr. Marie Hale, Dr. Paula Jameson, and Dr. Drusilla Mason, for supporting me in various ways throughout my journey or otherwise enriching my experience at the University of Canterbury.

Abstract

The extremely large internodes of the Characean algae have long served as a model system for biologists for investigations of membrane electrophysiology, the cell wall and the cytoskeleton, and the knowledge gleaned from these studies has facilitated subsequent discoveries in other systems, particularly higher plants. Despite this, the cytoplasmic organization of the streaming endoplasm and vacuole in the internodes remain poorly understood. Investigations of cytoplasmic architecture are typically conducted using a mixture of confocal laser scanning microscopy, expression of fluorescent proteins, and membrane-permeant fluorescent dyes. As Characean algae have not been successfully transformed, this study has used confocal microscopy with fluorescent dyes to image live cells. However, this encounters two notable problems, the light-absorbing chloroplast layer that encases all but the cortical regions of the cell, and the fast streaming rates of the endoplasm which distort imaging. Using confocal microscope settings optimized for high speed imaging, two complementary techniques have been used to image the interior of the cells. High intensity irradiation for 5 minutes with a 405 nm violet-laser generated windows in the cortical layer through which the endoplasm and vacuole could be imaged, while the vacuole and endoplasm could also be imaged in the structurally-related rhizoid cells. With these techniques, vivid image sequences of cytoplasmic architecture and dynamics within the endoplasm and vacuole have been achieved with a range of fluorescent dyes, notably neutral red and acridine orange, the cell marker Blue CMAC which loads into the central vacuole, the DNA stain Syto-13, and the tonoplast specific dye MDY-64. These results demonstrate that the streaming endoplasm and vacuole are considerably more structurally complex than previous investigations have described, and that the central vacuole is heterogeneous.

Abbreviations

20x	twenty times magnification
63x	sixty-three times magnification
Blue CMAC	7-amino-4-chloromethylcoumarin
$DIOC_6(3)$	3,3'-dihexyloxacarbocyanine iodide
DMSO	dimethyl sulfoxide
ER	endoplasmic reticulum
GFP	green fluorescent protein
NR	non-protonated neutral red
NRH^+	protonated neutral red

1: Introduction

This thesis investigates the organization of the vacuole and streaming endoplasm of cells of the Characean alga *Nitella hookeri*. Although the Characean algae, including various species of *Nitella* and ecorticate species of *Chara* (for example, *C. australis* and *C. corallina*) have been extensively used for various cell biological and electrophysiological studies for many decades, including investigations of cytoplasmic streaming, gravitropism, action potentials and membrane channels, the organization of the interiors of these cells has been difficult to study.

In this thesis, I have combined confocal microscopy and the use of various fluorescent dyes in an attempt to determine how the central vacuole and streaming endoplasm of these cells is organized. Because the layer of chloroplasts surrounding the internode of Characean algae strongly absorbs most wavelengths of light, two methodologies which allowed access to the centre of the cell were assessed. These were the use of the rhizoid cells, which typically lack (most) chloroplasts, and the generation of chloroplast windows.

In the remainder of this introduction, I explain the background of Characean algae, and why understanding the structure and organization of the central vacuole is important.

1.1: Characean Algae 101

This section covers the basic biology aspects of Characean biology, with a particular emphasis on *Nitella*.

1.1.1: Morphology

Characean algae are large, macroscopic multi-cellular algae that live in fresh (and sometimes brackish) underwater habitats such as lakes, streams, and rivers. The main plant body of Characean species is called a thallus (plural thalli). The thallus is divided up into stem-like axes, which includes long, cylindrical, single-celled, coenocytic (multi-nucleate) internodes punctuated by multi-cellular nodes, from which a variety of other plant structures emerge laterally. These include branchlet cells, cortical cells, stipulodes, rhizoids, gametangial initials, and protonemata. Periodically, side branches will emerge from the nodes, which form new apically dividing axes from the main axis. The intermodal cells are very large, and can reach 1-2 mm in thickness and several to tens of centimetres in length, and the thallus can reach lengths of up to 2 m or more. In *Nitella* species, these internodal

cells are ecorticate, and lack the layer of cortical cells that cover the internodes of many but not all *Chara* species (for example, *C. globularis* and *C. vulgaris*) (Hodick and Sievers, 1998, Beilby and Casanova, 2014).

Primary growth occurs at the apex of the axis, which is indeterminate and the result of a series of divisions from an apical dividing cell in a manner reminiscent of higher plant development. This single apical contains one nucleus. Continued division of this cell produces all subsequent cells and nuclei, with the daughter cells differentiating into spherical nodal cells or elongate internodal cells (Fritsch 1948). These nodal cells further differentiate into central cells and lateral cells which go on to produce the other node-derived cells (Bharathan and Sundralingam, 1984). Environmental factors such as light levels and water chemistry can influence the overall morphology of the plant (Beilby and Casanova, 2014). For example, higher light conditions such as those in shallower rivers produce a more compact thallus with shorter internodal spaces, while low-light conditions produce longer intervals between nodes (Wang et al., 2008).

The nodal complex is composed of numerous much smaller, roughly spherical cells. Leaf-like, branchlet cells emerge in rays (collectively called a whorl) from the node, which are similar in size and shape to intermodal cells but grow only deterministically, stopping after reaching a fixed size and number of cell divisions. In *Nitella,* these branchlets sometimes occur in two whorls, and often bifurcate into secondary and tertiary rays terminating in an end cell (Beilby and Casanova, 2014). However, some species lack these bifurcations and simply grow linear branchlet segments (Broady et al, 2012). While absent in *Nitella* species, stipulode and cortical cells also emerge from the node (Hodick and Sievers, 1998, Beilby and Casanova, 2014).Tip-growing rhizoids and protonemata also emerge from the nodal complex, although these are not always present at any given node. The downward-growing rhizoids playing a key role in anchoring the main axis of the plant to the substrate, whereas the upward-growing protonemata give rise to new thalli. These protonematal cells are much smaller than the intermodal and branchlet cell, being typically only 30 µm thick and generally no more than 1 cm in length. However, like the internodes, these structures are single cells (or uniseriate strings of single cells)(Gerber et al, 1995).

1.1.2: Sexual Reproduction and Development

Characean algae have male and female reproductive structures, with both monoecious (male and female organs on the same plant) and dioecious (separate make and female plants) species occurring. Initiation of sexual reproduction can be triggered by various factors including age and environmental parameters such as nutrient availability and warmth (Casanova 1994). Gametangial

initials develop from lateral cells along the node and sequentially differentiate into the female oogonium and male antheridium (plural oogonia and antheridia). Both the oogonia and antheridia arise from a single gametangial initial, which subsequently divides to produce the rest of the structure, and are protected by a layer of non-sterile cells (Pickett-Heaps 1986a, Leitch et al, 1990,). In oogonia, these cells (ten in *Nitella*) form a distinctive spiral structure around the cell called a coronula, inside of which is the fertile egg cell. At the base of the oogonia are one or more basal cells, which swell to create openings in the coronula when fertilization is ready. Antheridia are usually protected by eight shield cells, inside which are filamentous strings of sperm-producing cells attached via capitulum cells to basal manubrium cells (Picket-Heaps 1986b, Beilby and Casanova, 2014,).

In Characean algae, the product of fertilization is called an oospore. Like the gametes, the oospore is surrounded by a sophisticated structure formed from multiple levels with cells derived from both the coronula and developing zygote. These structures exist in various locations on the thallus: in *Nitella* species, the oospores tend to sit at the base of branchlet bifurcations of fertile rays (Beilby and Casanova, 2014). *Nitella* oospores can be very elaborately and diversely ornamented (John and Moore, 1987), and their color and level of oospore wall development can be indicative of maturity level in some species (Casanova 1991).

The gametes and plant body are haploid, consisting of *n* chromosomes, with gametes produced via mitotic division (Beilby and Casanova, 2014, Foissner and Wasteneys, 2014). The fertilized oospore is *2n*, or diploid, containing two complete sets of chromosomes. At an unknown point between fertilization and germination, the oospore undergoes meiosis, resulting in a return to the haploid cells of the main plant body. The first two cells produced are a positively gravitropic rhizoid initial that grows downward into the substrate, and a negatively gravitropic protonemata that grows upwards against the gravity vector. It is this upward growing cell that produces the first thallus. Growth uses the oospore's starch reserves until photosynthesis can achieved upon breaking the surface (de Winton et al., 2004), and the upward growing cell can travel upward of 100 cm through the substrate (Dugdale et al, 2001). Upon stimulation via blue light, the cell undergoes an extensive cytoskeleton reorganization transitioning from a tip-growing unicellular structure to a multicellular thallus via asymmetric divisions (Braum and Wasteneys, 1998).

Vegetative reproduction also occurs in Characean algae, with this being the primary mode of reproduction in some species. New growth and thalli can develop from structures called bulbils (which are starch-filled nodes), or from broken-off fragments that are able to develop into new thalli

(Casanova and Brock, 1999a). Life histories of Characean algae include monocarpic annuals, that survive for one year and reproducing once, or polycarpic perennials, lasting many seasons and reproducing many times (Casanova and Brock, 1999a).

1.1.3: Ecology

Characean algae occupy a variety of freshwater and brackish habitats, which can include rivers, lakes, streams, marshes, bogs, swamps, fens, and other types of watery habitats (Casanova and Brock, 1999b, Blindow 2000, Appelgren and Matilla, 2005). They can be found in water as deep as 40 m, and as shallow as a few centimeters (Casanova et al, 2007), and tend to prefer non-eutrophic (low-nutrient), calmer waters. Many of these habitats are ephemeral, with new plants emerging from substrate-borne oospores (of which there can be several generations worth built up) as water levels increase (Casanova and Brock, 1990). Spread occurs via the movement of sediments carrying oospores downstream (Bornette and Arens, 2002), or from ingestion and deposition by waterfowl (Proctor 1962), and attachment to people and animals (Beilby and Casanova, 2014).

Characean algae are often used as indicator species for the health of oligotrophic habitats (Krause 1981), which they help maintain by removing nutrients from the water column via above-ground thalli and rhizoids (Littlefield and Forsberg, 1965, Andrews 1987, Vermeer et al., 2003), dampening water currents, and stabilizing sediments (Scheffer et al, 1994, Kufel and Kufel, 2002). Research has shown that they are closely tied to phytoplankton diversity (Casanova and Brock, 1999b). Other ecological services rendered by Characean algae include providing shelter for fish, insects, and various epiphytes (Beilby and Casanova, 2014), and acting as a source of food (Pereyra-Ramos 1981, Proctor 1999, Noordhuis et al., 2002).

1.1.4: Phylogenetics

Characean algae have fossilized remains dating back to the Silurian period more than 400 million years ago, and form a long-established clade of the green algae (Villaba-Breva and Martin-Closas, 2011). The family Characeae is broken up into several genera (*Chara, Nitella, Nitellopsis, Tolypella, Lamprothamnium, Lychnothamnus*), with most species falling into either *Chara* or *Nitella*. Characeae itself is a part of order Charales, which is basally related to the land plants. Although not sister taxa (Wodniak et al., 2011), they are the land plants closest extant relatives (Karol et al, 2001). This close relation is responsible for the numerous similarities Characean algae bear to land plants and the early confusion they created with regard to their place in taxonomy (Fritsch 1948). Even after major advancements in such questions, they are still frequently referred to as being part of the plant kingdom, and as such plants themselves (Foissner and Wasteneys, 2014).

1.2: The World's Biggest Plant Cells

This section will cover known aspects of cytoplasmic architecture and dynamics of the Characean internode, as is pertinent to the purposes of this thesis. Internodal cells in *Nitella* are primarily composed of five main layers (Figure 1.1). These are:

i) The cell wall and membrane,

ii) The cortical region,

iii) The chloroplast layer,

iv) The fast-streaming endoplasm, and,

v) The large central vacuole.

1.2.1: The Cell Wall and Membrane

The overall organization of the internodal cells is strain-aligned, helical, and symmetrical. The cells can be divided into two halves, separated by a junction called the neutral line or indifferent zone. This zone slowly spirals along the length of internode, , with cytoplasmic streaming flowing in opposite directions on either side of the line.

The outermost layer of the cell is a cell wall composed of cellulose microfibrils embedded in a gel of pectin polysaccharides. The cell wall has both a primary wall and a secondary wall, and both layers combined can be up to 10 µm thick. The deposition of microfibrils is transverse in the primary cell wall of elongating cells, and random in mature cells. They are helicoidal in the secondary wall. These microfibrils are dependent upon a network of transverse cortical microtubules and are ultimately responsible for the shape of the cells, as treatment with microtubule-depolymerising compounds such as colchicine and oryzalin results in spherical cells (Delay, 1957, Wasteneys and Williamson, 1987, Wasteneys, 1992).

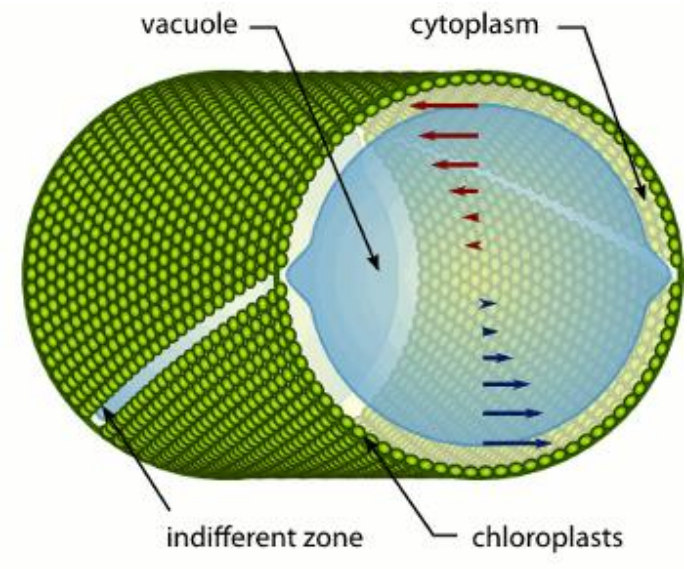

Figure 1.1. The conventional view of the organization of the internodal cells of Characean algae. Inside the plasma membrane and cell wall lies the cortical zone, neither of which are shown in this figure. The chloroplast zone surrounds a narrow layer of cytoplasm, referred to as the endoplasm in which rapid cytoplasmic streaming is generated. In the middle of the cell is the central vacuole. This undergoes some streaming, dragged along with the endoplasm through hydrodynamic flow. The direction and magnitude of cytoplasmic streaming in the endoplasm and vacuole are indicated with arrows. Source: Verchot-Lubicz and Goldstein, 2010

1.2.2: The Cortical Layer

The second layer is the cortical layer (or ectoplasm), consisting of the outermost layer of the cytoplasm. The ectoplasm contains numerous organelles such as cortical endoplasmic reticulum (cortical ER), mitochondria, peroxisomes, actin microfilaments, microtubules, and assorted vesicles. Cortical microfilaments are mostly transverse in growing cells, but randomly-orientated in mature cells, and are associated with the trafficking of vesicles to, from, and along the plasma membrane (Collings et al., 1995, Wasteneys et al., 1996). These actin microfilaments may also play a role in stabilizing the cortical ER. Similar to microfilaments, cortical microtubules are mostly transverse in growing cells, but randomly orientated in mature cells (Wasteneys, 1992). Cortical ER is flat and largely reticulated. Younger cells have much greater cortical ER coverage, covering nearly the entirety of the cortical region before elongation, 50% upon commencing of elongation, and are predominately orientated in transverse meshes. These transverse meshes result from transversely-orientated cortical microtubules. Coverage ultimately drops to 20% at maturity. Continuations between the cortical ER and the outer chloroplast membrane have been reported (Foissner et al., 2009). Lipid droplets appear to be associated with the cortical ER, and increase in size and number with age (Foissner 2009). Cortical mitochondria are rare in younger and mature cells (residing

primarily in the endoplasm), but become abundant in rapidly-elongating cells. They are influenced by light intensity, being larger and more amorphous. Their organization is influenced by both the actin and microtubule networks, indicating an affinity for both kinesin and myosin motors (Foissner 2004). They will undergo fusion and fission, and change shape over time. Structurally, Characean mitochondria are similar to that of land plants. They have similar enzymatic composition to plants and presumably play a role in photorespiration and in fatty acid oxidation.

1.2.3: The Chloroplast Layer

Inside the cortical layer is the chloroplast layer. The chloroplasts align in helical files that twist along with the rest of the cell, and the neutral line where streaming polarity reverses is a thin band that lacks chloroplasts. Chloroplasts are small initially as the cell grows, but rapidly increase in size at maturity, overlapping one another in a tight mesh. Microfilament bundles composed of polymerized actin are attached to the inner side of the chloroplast layer, and it is these stationary microfilaments that drive the rapid cytoplasmic streaming that is characteristic of Characean internodes (Williamson, 1974). The cortical ER also has strands traversing the chloroplast layer connecting cortical ER and endoplasmic ER (Foissner et al., 2009). Chloroplasts can be seen detached from the chloroplast layer streaming freely within the endoplasm. They are often ringed by actin, as are those chloroplasts near the neutral line (and are generally smaller and more roundish), allowing them to, similar to nuclei, perform rotational movements (Wasteneys and Williamson, 1991, Wasteneys et al., 1996). They are often detached in rows still strung together by microfilaments.

1.2.4: The Streaming Endoplasm

The innermost layer of the cytoplasm is the fast-streaming endoplasm. Cytoplasmic streaming which can reach rates of up to 70 μm/s, is dependent on the actin microfilament bundles that are attached to- the chloroplast layer (Williamson, 1974). Streaming originates from the interaction of myosin-coated organelles (for example, mitochondria, peroxisomes, assorted vesicles, nuclei and endomembranes) with the actin bundles (Grolig et al., 1988). The endoplasmic ER is extensive, pervading the entirety of the endoplasm in a network of tubes, but its structure has not been well defined in the literature because of difficulties in imaging the endoplasm. This ER is closely associated with the subcortical actin network, suggesting myosin motors on the ER. Mitochondria are also abundant in the endoplasm and appear to be similarly associated with the actin. The multinucleate internodal cells contain thousands of nuclei each within the streaming endoplasm, and derive without a spindle from a single progenitor nuclei in the tip-growing regions of the thalli. They are flattened structures about 2/3 of the thickness of width, and in internodal *Nitella* cells,

dumbbell shaped. They vary considerably between species, cells within a thallus, and within individual cells. Nuclei are more abundant in mature cells, but contain generally smaller, more rounded nuclei. Nuclei in elongating cells sometimes have associated microtubules on their surface and in *Nitella* (but not *Chara*), the nuclei have rings of actin, allowing them to perform rotational movements (Wasteneys and Williamson, 1991).

1.2.5: The Central Vacuole

The central portion of the cell is dominated by a large vacuole which occupies over 95% of the cell volume (Beilby and Shepherd, 1989). These vacuoles accumulate large volumes of sucrose, indicating a predominately storage-based function (Sakano and Tazawa, 1984, Oikawa et al., 2011). The levels of sucrose can change from species to species and across time, with the production of gametes corresponding with an increase in sucrose content (Beilby and Casanova, 2014). The vacuole only contains trace amounts of free amino acids (0.31 mM), which can increase up to five-fold in continuous darkness or light (Sakano and Tazawa, 1984). The central vacuole is acidic, as per experiments with numerous dyes such as Lysotracker yellow (Klima and Foissner, 2008) and neutral red, which accumulates into acidic compartments and become protonated and sequestered (Hitchcock 1919, Shimmen and MacRobbie, 1987, Beilby and Shepherd, 1989).

The central vacuole is not, however, the continuous or homogenous structure that conventional images of the internodal cell (Figure 1.1) suggest it to be. The vacuole is perfused by cytoplasmic tubules in young cells that have not yet begun elongation (Wasteneys et al., 1996). The central vacuole also contains numerous inclusions such as small vesicles containing solid bodies thought to play a role in plugging punctures in the cell. These wound plugs are generally surrounded by a lipid membrane classically thought to be derived from the ER, and are polysaccharides with protein. This is further supported by the fact that the wound plugs can occasionally be seen in the endoplasm of internodes (Own unpublished results).

1.3: Fluorescence Microscopy

As this thesis relies on the use of fluorescence and confocal microscopy, the following two sections of this introduction provide background to these techniques.

Fluorescence is a phenomenon where an electron within a fluorescent substance absorbs a photon, causing it to become excited from a ground state to a higher state, subsequently returns to the ground state by emitting a photon. Various physical processes such as vibrational relaxation cause the electron to lose energy after becoming excited and before emission, and because of relaxation

and energy loss, the released photon is lower than that of the absorbed photon. This means that the fluorescence occurs at a longer wavelength, and the difference in the wavelengths of strongest absorption and emission is referred to as the Stokes shift. Different substances have distinct absorption and emission spectra, and these spectra are dependent on the chemical environment of the fluorescent substance in question. The ratio of photon absorption to photon emittance is called quantum yield, and higher quantum yields result in more efficient fluorescence. Typically, the fluorescent dyes used for live cell imaging have high quantum yields, which means that bright signals can be generated with lower levels of excitation radiation. Various types of quenching can reduce the intensity of fluorescence. The average time between emittance and emission is called the fluorescence lifetime, and is generally in the 0.5-20 nanosecond range, which can be contrasted with phosphorescence, a related phenomenon that occurs over longer timescales (up to hours) (Lakowicz 2006).

1.3.1: Fluorescence in Cell Biology

Fluorescence is prevalent throughout nature, with many molecules present in animals, plants and other organisms being naturally fluorescent, a phenomenon that is called autofluorescence (Andrews et al.,2007, Sparks et al., 2014). Examples of this include the plant photosynthetic pigment chlorophyll, compounds found in the exodermis of spiders and scorpions that make them fluoresce under ultra-violet light, and the range of proteins found in marine organisms related to green fluorescent protein, first characterised in the jellyfish *Aequoria* (Chudakov et al., 2005).

For cell biologists, many thousands of different fluorescent dyes have now been developed, many of which can be used to label specific components of cells (Lakowicz 2006, Johnson and Spence, 2010). The spectral properties of fluorescent dyes have allowed researchers to learn much about the structure and dynamics of various cellular systems. Dye concentrations are generally optimized to have just enough dye to produce a sufficient amount of fluorescence, as the presence of the dye can cause biological disruptions or cell death. Dyes can also be used as vital stains, with dead cells staining differently from live cells (Sousa et al., 1997). These dyes can often be combined to reveal several aspects of a cell at once. Transformable cells can utilize green fluorescent protein hybrids create proteins with GFP tags, allowing for the localization of certain proteins to be visualized with minimal disruption to the cell (Snapp 2010).

1.3.2: Variable Spectral Properties of Fluorescent Dyes

The use of fluorescent dyes in living cells can be problematic. Numerous parameters are capable of influencing the fluorescent properties of dyes. For example, neutral red is a weak acid that exists in both its protonated (NRH^+) and non-protonated (NR) form, in addition to forming aggregates at sufficient concentration. In aqueous solution, NR absorbs with a maximum in the blue part of the spectrum at 450 nm, NRH^+ at 530 nm (green), and both fluoresce with a peak in the red part of the spectrum at 637 nm. These changes are significant because when NR is accumulated into compartments such as acidic vacuoles, it protonates to become the membrane impermeant form NRH^+. The polarity of the solvent is important in regards to the fluorescent properties of neutral red: switching the solvent from water to a non-polar organic molecule such as dioxane shifts the fluorescence of NR from 637 nm (water, polar) to 540 nm (Sousa et al. 1997). Quantum yield is also affected by things such as solvent (Singh et al., 1998). For neutral red, these solvent-dependent changes in fluorescent properties are not typically important for living cells, where neutral red will be present predominantly in its aqueous form, but should the neutral red accumulate in lipid bilayers, then changes in fluorescence might be possible. Such effects are known for the dye Nile red, which fluoresces red (peak above 600 nm) when dissolved in membranes, but a bright yellow colour with a fluorescence peak at about 550 nm when in lipid droplets (Greenspan, 1985).

Neutral red can also form aggregates, and these too change its spectral properties, with absorbance shifting from 440 nm (monomeric) to 518 (aggregate) (Sousa et al. 1997). Numerous other dyes exhibit similar changes based on things such as pH, concentration, and solvent. This means that it can often be somewhat unreliable to depend on “known” spectral behaviours of a dye, making it necessary for one to be constantly vigilant of any possible factors which could be affecting the fluorescence of the dye. On the positive side, these shifts in spectral behaviour can serve as useful clues as to the physiological parameters present inside of various parts of the cell, for example determining the pH of different cellular compartments using dyes such as acridine orange (Johannes and Felle, 1990).

1.4: Confocal Microscopy

Confocal microscopy is a microscope technique that selectivity eliminates out-of-focus light. A light source, which in modern confocal systems is typically a laser or a series of lasers of different colours, is focused through a small aperture (the pinhole) through an objective lens onto the specimen. The lasers scan across the focal plane dot-by-dot, line-by-line, across the entire imaging area. The reflected light and fluorescence is collected by the same lens (this configuration is referred to as

epifluorescence), and on its return hits a beam splitter which only passes the fluorescence signal. This light is passed through another pinhole which effectively selects light only from a single focal plane within the specimen (Figure 1.2). This eliminates out of focus light, allowing microscopists to create thin optical sections of translucent specimens. It is then picked up by a light detector, transforming it into an electrical signal to create a digital image. Due to the nature of the laser scanning process, this means that each "dot" imaged by the microscope can correspond with pixels in the resulting digital image (Webb 1996). It is this ability to remove out-of-focus light from the image which allows the confocal microscope to be so important for live cell imaging experiments.

In the Leica SP5 confocal microscope used in these experiments, the fluorescence from the cell is split by a prism into its different wavelengths / colors. A series of mirrors and barriers allows the user to define multiple channels based on their emission wavelengths and, unlike other confocal systems, this means that the system is not limited to the specific wavelengths based on filters (Figure 1.3) (Collings, 2013).

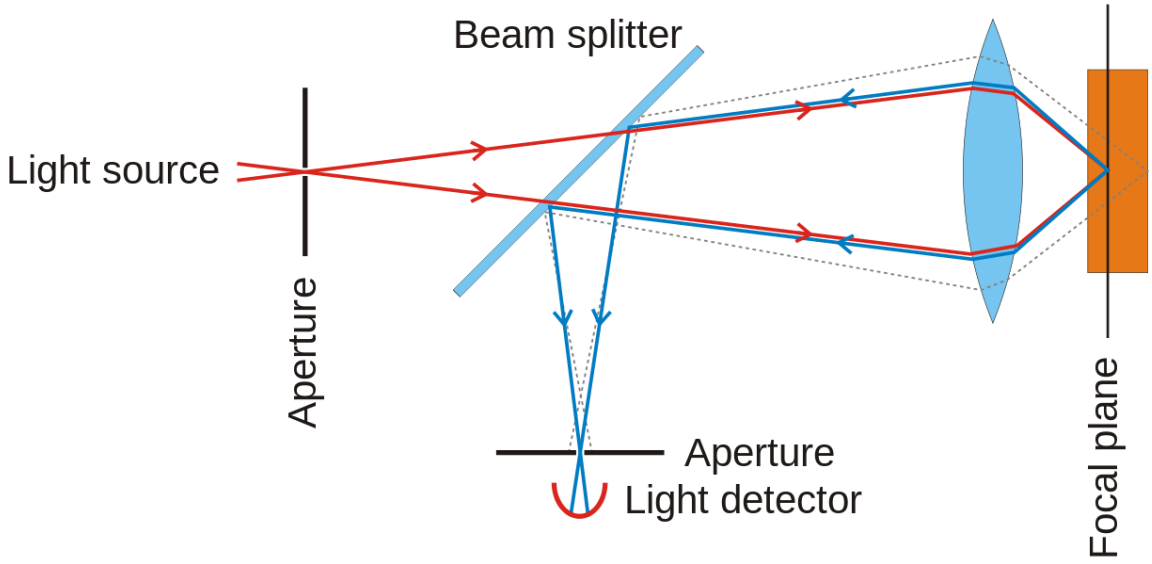

Figure 1.2. Basic principles of confocal microscopy. The use of the pinhole allows the removal of out-of-focus light. Image from Wikipedia, used under the Wikimedia Commons license.

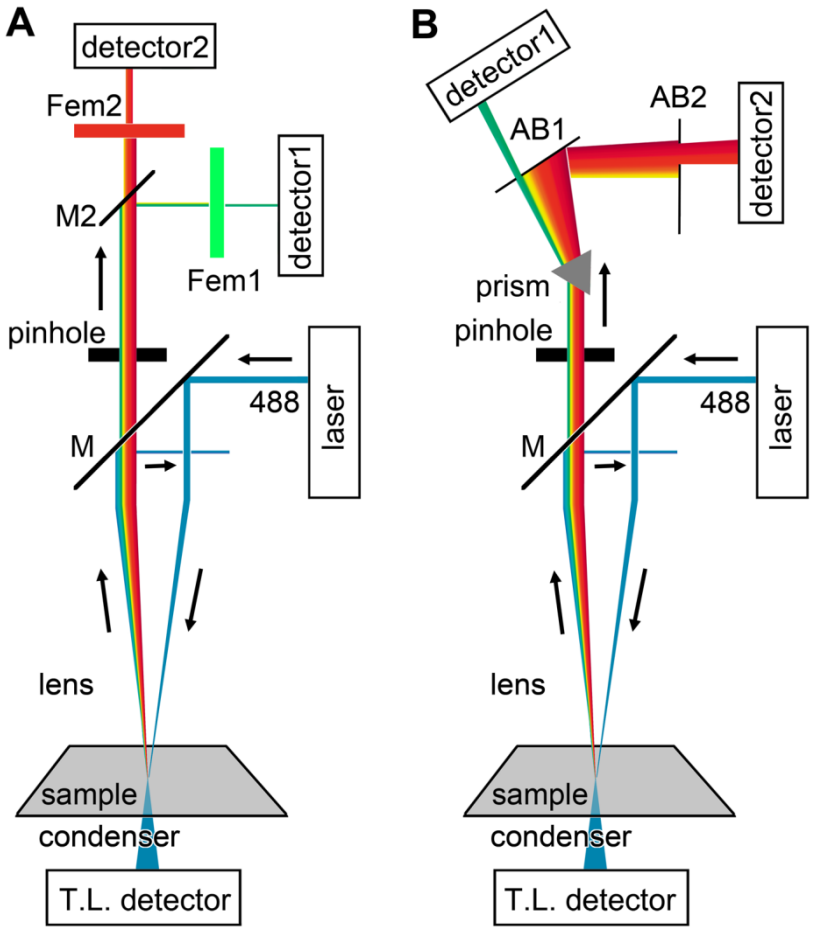

Figure 2.3. Spectral scanning in the Leica confocal microscope. Unlike a conventional confocal microscope (A), in which specific emission filters (Fem1 and Fem2) control light going to the detectors, the Leica confocal microscope (B) uses a prism which separates light into its different wavelengths. A set of mirrors acts as a barrier to the first detector, and reflects light to the second detector. Because the barriers can be precisely controlled, the wavelengths received by the detector can be tuned to specific dyes. Image modified from Collings (2013).

1.4.1 Advantages and Disadvantages of Confocal Microscopy

One of the main benefits of confocal microscopy is that it is comparatively non-invasive, allowing for the optical sectioning of living cells. This technology, along with the introduction of a wide range of targeted dyes and the development of fluorescent protein technologies, has revolutionized cell biology. The confocal is not, however, without significant limitations.

Although the confocal image removes out-of-focus light through the use of the pinhole, the maximum resolution achievable in a confocal image remains limited to about half the wavelength of the excitation light, as with other light-based imaging systems, and considerably worse than achievable with electron microscopy. While several different approaches to super-resolution

imaging, each with increased resolution, have been developed in recent years (Galbraith and Galbraith, 2011), these too have their limitations. Nevertheless, while confocal microscopy lacks the resolution achievable by electron microscopy, it has the considerable advantage that live cell imaging and optical sectioning is possible, something that cannot be achieved with electron microscopy. During confocal imaging, the actual image resolution achieved can be controlled by changing the rate at which the laser is scanned across the sample, with slower scan speeds producing higher resolution images. This can allow microscopists to achieve faster scanning speeds when high resolutions are unnecessary, or to help capture high speed objects. The scanning speed can be similarly boosted by reducing the size of the imaging area, useful when scanning smaller objects with weaker lenses. This is, however, another of the fundamental limitations of the conventional confocal microscope: With a 20x lens on the Leica confocal microscope used in this study, a 775x755 µm scan area takes over a second to image at high quality, making capturing fast-moving events without distortion difficult (Semwogerere and Weeks 2005).

Confocal microscopes do have several other advantages. Multiple emission wavelengths can be imaged at the same time without interference from one another, and concurrent transmitted light imaging is also possible. This allows different dyes to be imaged in a single system, and the results to be compared to the transmitted light image. The confocal system is also extremely sensitive, with the gain in the detection system adjustable. These higher gains producing brighter images at the cost of introducing noise. This can be useful for picking up a weak signal (for example, when using higher magnification lenses that get less light), especially if the introduced noise can be rectified. It can also be useful for dampening a powerful signal. The depth of the focal plane can also be controlled by changing the size of the pinhole, which produces thicker sections but does increase the amount of light recovered.

1.5: Nitella as a Model System

1.5.1: Classical Studies

Nitella and other Characean algae have long-served as a model system in cell biology. The algae were described in pre-Linnaean times as “equisetum” due to their resemblance to horsetails (Bauhin, 1623), cytoplasmic streaming was first described in algae and plants by the Italian abbot Bonaventura Corti in 1774 (Corti, 1774). . Characean internodes have also been a classical system for electrophysiological studies (reviewed in Beilby, 2016), and can generate an action potential that release calcium into the cell (Williamson and Ashley, 1982). Numerous other aspects also contribute to their experimental value. Their large, helically symmetrical, easily-manipulated cells have made

them ideal for experimental procedures such as microinjection, usage of pressure probes, injection of electrodes, intracellular perfusion with a foreign media, and the generation of cytoplasmic droplets. With this array of techniques, Characean algae have been used in various kinds of research such as studying the electrophysiology of membrane potentials, which were discovered in Characean algae before their subsequent discovery in neurons. They have also been used for studies of cytoskeletal organization, organelle interaction, and photosynthesis (Foissner and Wasteneys, 2014, Beilby 2016). Many general principles of plant biology were first discovered in Characean algae. For example, actin was discovered in *Chara* before their discovery in plants (Williamson, 1974), as was myosin's association with actin before a similar discovery in *Arabidopsis* (Grolig et al., 1988, Knight and Kendrick-Jones, 1993). As they are such a model system for numerous types of study, it then becomes prudent to have a fuller understanding of the biological context these experiments are taking place in, which can have major implications on experimental design and the understanding of results.

1.5.2: An Aging System

Despite these successes, however, the field of Characean cell biology has struggled to keep up with recent advances in cell and molecular biology. There are, for example, no methods to transiently or stably transform the Characean cells despite the obvious use for such protocols in electrophysiological research and for the expression of GFP fusion proteins. For developmental biology, there is also a lack of mutants, and as yet there are no full genome sequences available for Characean algae, although it might be expected that this will change in the near future.

There are, moreover, significant issues in the microscopy of Characean algae. An often understated problem is the fact that the fast-streaming endoplasm and large central vacuole are difficult to image using fluorescence and confocal microscopy. By the time a scan has run from start to finish, any object in motion is likely to have moved dozens of micrometers (given scan times up to 1 second or more and an endoplasmic streaming rate of up to 70 μm/s), resulting in a distorted image. There is also the problem of the cylindrical tube of chloroplasts that covers the length of the cell which significantly absorb any light passing through and limiting the ability to excite most fluorescent dyes in the lower layers. This leaves only the cortical and chloroplast layers with a good, comprehensive body of image data for live cells. Most of what we know about the organization of the endoplasm comes from electron microscope work. Good sample preparation can do much to preserve cellular organization, but electron micrographs can offer little in the way of showing active cell dynamics, which only live cells can demonstrate with certainty.

1.6: Experimental Aims

In this thesis, I use two complimentary methods which bypass the chloroplast layer: The utilization of rhizoids in place of internodes, and the creation of chloroplast-free windows. These allow effective fluorescent imaging of the endoplasm and vacuole. I also propose scanning protocols that achieve fast enough imaging rates to capture the dynamics of the vacuole at sufficient image quality and minimal distortion. As a comparatively understudied organelle, the vacuole and endoplasm will be the main foci of study, and observations of the cortical region of the cell will be minimized. In addition, this study will also be an exploratory study investigating the usefulness of assorted dyes for imaging in *Nitella*.

1.6.1: Exploration of New Imaging Techniques

The first method involves using the small, root-like rhizoid cells, which are largely or completely devoid of chloroplasts and have similar cytoplasmic architecture and dynamics as internodal cells. The rhizoids, due to their smaller size may be more effective at absorbing dye then their internodal counterpart. Further, because the rhizoids are considerably smaller than the internodes, this means that the imaging area is also smaller, readily accommodating faster scanning speeds which are used to help overcome the imaging speed problem.

The second method involves irradiating a small square-shaped area on the surface of an internodal cell with the violet (405 nm) laser, burning out the chlorophyll and causing the chloroplasts to subsequently detach, creating a chloroplast-free window. While this technique has normally been used in studying various aspects of wounding response, it has not previously been used to create chloroplast-free windows in the cell specifically through which to fluorescently image the endoplasm or vacuole. One concern is that this approach, which damages the cortical layer, might possibly damage the endoplasm as well. Previous experiments, however, have shown that if the irradiation is not severe, then the actin bundles that normally sit underneath the chloroplast layer and which drive cytoplasmic streaming can regenerate (Williamson et al., 1984). This suggests that intermixing and fast streaming rates should minimize any disruption to the endoplasm and vacuole.

1.6.2: Exploration of New Staining Protocols

Beyond dyes for structures in the cortical regions of the cell, a suite of dyes with standardized protocols exists only in limited form for Characean algae. In order to effectively image cell structures, the most optimal dyes need to first be ascertained. Dyes will be tested at a variety of concentrations, incubation periods, and excitation/emission spectra until an optimal protocol is

determined. As part of the experimental regimen will involve using a variety of dyes that have never been used in Characean systems (or in plant systems), serendipitous observations of interest are likely to occur.

1.6.3: Aims in This Thesis

It is intended that these investigations will lead to a keener understanding of the cytoplasmic architecture and dynamics of model Characean algal species. This will not only provide a better cellular context for scientist investigating fields such as membrane electrophysiology in which Characean algae continue to be popular, but also potentially provide insight into the roadblocks that prevent us from performing techniques such as genetic transformation, allowing us to find ways to overcome them. Characean algae have already been a treasure trove of knowledge about cell biology for us in the past. With the overcoming of the chloroplast problem and the other hurdles facing the field, it can once again become one of the premier fields for research into cell biology.

2: Methods

2.1: Collection, Identification and Culturing

Characean algae and soil were collected by hand from Okeover Stream at the University of Canterbury. The alga was identified as *Nitella hookeri* on the basis of three-segmented branchlet terminations, as well as the lack of a secondary whirl of branchlets that occurs in *Nitella hyalina,* the only other species of *Nitella* present in New Zealand (Broady et al., 2012).

Algal samples were grown in an aquarium (0.5 x 0.25 x 0.25 m) filled up with trap water and ~5 cm of soil. In order to generate rhizoids, aquarium water levels were only topped up with distilled water, without any additional nutrients being added during the experiments. The water was aerated with a tube connected to an air feed from the wall, connected to the School of Biological Sciences compressed air freed. Algae were grown on a laboratory bench with room lighting, and weak, indirect sunlight. This culture was maintained through the course of the experiments.

2.2: Experimental Manipulation of Algae

Samples for experiments were collected from the culture tanks using scissors to snip beneath the second or third node, with efforts made to keep the overall length of the samples roughly the same (~4-5 cm).

For sample staining, cells were placed on a glass slide and briefly washed with distilled water for 5 to 10 seconds, using a wash bottle to remove as much debris as possible. This method was chosen as it was strong enough to remove the debris that tended to collect near nodes without damaging the delicate rhizoids and other cells that sprout from there. Approximately 500 µl of diluted dye solution (see below) was pipetted evenly across the sample, and the cells left to absorb the stain for varying lengths of time. Samples were then washed for 5-10 seconds with distilled water to remove excess dye. The sample was then enclosed by a coverslip (22 x 40, or 22 x 50 mm), and any excess water wicked off with a paper towel.

2.3: Fluorescent Dyes

Numerous fluorescent dyes were used during the course of this study. These dyes, whose characteristics and sources are listed in Table 2.1, localise to different compartments within the cell.

The experimental dyes were kept as stock solutions in dimethyl sulfoxide (DMSO) and stored within Eppendorf tubes in the freezer at -20^{o}C when not in use. Dyes included neutral red, acridine orange, CMAC Blue, MDY-64, Syto-13, $DIOC_3(6)$, and Nile red. Further details concerning each of the different dyes used in this study have been included in Appendix 1.

Dyes were diluted by pipetting distilled water into a fresh Eppendorf tube, then pipetting the required amount of dye in and mixing, with further dilutions and mixing as required. Control treatments demonstrated that the DMSO solvent used for the dye did not affect cytoplasmic streaming, and thus did not appear to harm the cells.

Table 2.1. Fluorescent dyes and fluorophores

Dye	Localisation	Supplier	Excitation (nm)	Emission range (nm)	Stock concentration (mM)	Staining concentration (μM)	Staining (min)
Acridine orange	DNA, acidic organelles	Sigma	488 or 514	500 - 550, 650 - 700 [1]	50	20	360
Blue-CMAC	Vacuole	Molecular Probes	405	415 - 465	10	100	30
$DIOC_6(3)$	Mitochondria, and ER	Molecular Probes	488	500 - 550	20	10	20
MDY-64	Tonoplast	Molecular Probes	456	465 - 515	10	10	30
Neutral red	Acidic organelles	Sigma, Molecular Probes (high purity)	561	570 - 620	10	10	10
Nile red	Oil droplets, membranes	Sigma	561	580 - 620	10	50	30
Syto-13	DNA	Molecular Probes	488	500 - 550	5	5	30

[1] Wavelengths for imaging acridine orange were highly variable, and depended on the specifics of staining. Numbers give general indications only.

2.4: Confocal Microscopy

A Leica SP5 confocal microscope running on a DMIRB inverted microscope was used for these experiments. Imaging used either a 20x NA 0.7 glycerol immersion lens or a 63x NA 1.3 glycerol immersion lens.

The Leica confocal was equipped with 4 different lasers, giving excitation wavelengths of 405 nm (violet light), 458, 488 and 514 nm (various shades of blue light), 561 nm (green light) and 633 nm (red light). On the Leica system, emission wavelengths can be set using the spectral scanning system, and are not limited by specific filters. Excitation and emission wavelengths were varied according to the dyes used, and are described in the results section. Transmitted light images were recorded wherever appropriate.

To increase confocal imaging speed, necessary for the rapidly-streaming *Nitella* internodes, several non-standard approaches to imaging were taken. All of these resulted in faster images, but decreased image quality:

- The imaging area was reduced to as small an area as possible. The limitation with this was that internodal cells were typically large, and required lower zoon settings so that the entire cell could be imaged.
- Bidirectional scanning was used in which scanning was conducted in both directions across the sample.
- Laser power was increased so that fluorescence levels were high, noise levels low, and averaging required reduced. Increasing the laser power too high, however, caused irreversible damage to the cell, notably in the rhizoids.
- Imaging used all lasers concurrently, rather than sequential scanning. This introduces the potential for cross-talk between different fluorescent molecules although as most experiments were limited to a single dye, this was less of a problem.
- The scan speed was increased from the default speed of 400 Hz to frequencies as high as 1400 Hz. Increasing the scan speed too high, however, required the system to run at higher zoom settings, and resulted in only small areas being scanned.
- Imaging averaging was reduced to a minimum. While line averaging was set to 3 to improve image sharpness in some cases, in other cases averaging was set either to 2, or no averaging was used. When averaging was used, this was always line averaging, rather than frame averaging, which meant that it was the individual lines of the image,

rather than whole frames that were averaged, thus reducing movement artefacts. However, reduced averaging resulted in increased noise within the images.

- The images were taken at a variety of resolutions, including 512x512 and 1024x1024. However, image size was often reduced so that imaging speed was increased. This caused a reduction in image resolution, and thus lost information.

2.5: Image Processing

Images were processed using ImageJ and Photoshop. ImageJ was used to select frames, then crop and separate them from image stacks created by the Leica software. The frames were then processed further in Photoshop to adjust brightness and contrast, collate them into single images, adjust dimensions and dpi, and add labels, borders, and scale bars. Finalized images were saved as *.tif files.

2.6: Generation of Chloroplast-Free Windows

Chloroplast windows were made by mounting an unstained internode on a slide and then irradiating a 400x400 µm square region for 5 minutes using the 405 nm violet laser running at 50% power. The cells were then carefully recovered from the slide. Lens wipes were used to gently wick away as much glycerol/oil as possible from the coverslip. The slides were then placed in a Petri dish containing distilled water, and the coverslip carefully removed so as to preserve the orientation of the sample. This was necessary, as subsequent location of the window could be difficult. The cells were then removed from the Petri dish and placed in a different dish with a fresh sample of distilled water to incubate while the chloroplast layer in the windows detached. Cells were incubated for varying lengths of time and, once ready, the slides were removed, and water removed, and the cells stained and mounted as described above.

2.7: Plasmolysis Experiments

Cells were opportunistically plasmolyzed with glycerol. This was achieved by rotating the lens to the edge of the slide so that some of the glycerol normally used for the 20x or 63x immersion lenses would leak under the coverslip. This allowed for the lens to then be quickly brought back to the sample to start imaging as the cell started to plasmolyze. This method, which was initially developed by accident, was used in preference to others because of the difficulties associated with getting plasmolysis solutions under a coverslip on an inverted microscope.

3: Results

These experiments developed and explored the validity of two new imaging methodologies, and sought to compare their results to imaging obtained with unadulterated internodes. The experiments used a combination of well-established and novel fluorescent dyes. As such, these methods are complementary to each other, and can be used in combination to increase the certainty of results.

3.1: Control Imaging

3.1.1: Chloroplast Absorbance

As the chloroplast layer, and its ability to absorb both incoming and outgoing light, are a major focus of these experiments, an initial exploration of the chloroplasts and their properties was conducted in order to provide a framework of understanding for later experiments. Chloroplasts contain a variety of photosynthetic pigments such as chlorophylls a, b, and ß-carotene. Collectively, these photosynthetic pigments absorb light across the entire visible spectrum, with peaks in blue (~450 nm) and red (~680 nm) wavelengths, but with a significant drop in green (~500-575 nm) wavelengths. This low absorbance of green wavelengths, and moderate-to-strong absorbance of other wavelengths, is responsible for the green coloration of chloroplasts and *Nitella* plants as a whole, as the light transmitted by the algae is predominantly green.

The effects of chlorophyll absorption by chloroplasts were demonstrated by observing the brightness along the neutral line with transmitted light (Figure 3.1C, arrow). This brightness coincides with the lack of chloroplasts, and was confirmed by imaging chloroplast autofluorescence (Figure 3.1B, arrow). From such imaging, the tube-shaped encasement of the endoplasm by the chloroplast layer can be seen. Chloroplasts circulating through the endoplasm cast clear shadows with visible outlines in imaging wavelengths (Figure 3.2A-C, arrow) (Figure 3.3, carets). Even for dyes such as neutral red, a noticeable increase in brightness along the neutral line was observed. This is due to the fact that while the exciting 561 nm green light can readily pass through the chloroplast layer, the 570-620 nm yellow-orange light the neutral red re-emits cannot (Figure 3.4A, B, arrow). These sorts of results make it clear that getting the excitation wavelength into the cell was only one half of the problem- getting the fluorescence emission out of the cell can also be problematic. For dyes not excited with green light such as $DIOC_6$(3), imaging was much more difficult, as although the green fluorescence can readily pass back through the chlorophyll, the lack of initial excitation

resulted poor imaging and revealed only faint mitochondria in the upper endoplasm (Figure 3.5). Equivalent images in rhizoids with $DIOC_6(3)$ (Figures 3.6, 3.7), or in internodes with neutral red (Figures 3.8, 3.9), were much more vivid and detailed, with fluorescence bright enough to take optical sections through the middle of the vacuole and image structures throughout the entirety of the cell. This makes it clear that given a choice between excitation absorption and emission absorption, it is better to sacrifice emission.

3.1.2: Observations of Autofluorescence

Whenever fluorescent dyes are used in live cell imaging experiments, the autofluorescence of the cell needs also to be investigated. This control imaging was achieved under similar conditions compared to when dyes were present. By identifying the autofluorescent structures present in *Nitella*, it was then possible to determine to where dyes were actually localized.

In *Nitella hookeri*, autofluorescence came primarily from two sources. The most significant source was chlorophyll in chloroplasts which had its greatest excitation with 633 nm excitation, and emission in the far red and near infra-red from 650-700 nm. However, chloroplasts have a wide range of excitation and emission wavelengths, including weak green and yellow fluorescence. A faint outline of the chloroplasts was typically seen whenever internodes were imaged, even with blue excitation and green emission (Figure 3.10A, arrow, C). On occasion, chloroplast autofluorescence would bleed strongly enough into imaging wavelengths to interfere with imaging (Figure 3.1A, arrow, Figure 3.11A, arrow, Figure 3.7A, B, carets, Figure 3.12A, B). On rare occasions, dislodged autofluorescent chloroplasts were observed that streamed in the endoplasm. Such chloroplasts, like the stationary chloroplasts, could always be identified in the concurrent transmitted light images.

As the chloroplasts were in defined locations in the periphery of internodal and nodal cells, and as their development in rhizoids was also in defined locations, even this strong autofluorescence did not confound imaging of the streaming endoplasm and vacuole. Instead, it acted as a frame of reference when imaged concurrently with other fluorescent dyes. As such, 633 nm laser illumination and a 650-700 nm emission window were included in all imaging experiments.

The second source of cellular autofluorescence was from the wound plug cores (Figure 3.10B, D, arrow) (Figure 3.13A, C, arrows) (Figure 3.14A, C, arrows). These emitted their strongest fluorescence with 561 nm excitation in the 570-620 nm emission range (orange to red). Their

level of autofluorescence was lower than the chloroplasts, and was generally minor. These wound plugs would sometimes aggregate into extensive mats (Figure 3.13, arrow) and gyres (Figure 3.14, arrow). The mats had little internal movement and were spatially dispersed, but could migrate up and down the length of the cell, often taking up most of the intervening space between tonoplasts. Gyres were more spatially compact, and could rotate freely along all three axes, as well as migrate up and down the length of the cell (Movie 1). No other sources of consistent autofluorescence were present.

3.2: Imaging Internodes

Imaging of unadulterated internodes (that is, internodes that had not been subjected to the generation of chloroplast windows - see below) was completed in order to achieve two things. First, this gave certainty about whether or not cell dynamics shown through chloroplast-free windows is true to the dynamics that exist in non-treated cells. Second, it determined to what extent the basal streaming region of rhizoids resembles the structure and dynamics of internode and branchlet cells, and hence their ability to serve as superior proxies. For the purposes of these experiments, branchlet cells and internodal cells are grouped together as "internodal-type" cells.

Internodes could on occasion be used to successfully image the endoplasm and vacuole, particularly neutral red, and to a lesser extent, MDY-64, Blue CMAC and acridine orange. On one rare occasion $DIOC_6(3)$ produced vivid imaging in internodes, however this was not being readily replicated. Dyes such as Blue CMAC and MDY-64 have both their excitation and emission wavelengths absorbed (405/415-465 nm and 456/465-515 nm, respectively) by the chloroplast layer, however their high quantum yields allowed them to be somewhat successful in imaging unadulterated internodes. The specifics of what each of these dyes demonstrated are discussed in the following sections.

3.2.1: Imaging the Tonoplast

Experiments with neutral red and MDY-64 revealed the tonoplast to be a highly dynamic membrane that is often undulating, causing it to bulge significantly into the endoplasm and vacuole. Neutral red demonstrated a network of tubules and membranes was often associated with the tonoplast, with this at times extensive and up to 14 µm thick (Figure 3.15A, carets), while in other cases being sparse, and only 5 µm thick (Figure 3.8A, caret). The tonoplast stain MDY-64 could also image these networks (Figure 3.16A, caret).

3.2.2: Imaging the Internodal Endoplasm

Other membranes within the endoplasm appeared to be stained by neutral red as well, giving it a textured, heterogeneous appearance from above (Figure 3.9A, caret) (Figure 3.17A, carets). $DIOC_6(3)$, a mitochondria stain, labelled numerous punctate structures likely to be mitochondria in the endoplasm (Figure 3.18A, carets) (Figure 3.19A, asterisk). MDY-64 also labelled similar punctate structures (Figure 3.20A, carets) however it is better known as a tonoplast dye. Embedded within these membranes and mitochondria were multiple disk-shaped nuclei. Neutral red (Figure 3.9A, arrow), MDY-64 (Figure 3.20A, arrows), and $DIOC_6(3)$ (Figure 3.18A, arrow) (Figure 3.19A, arrow) acted as negative stains, and acridine orange (Figure 3.3A, C, arrows) and Syto-13 (Figure 3.12A, arrows), both nucleic acid dyes, acted as positive stains. These nuclei would stream with the rest of the endoplasm (Movie 2), and could bulge the tonoplast noticeably into the vacuole (Figure 3.19A, caret). They were variable in size, ranging from 7x14 µm (Figure 3.9, 48) to 10x27 µm (Figure 3.18) to 15x15 µm (Figures 3.12, 3.20). As they were disk shaped, they would usually appear as either rods or circles depending on viewing orientation.

3.2.3: Imaging the Internodal Vacuole

The vacuole contents could be imaged effectively with Blue CMAC which localizes into the vacuole without any non-specific staining in the endoplasm. This allowed the dynamism and undulations of the tonoplast to be demonstrated (Figures 3.21A, arrow). The neutral line greatly increased the brightness of imaging with Blue CMAC (Figure 3.22A, C, asterisk), as both incoming (405 nm) and outgoing (415-465 nm) radiation were heavily absorbed by chloroplasts.

Wound plugs are membrane-bound compartments that exist inside the vacuole, and the membranes surrounding wound plug cores could be labelled with MDY-64 and neutral red. In a comparison image using both dyes, neutral red stained the membranes more vividly than MDY-64 (Figure 3.16A, caret), likely a result of the 561 nm laser able to penetrate the chloroplast layer more effectively and hence deeper into the cell than the 456 nm laser used to excite MDY-64. Blue CMAC wound stain these wound plugs in one of two ways, either positively by filling the contents and fluorescing brightly (Figure 3.22A, C, caret, Figure 3.23A, C, caret), or by negatively such that the wound plugs left noticeable shadows on imaging wavelengths (Figure 3.22A, C, arrow, Figure 3.23A, C, arrow).

Other vesicles lacking a wound plug core could also be stained, and they were often tethered to each other by tubular strands of material, having a viscous character as they moved through the vacuole, as shown with neutral red (Figure 3.24A, arrows). These tubules could extend for dozens of micrometers along the length of the cell.

3.3: Chloroplast-Free Windows

3.3.1: Irradiation Treatment

The literature suggests that it is possible to selectively remove the chloroplast layer to create windows into the endoplasm and vacuole by high levels of irradiation (Kamitsubo 1972).

Irradiation of a small region of chloroplast layer, about 40 by 40 µm, for 5 min with the 405 nm laser running at 50% power caused dramatic changes to cellular organisation. This laser strength was at least 10-fold higher than would normally be used for live cell imaging. The most immediate effect was that the chlorophyll in the chloroplasts became bleached, creating stark boundaries of increased brightness within the irradiated area when viewed by transmitted light (Figure 3.25A, B arrow). This increased brightness contrasted with the relative freedom through which 561 nm light could pass through the chloroplast layer, where the differences in brightness inside and outside of the irradiation area were minimal (Figure 3.25D, arrow). A sort of chloroplast “skeleton” of fluorescence was left behind after the irradiation treatment (Figure 3.25C, arrow).

By 24 hours later, the chloroplasts detached, creating a true chloroplast-free window (Figure 3.26). There were a few anomalies along the peripheries of the window. Membrane-bound, weakly-fluorescing chloroplasts were present (Figure 3.26A, B, caret), as well as chloroplasts exhibiting unusual autofluorescence patterns, with a doughnut-shaped ring of fluorescence around an internal structure bearing the usual “coffee bean” appearance of a chloroplast (Figure 3.26C, D, arrow). These assorted unknown structures were perhaps chloroplasts in various stages of either being recycled or incorporated.

3.3.2: Imaging Through Chloroplast-Free Windows

The creation of chloroplast-free windows greatly enhanced imaging. MDY-64 was successfully imaged through such windows, and provided detailed observations of the streaming endoplasm and vacuole (Figures 3.2, 3.27-3.28). This dye was chosen on the basis of its performance in rhizoid experiments (see below). In the upper endoplasm, punctate structures were labelled and were the most predominant feature (Figure 3.2A, caret), flowing with the bulk of the endoplasm. Deeper into the endoplasm, nuclei were negatively stained and flowed throughout the endoplasm (Figure 3.2B, arrows). The nuclei were sometimes discernible in the transmitted light imaging (Figure 3.2C, arrows), and their size (~4 x 15 μm) matched other observations of nuclei (see below). These nuclei were often associated with stacks of membranes (Figure 3.2B, C, carets), which appeared near the disks, and were 5 μm at their thickest, and 8 μm at their widest.

Near the tonoplast, the extreme dynamism of the tonoplast could be observed with MDY-64, with bulges extending into the endoplasm (Figure 3.27A, caret). On the endoplasmic side, the tonoplast appeared to be associated with a complex network of tubules and membranes. This network could reach up to 4.5 μm in thickness, and contained internal spaces 1 μm long and 3 μm wide (Figure 3.27A, arrows). However, these tubules were not always this thick and intricate, sometime being as thin as 1 μm wide (Figure 3.27B, caret). The membranes surrounding wound plug cores were also strongly labelled with MDY-64 (Figure 3.27D, arrow). An unknown, unstained object appeared in the transmitted light (Figure 3.27C, arrow) which may have been an out-of-focus nucleus.

Imaging results through winds were consistent with MDY-64 imaging obtained from rhizoids (see below) and unadulterated internodes (see above). This indicates the success of the technique overall, which did not appear to produce any experimental artefacts. However, without the chloroplast layer to shield the streaming endoplasm, it was more vulnerable to photodamage, with bunching, ripples, and arrest of endoplasmic streaming occurring after prolonged scanning (Movie 3). Because of this, it becomes necessary to ensure that imaging is done quickly and without excessive laser strength, and for individual windows to not see prolonged usage. Otherwise, there is a risk of experimental artefacts.

3.4: Imaging With Rhizoids

Rhizoids were another avenue through which detailed imaging of the vacuole and streaming endoplasm could be achieved, as in these cells, the highly-absorbent chloroplasts were typically absent or, when present, were sparsely dispersed. This eliminated the need for creating chloroplast-free windows, and reduced the possibility of associated experimental artefacts.

3.4.1: Classifying Rhizoids

Rhizoids are cells that grow laterally from the nodes, and have some similarities but some differences to internodes and branchlet cells in miniature. Their similarities include a large central vacuole that comprises the majority of the volume of the cell, a cylindrical / helical arrangement, and the presence organelles such as mitochondria, Golgi bodies, and extensive endoplasmic reticulum throughout the streaming endoplasm. Their differences, however, include the overall growth and cellular architecture. Unlike the branchlet and internodes that exhibit diffuse growth along their entire cell length, rhizoids elongate by tip growth, adding new cell volume solely at the tip (Hodick and Sievers, 1998). They also, characteristically, show a different cellular organization, and consist of a basal streaming region, a non-streaming sub-apical region containing the nucleus, and a tip-growing apical region containing the Spitzenkörper (Hodick and Sievers, 1998).

In this study, the *Nitella* cells growing in culture developed extensive rhizoids. These rhizoids showed a range of different growth patterns and structures, and were classified according to the following criteria. S-rhizoids were small (20 µm diameter) and had minimal chloroplasts (Figure 3.29A-B). M-rhizoids were slightly larger (30 µm diameter) and had sparse but noticeable chloroplast coverage (Figure 3.29C-D) while l- rhizoids were the largest (40 µm diameter) and had thorough chloroplast coverage (Figure 3.29E-F). The chloroplast coverage, even in the broadest l-rhizoid was not, however, as dense as found in internodal or branchlet cells, and the fluorescence from the rhizoid chloroplasts was distinctly patchy (Figure 3.29E, F, asterisk) rather than even as in internodes. Moreover, the diameter of even the largest L rhizoids was considerably narrower than even the smallest brachlet cells whose diameters were about 80 µm. These l-rhizoids also showed a characteristic and distinct anatomy where they joined adjacent cells (see below). Thus, l-rhizoids were a form of rhizoid rather than a modified internode or branchlet.

3.4.2 Imaging Dynamic Rhizoids

The lack of chloroplasts in rhizoids significantly improved the quality of imaging. Whereas the best imaging of $DIOC_6(3)$ in internodes was typically underwhelming (Figure 3.5), the entirety of $DIOC_6(3)$ labelled-rhizoids fluoresced brightly in (Figures 3.6, 3.7). Even neutral red imaging was enhanced (Figures 3.30, 3.31, 3.32), as it was along the neutral line in internodes.

Some limitations existed with rhizoid imaging. As with imaging through chloroplast-free windows, care needs to be taken when imaging s-rhizoids (and, to a lesser extent, m-rhizoids) as they lack the chloroplast layer to protect the endoplasm from photodamage. A breakdown of cytoplasmic architecture and dynamics began in s-rhizoids within several seconds of being imaged, even at low laser strength (Movie 4). To ensure the minimization of artefacts resulting from photodamage, it was necessary to image each rhizoid only once, and only for a maximum period of 10-15 seconds.

3.4.2.1 Streaming Endoplasm

The streaming endoplasm contained many small organelles that could be labelled with different fluorescent dyes. For example, the mitochondria could be seen stained as punctate structures flowing through the endoplasm when stained with $DIOC_6(3)$ (Figure 3.6A, asterisk) and the DNA-label Syto-13 (Figure 3.33A, caret). Other punctate structures included lipid droplets labelled by Nile red (Figure 3.34A, carets, Figure 3.35A, caret, Figure 3.36A, asterisk). Somewhat stationary tubules of endoplasmic reticulum near the cortical region of the cell were labelled with $DIOC_6(3)$. These tubules were not completely still, however, and would interact and change shape somewhat with the endoplasm (Figure 3.7A, arrow).

3.4.2.2 Tonoplast

In rhizoids, the tonoplast was a stained by a variety of dyes, including neutral red, MDY-64, Nile red, and $DIOC_6(3)$. The tonoplast was typically undulating as it flowed with streaming (Figure 3.30A, arrows, Figure 3.37, asterisk, Figure 3.6, caret), often bulging several micrometers into the vacuole. At times, however, the tonoplast would be highly infolded with a complex topography of tubules and membranes (Figure 3.38, arrows, Figure 3.39A, C, caret, arrow) (Movie 5). Other times, it would appear as a simple membrane, particularly under 63x imaging (Figure 3.37, asterisk, Figure 3.40, Figure 3.41, arrow), with numerous, often close membranes throughout the endoplasm.

3.4.2.3 The Central Vacuole and Vacuolar Inclusions

The central vacuole of rhizoids could be imaged with the far-red fluorescence of acridine orange which loaded into the vacuole as it is a weak acid. The vacuolar contents could be labelled with acridine orange, where it would fluoresce from the 650-700 nm (Figure 3.42B, Figure 3.43B). The second vacuolar stain used in internodal cells, Blue CMAC, was not used here.

The central vacuole was not, however, a uniform structure. Of particular note were strings of variously-sized and shaped vesicles that were inside and adjacent to the tonoplast (Figure 3.37, arrow, Figure 3.40A; C, arrows), and which seemed to be tethered by a small strand (Figure 3.41A, B, caret). These tethered complexes moved along with the tonoplast as it streamed. Other inclusions streaming freely in the interior of the vacuole were also present and as with the inclusions affixed to the tonoplast, were often formed of several small vesicles attached along a strand (Figures 3.32, 3.42, 3.44). In simultaneous staining with MDY-64 and neutral red, these inclusions would fluoresce internally across neutral red's yellow-orange emission wavelength of 570-620 nm (Figure 3.32B, arrow), while the surrounding membranes fluoresces in MDY-64's blue-teal 465-515 nm emission wavelength (Figure 3.32A, arrow). These inclusions could also be stained with acridine orange (Figure 3.44A, arrows). Not all of the elements in the vacuole took on this stringy nature. Sometimes, they would maintain a rigid shape as they flowed through the vacuole (Figure 3.31A, caret). Other times, they would appear as thin, bunched, clusters of material with a distinctive angular arrangement, which could be seen particularly well with MDY-64 under 63x magnification (Figure 3.37A, caret). These elements were more common near the upper region of the vacuole (Figure 3.45, arrow).

Wound plug membranes were noticeable and stained by neutral red, MDY-64, Nile red, and acridine orange (Figure 3.46A, B, caret, Figure 3.36A, arrow, Figure 3.44A, asterisk). When neutral red and MDY-64 were used concurrently, the membranes were stained better in neutral red. As this occurred in a rhizoid with limited chloroplast coverage, this could indicate that the neutral red is somehow excluding the staining of the MDY-64.

3.4.2.4 Acridine Orange

The dye acridine orange shows complex localization and fluorescence patterns. As a DNA stain, it localizes nuclei (McMaster and Carmichael, 1977), although unlike Syto-13, it is not sensitive enough to reveal the localization of mitochondria. Acridine orange also accumulates into the

central vacuole and other acidic organelles as a weak acid, and its fluorescence has pH-dependent spectral properties (Zoccarato et al., 1999). Using 488 nm excitation, it has two distinct emission peaks, one of which peaks at 500 nm (teal fluorescence) and extends to 550 nm (yellow-green) and a second peak at or 650-700 nm (orange-red to red) (Figure 3.42B, Figure 3.41B).

This meant that the neutral endoplasm had green-yellow fluorescence, as did the interior of some vacuolar inclusions (Figure 3.42A, arrow) while red emission came from the interior of the vacuole (Figure 3.42B). Areas which fluoresced one colour appeared as dark regions in the other parts of the emission spectrum. Interestingly, the vacuolar inclusions did not all behave the same way. For example, the surface of one of a pair of vacuolar inclusions fluoresced green, although its interior did not (Figure 3.42A, left caret) while the interior of the inclusion next to it fluoresced green, similar to the endoplasm (Figure 3.42, right caret), and appeared as a dark region in red emission channel (Figure 3.42B, caret). The former inclusion does not appear in the red emission, indicating that it is either fluorescing similarly to its surroundings or drowned out by the vacuolar fluorescence. This indicates that the various internal compartments within the vacuole have differing topographies in terms of pH.

This effect could also be seen when imaging the sub-apical region of a tip-growing rhizoid (Figure 3.43). Excitation with 488 nm produced the same two strong emission band from 500-550 nm (green) and 650-700 nm (far-red). The nucleolus (Figure 3.43A, N) showed bright teal-green fluorescence, and the nuclear compartment around it (Figure 3.43A, caret) fluoresced mildly, as well as numerous other compartments around them, which contrasted with distinct dark regions (Figure 3.43A, arrows). In the far-red, however, these dark regions were the brightest, with an extensive compartment with mild deep red fluorescence (Figure 3.43B, arrow) containing numerous smaller, bright vesicles (Figure 3.43B, caret). Some mild far-red fluorescence also came from the nucleolus (Figure 3.43B, N).

3.4.2.5 Rhizoid Greening and Tip Divisions

One of the developmental abnormalities noted during this study was rhizoid greening. In the literature, rhizoids are frequently described as colorless cells functioning in affixing the thallus to the substrate and functioning in gravitropic sensing (Ackers et al., 2000). However, when exposed to light, rhizoids begin “greening”, increasing in size and becoming increasingly covered in chloroplasts (Figure 3.29). These differences in rhizoid structure lead to their description as s-, m- and l-rhizoids, with the chloroplasts being most common and developed

in the l-rhizoids These chloroplasts would sometimes cause fluorescence to bleed through into imaging wavelengths (Figure 3.7A, caret) when present, but the sparse coverage of the chloroplasts and their known location within the cell prevented them from confounding imaging.

Another developmental abnormality noted was internode-like lateral tip divisions (Figure 3.47). In this instance, the rhizoid tip had developed into three segments (Figure 3.47A, carets) ~25-40 µm long and 40 µm thick. These segments were filled with numerous membrane-bound compartments of various sizes that stained with MDY-64 (Figure 3.47A, arrows). They had minimal autofluorescence in the 650-700 nm range, indicating a lack of chloroplasts (Figure 3.47B). At the very tip of the third segment, a region of bright staining 5 µm across appeared (asterisk), which had a 7 µm "tail" extending out of it and a pair of small, particularly brightly stained spots.

3.4.2.6 Abnormal Rhizoid Nuclei

Several rhizoids exhibited other abnormalities associated with the nucleus. Normally, rhizoids have a 23-28 µm diameter nucleus with a 14-16 µm diameter nucleolus situated in a sub-apical region near the tip of the cell that lacks streaming and contains an extensive network of surrounding compartments (Figure 3.48, caret, arrow, Figure 3.43, caret, N). On occasion, rhizoids terminating in simple curves were observed (Figure 3.46, arrows), suggesting that normal tip organization had broken down and that tip growth had ceased. On another occasion, an s-rhizoid with an apparent nucleus located away from the subapical zone (Movie 6) (Figure 3.38) but a diminished network of surrounding membranes (carets) and streaming moving past it (arrows) was observed.

L rhizoids contained nuclei flowing throughout the endoplasm just like an internodal cell. These nuclei were 15-18 µm long, 8.5 µm wide, and 3-5 µm thick, which corresponds to nuclei size in internodal cells. They could be negatively stained with Nile red (Figure 3.34A, arrows), and positively labelled with the DNA-staining dyes acridine orange (Figure 3.44A, carets) and Syto-13 (Figure 3.33A, B, arrows). They would on occasion appear attached to one another (Figure 3.33B, arrow), or flowing independently (Figure 3.33A, arrows). These junctions were likely nucleus amitosis, and are typical of a young dividing internode cell. They also imaged with neutral red similarly to internodal cells (Figure 3.49A, arrow) (Figure 3.17A, caret), and had a similarly thorough level of chloroplast coverage (Figure 3.49B, C, arrow), although the

chloroplasts were larger and rod shaped (up to 18 µm long), unlike the smaller (~10 µm long), coffee bean shape characteristic of internodes (Figure 3.25).

3.4.2.7 Rhizoid Junction Cells

Rhizoids form junctions that have the appearance of a pair of hands clasping. However, at such junction points, two or three roughly spherical, 40-70 µm diameter "junction cells" were sometimes seen (Figures 3.35, 3.50, 3.51). Each appeared to contain a single nucleus. These nuclei could be negatively stained with Nile red (Figure 3.35A, arrow) (Figure 3.51A, arrow), and positively with Syto-13 (Figure 3.50A, arrows). The nuclei were 20-25 µm in diameter with a 15 µm diameter nucleolus, which corresponds in size with nuclei normally seen in tip-growing rhizoids (Figures 3.48, 3.43). These cells had discernible boundaries from the rhizoids and were not simple extensions (Figure 3.50A, C, caret) (Figure 3.51C, arrow).

3.5 Plasmolysis

Plasmolysis was initially induced in *Nitella* accidentally, through contamination of the water-based mounting medium with glycerol used for the immersion lens on the inverted microscope when the lens was moved too close to the edge of the coverslip. Subsequent and deliberate experiments confirmed that this was a reliable approach to generating plasmolysis in *Nitella* internodes and rhizoids.

Experiments with plasmolysis revealed the existence of Hechtian strand, thin connections that link the retreating cytoplasm to the cell wall. This shrinking of the cytoplasm takes the chloroplast layer with it (Figure 3.52B, arrow). Hechtian strands were seen in both internodes with the tonoplast stain MDY-64 (Figure 3.53, arrows) and in rhizoids with neutral red (Figure 3.52A,C, arrows). These strands were from several to more than ten micrometres in length, but were very ephemeral, breaking down within 10 to 20 seconds. Thus, they required rapid imaging after plasmolysis in order to be seen.

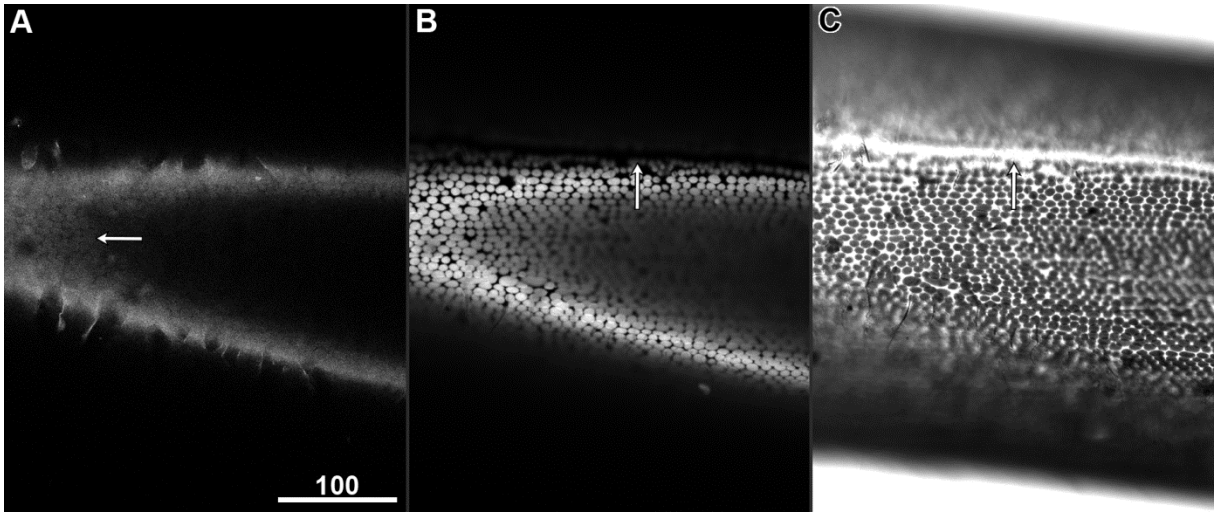

Figure 3.1. Unstained control image of an internodal cell focused at the chloroplast layer. The neutral line is clearly visible. 458+633 nm excitation. Scale bar = 100 µm.

A. 470-520 nm emission. In addition to problems caused by laser absorption and shadowing, chloroplast autofluorescence would also frequently bleed into images at shorter wavelengths (arrow), obscuring other features of the cell.

B. 650-700 nm emission. Chloroplast autofluorescence.

C. Transmitted light, demonstrating the strong absorption of the blue (456 nm) and red (631 nm) lasers, as indicated by the much darker chloroplasts flanking the neutral line (arrow). Unless the 561 nm laser is included in the excitation wavelengths, penetrating into the interior of the cell was difficult.

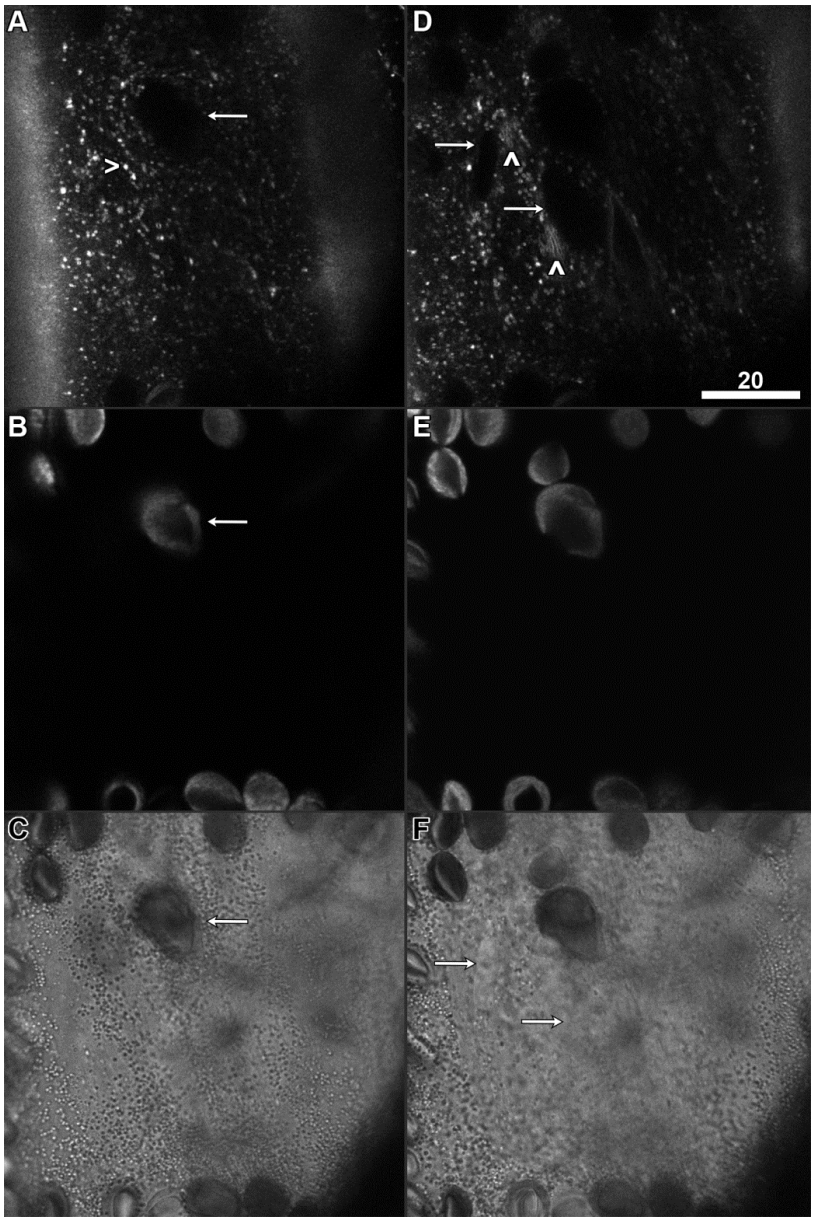

Figure 3.2. MDY-64 imaging of an internode through a chloroplast window, focused on a plane at the upper (A-C) and lower (D-F) endoplasm. Imaging was similar to that of MDY-64 when successful in internodes, with numerous punctate structures and dark disks. Scale bar = 20 µm.

A. MDY-64 (10 µM, 30 min) fluorescence from 470-520 nm. Numerous punctate structures (caret) were especially prominent in the upper regions of the endoplasm. Chloroplasts created clear shadows (arrow).

B. 650-700 nm emission. Chloroplast autofluorescence, with the chloroplast casting the shadow in A labelled (arrow).

C. Transmitted light, with the chloroplast casting the shadow in A labelled (arrow).

D. MDY-64 (10 µM, 30 min) fluorescence from 470-520 nm. Deeper into the endoplasm, dark disks (arrows) and unknown organelles (carets) were present.

E. 650-700 nm emission. Chloroplast autofluorescence.

F. Transmitted light, with the disks labelled (arrows).

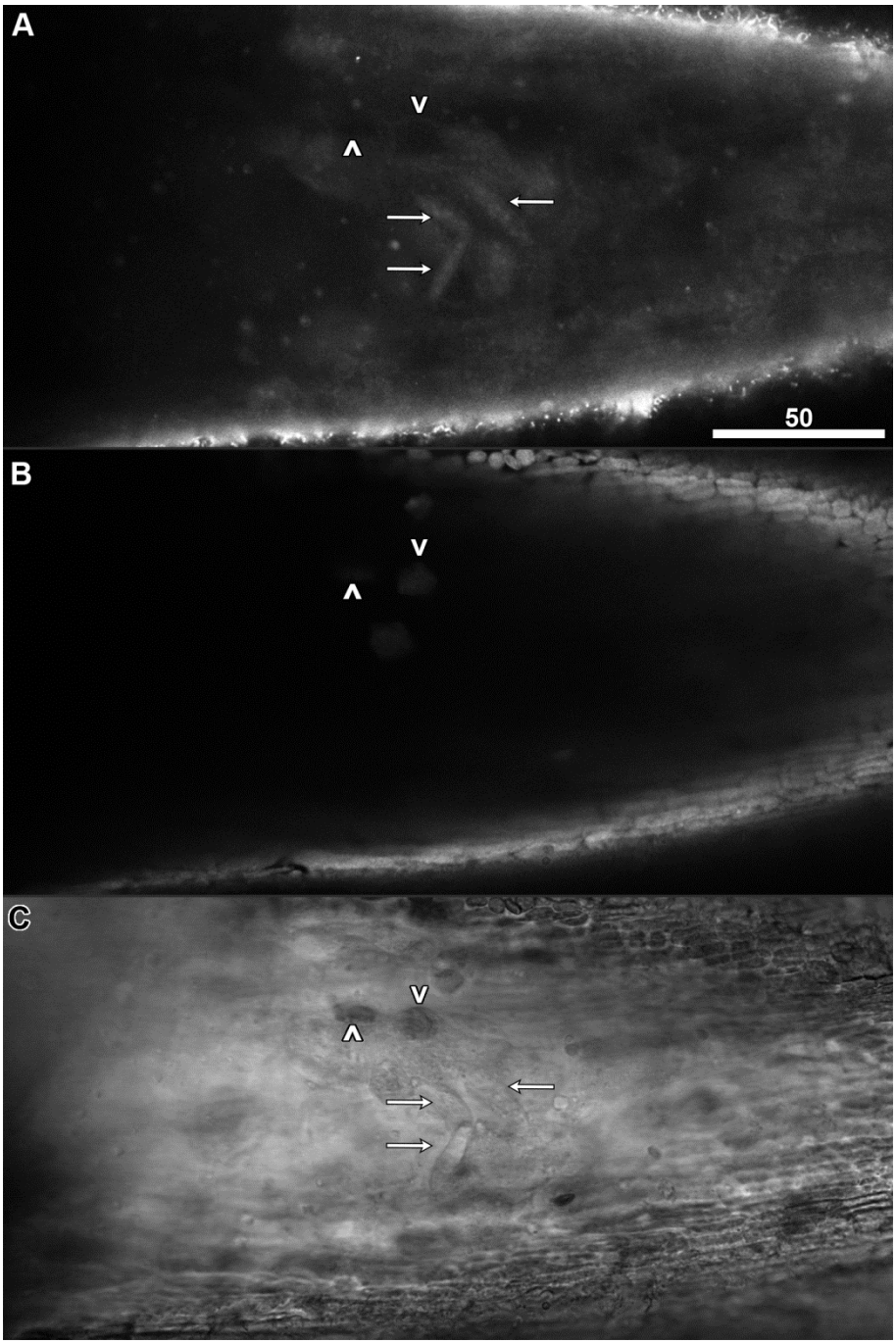

Figure 3.3. Acridine orange staining of an internodal cell focused on a plane near the lower endoplasm. 514+633 nm excitation. Scale bar = 50 µm.

A. Acridine orange fluorescence (20 µM, 6 h) from 525-575 nm. Disks were stained suggesting that they are nuclei (arrows). Chloroplast shadows are marked (carets).

B. 650-700 nm emission. Chloroplasts stream throughout the endoplasm (carets), casting shadows marked (carets in A).

C. Transmitted light.

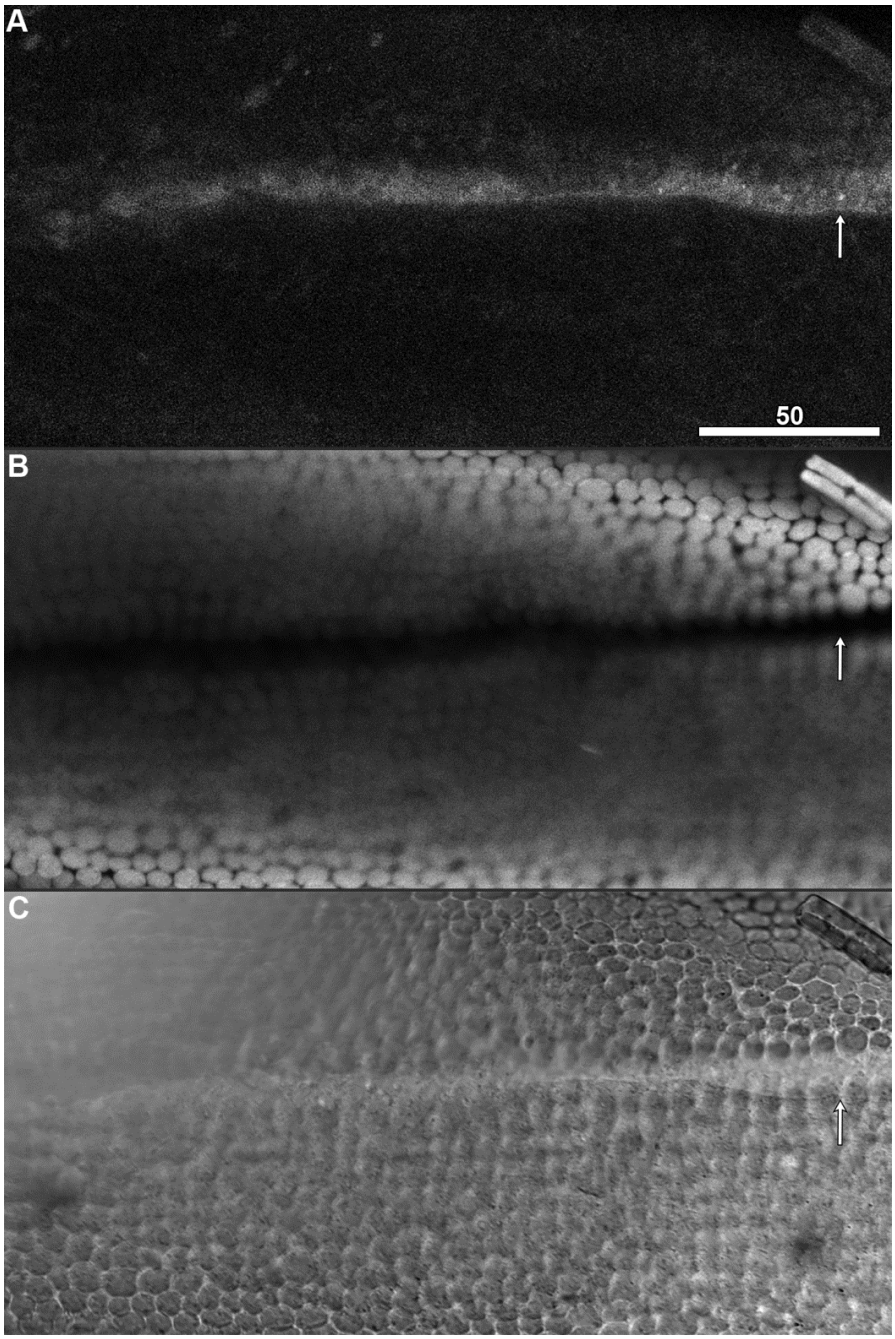

Figure 3.4. Neutral red imaging of the endoplasm and vacuole beneath the neutral line of an internodal cell. 561+633 nm excitation. Scale bar = 50 µm.

A. Neutral red (10 µM, 10 min) fluorescence from 550-600 nm. The fluorescence visible in the neutral line (arrow) demonstrated how chloroplasts block excitation of dyes further inside the cell regardless of the wavelength used. Some brightly-stained punctate organelles were visible in the neutral line (arrow).

B. 650-700 nm emission. Chloroplast autofluorescence, showing the gap in chloroplasts along the neutral line that coincides with the increased brightness in A.

C. Transmitted light.

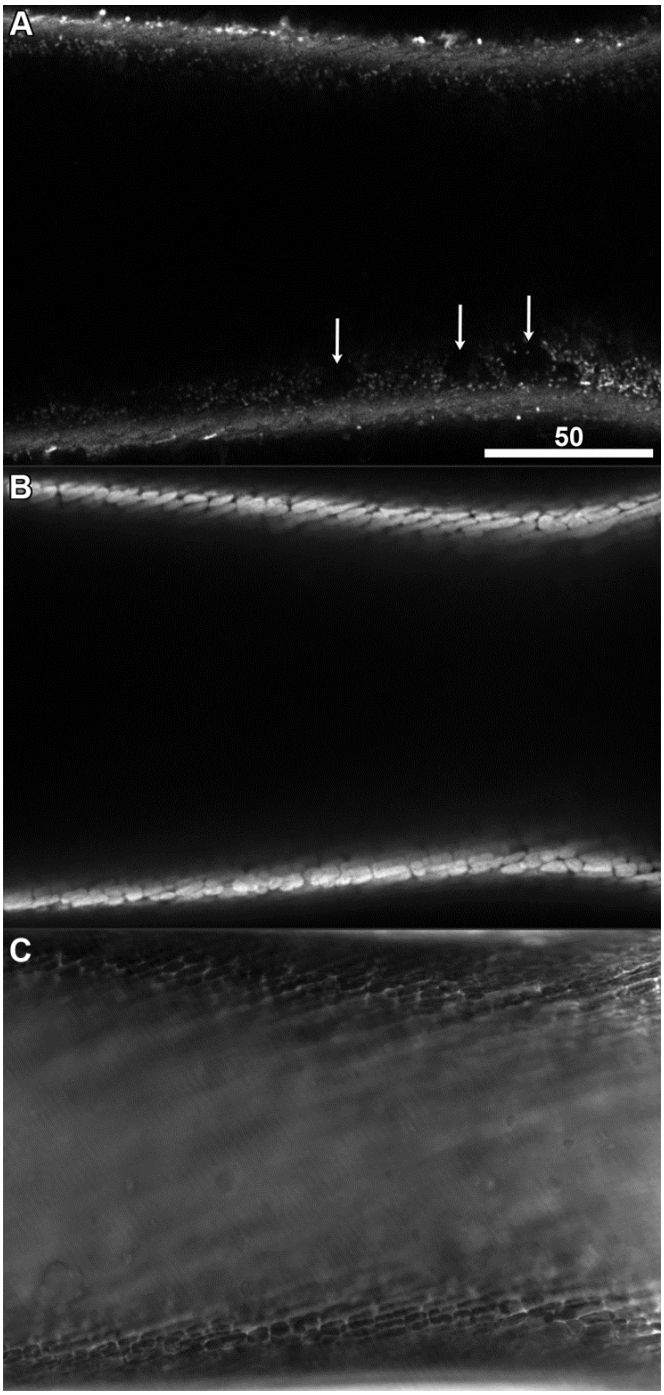

Figure 3.5. $DIOC_6(3)$ imaging of an internodal cell showing a cross section through the vacuole. 488+633 nm excitation. Scale bar = 50 µm.

A. $DIOC_6(3)$ (10 µM, 20 min) fluorescence from 500-550 nm. The numerous punctate mitochondria form an outline around dark disks, probably nuclei (arrows).

B. 650-700 nm emission. Chloroplast autofluorescence.

C. Transmitted light.

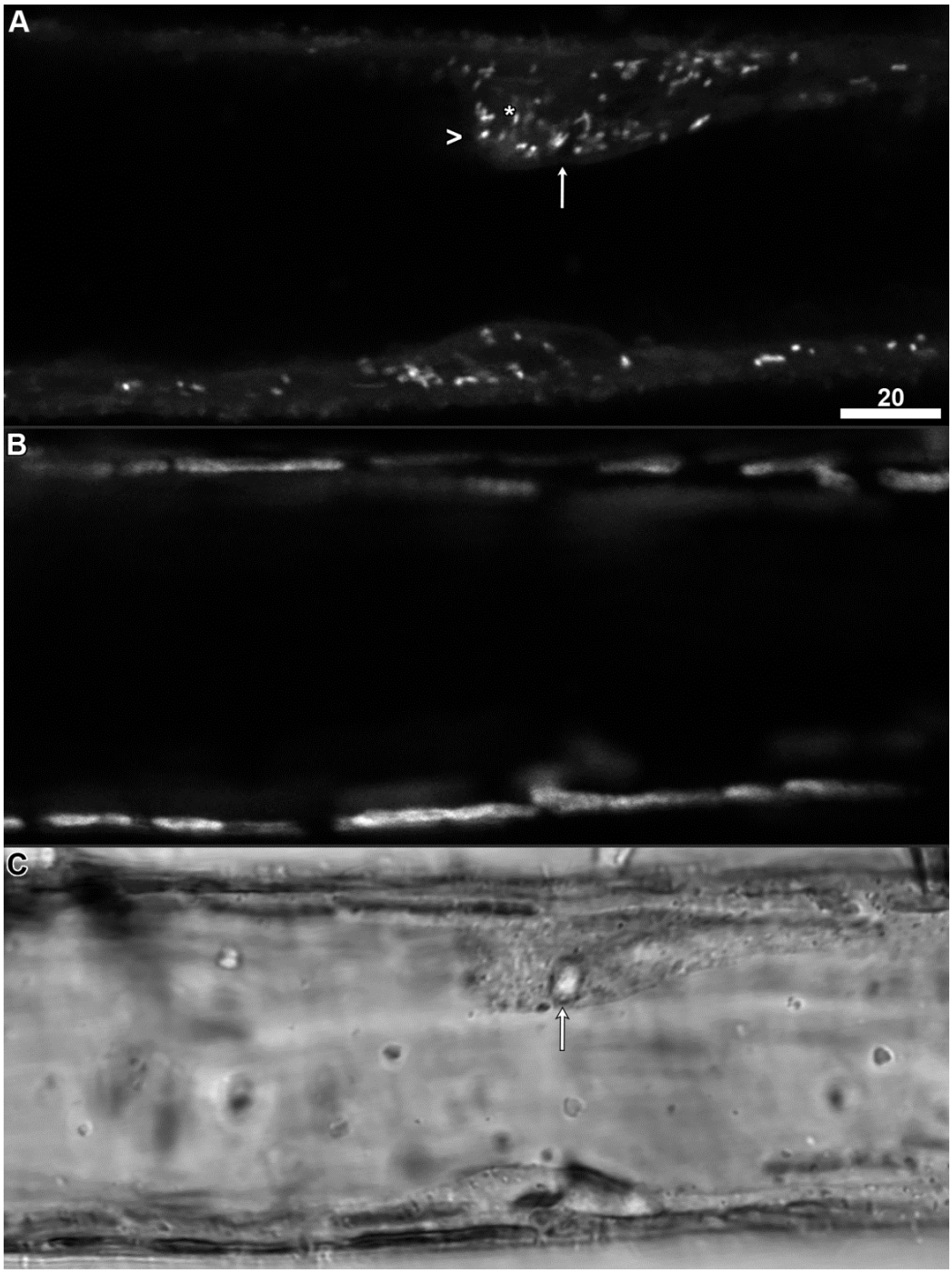

Figure 3.6. $DIOC_6(3)$ imaging of an l-rhizoid focused through the middle of the vacuole. 488+633 nm excitation. Scale bar = 20 µm.

A. $DIOC_6(3)$ (10 µM, 20 min) fluorescence from 500-550 nm. $DIOC_6(3)$ labels the mitochondria (caret) but did not stain wound plug cores (arrow).

B. 650-700 nm emission. Chloroplast autofluorescence.

C. Transmitted light. Note the wound plug core inside of the endoplasm (arrow).

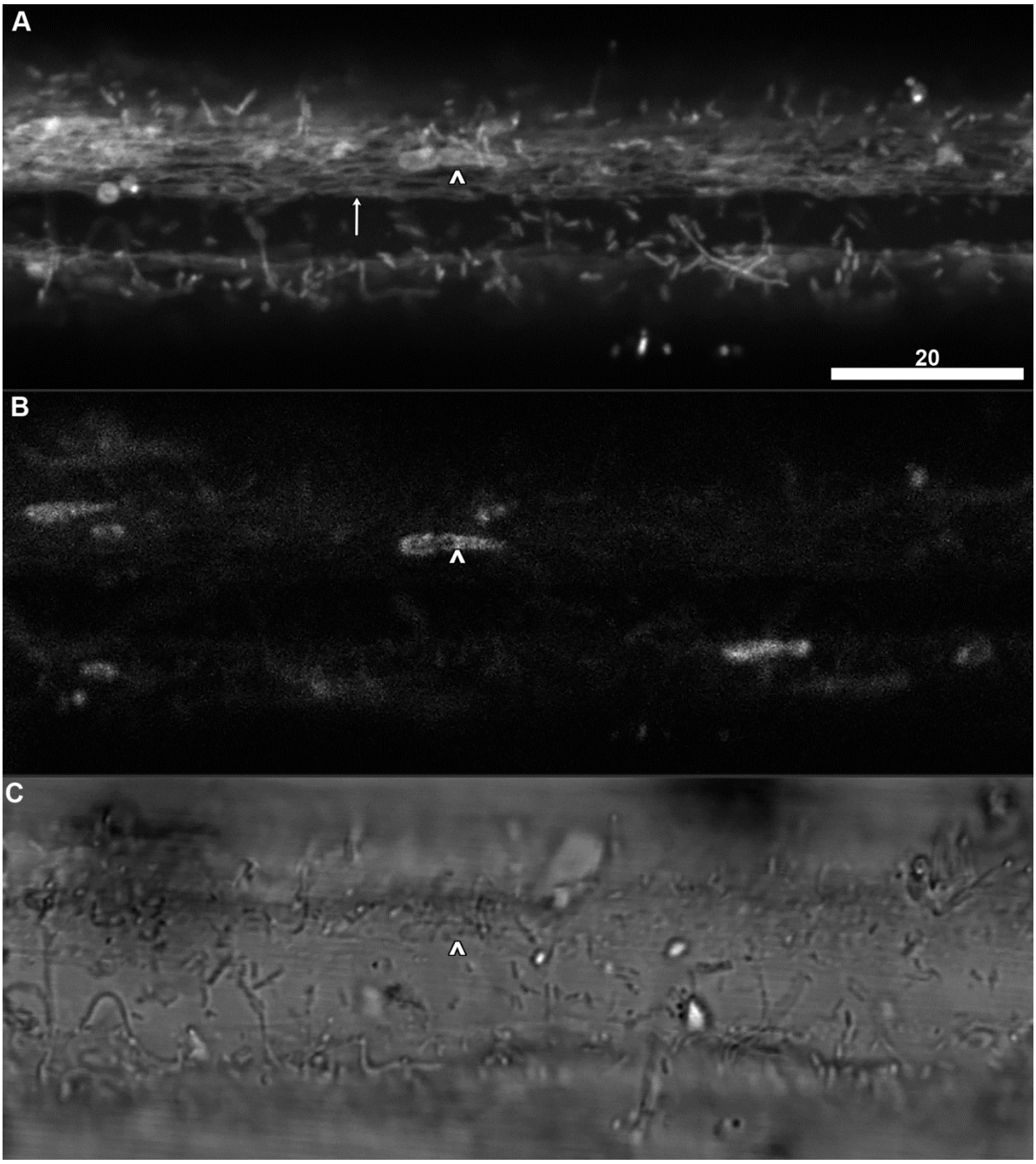

Figure 3.7. $DIOC_6(3)$ imaging of an m-rhizoid focussed in the cortical region. A stationary network of tubules was located above the streaming endoplasm. Scale bar = 20 µm.

A. $DIOC_6(3)$ (10 µM, 20 min) fluorescence from 500-550 nm. Thin, stationary tubules (arrow) sat near the chloroplast layer (caret).

B. 650-700 nm emission. Chloroplast autofluorescence, with a chloroplast labelled (caret).

C. Transmitted light. A chloroplast is labelled (caret).

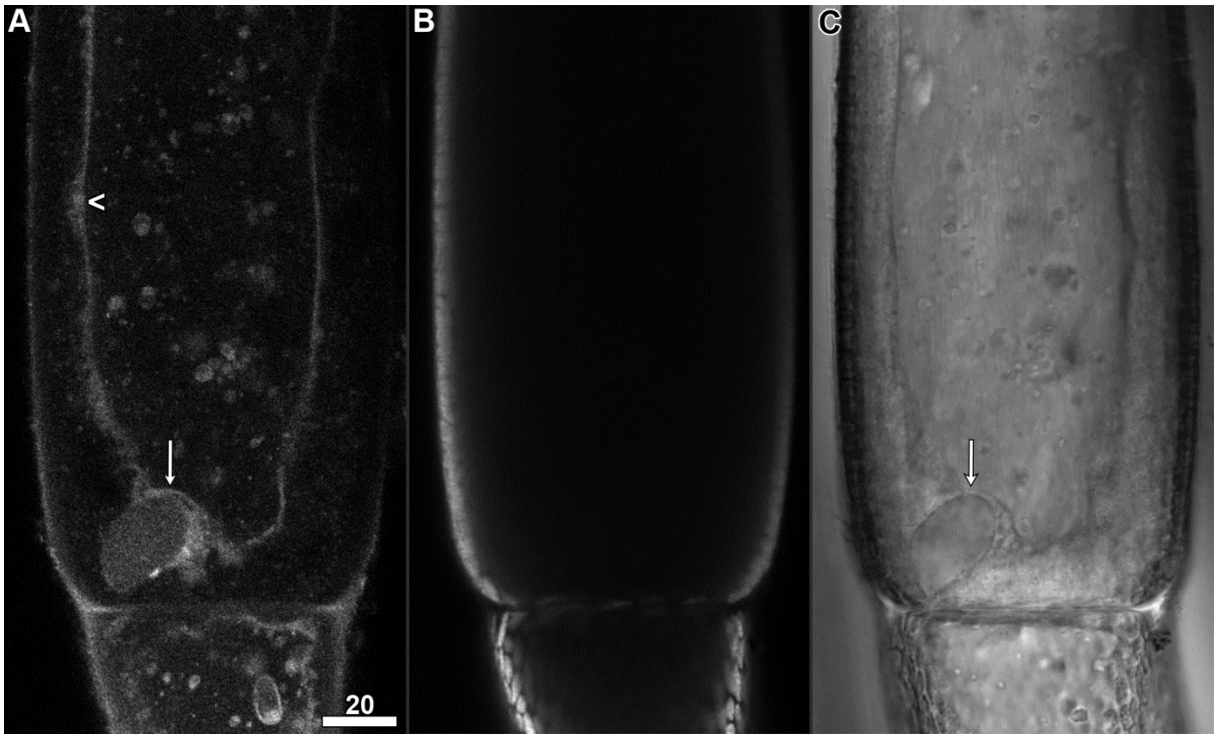

Figure 3.8. The boundary between a primary and secondary branchlet cell stained with neutral red, showing a cross-section mid-way through the vacuole. 561+633 nm excitation. Scale bar = 20 µm.

A. Neutral red (10 µM, 10 min) fluorescence from 550-600 nm. The tonoplast is clearly labeled. Numerous convoluted regions were present near the tonoplast (caret). A large, membrane-bound structure in the endoplasm (arrow) appeared to be filled with neutral red.

B. 650-700 nm emission. Chloroplast autofluorescence.

C. Transmitted light. The arrow indicates the same large, membrane-bound structure in the endoplasm that was visible by neutral red fluorescence.

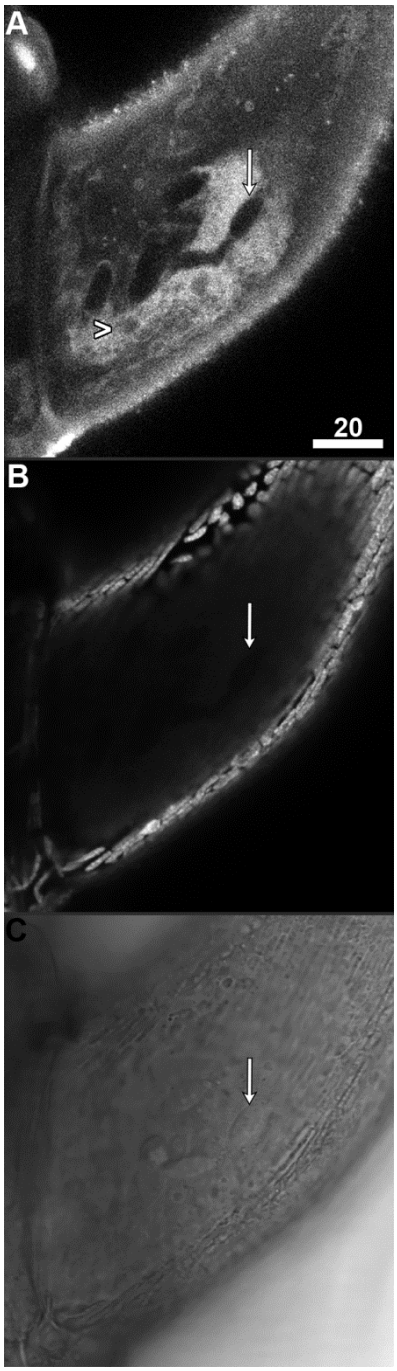

Figure 3.9. Neutral red staining of the boundary between an internodal and branchlet cell, showing the highly-differential staining of the tonoplast. 561+633 nm excitation. Scale bar = 20 µm.

A. Neutral red (10 µM, 10 min) fluorescence from 550-600 nm. The tonoplast appeared to be a dynamic mesh of tubes and layers (bottom arrow). Dark disks devoid of fluorescence streamed in the endoplasm (top arrow).

B. 650-700 nm emission. Chloroplast autofluorescence.

C. Transmitted light. Despite lacking fluorescence in A, the disks can be seen as concrete objects here (arrow) contained within compartments that exclude dye.

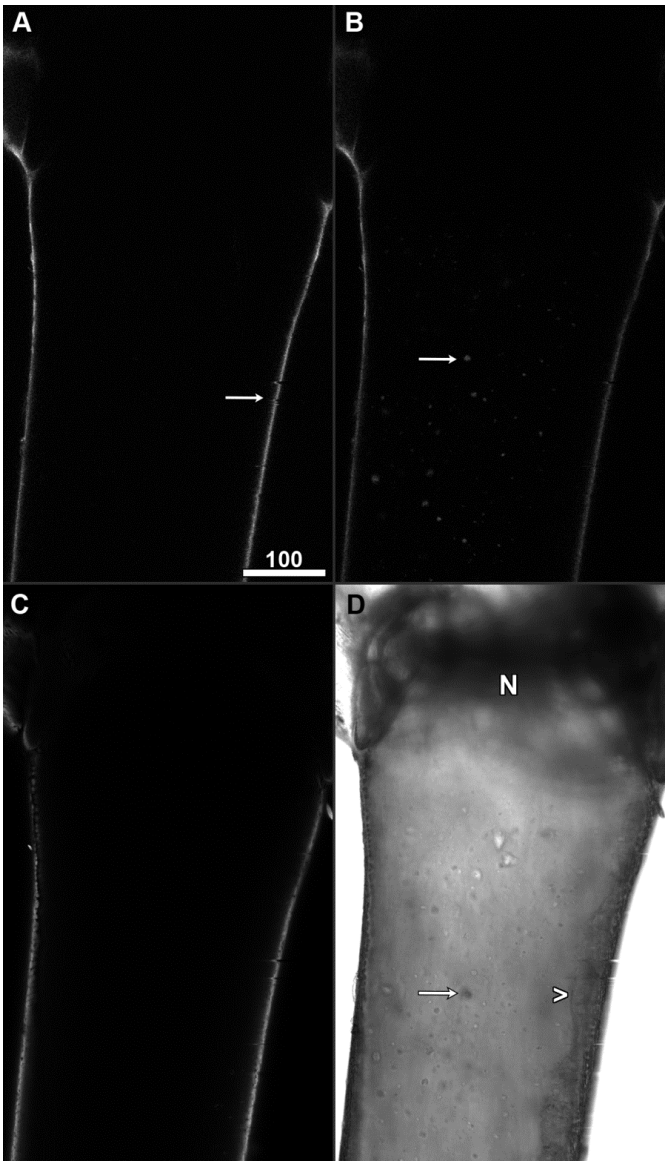

Figure 3.10. Unstained control image of an internodal cell near the nodal junction, focused mid-way through the cell, showing autofluorescence from multiple excitation wavelengths. 405+561+633 nm excitation. Scale = 100 µm.

A. 415-465 nm emission. 405 nm excitation generates little autofluorescence, although the inability of the laser to penetrate well into the cell contributes to this. However, the line of chloroplasts (arrow) fluoresce regardless of excitation or emission parameters.

B. 570-620 nm emission. 561 nm excitation generates more autofluorescence than the other lasers due to its ability to penetrate the chloroplast layer. The wound plug cores (arrow) are the only other significant source of autofluorescence within the cell.

C. 650-700 nm emission. Chloroplasts fluoresce strongest in the 650-700 nm range.

D. Transmitted light. The tonoplast is highly dynamic, showing significant waves and bulges (caret). The arrow shows a visible wound plug core, translucent specks that can be seen ubiquitously distributed throughout the vacuole and endoplasm. The node junction is marked (N).

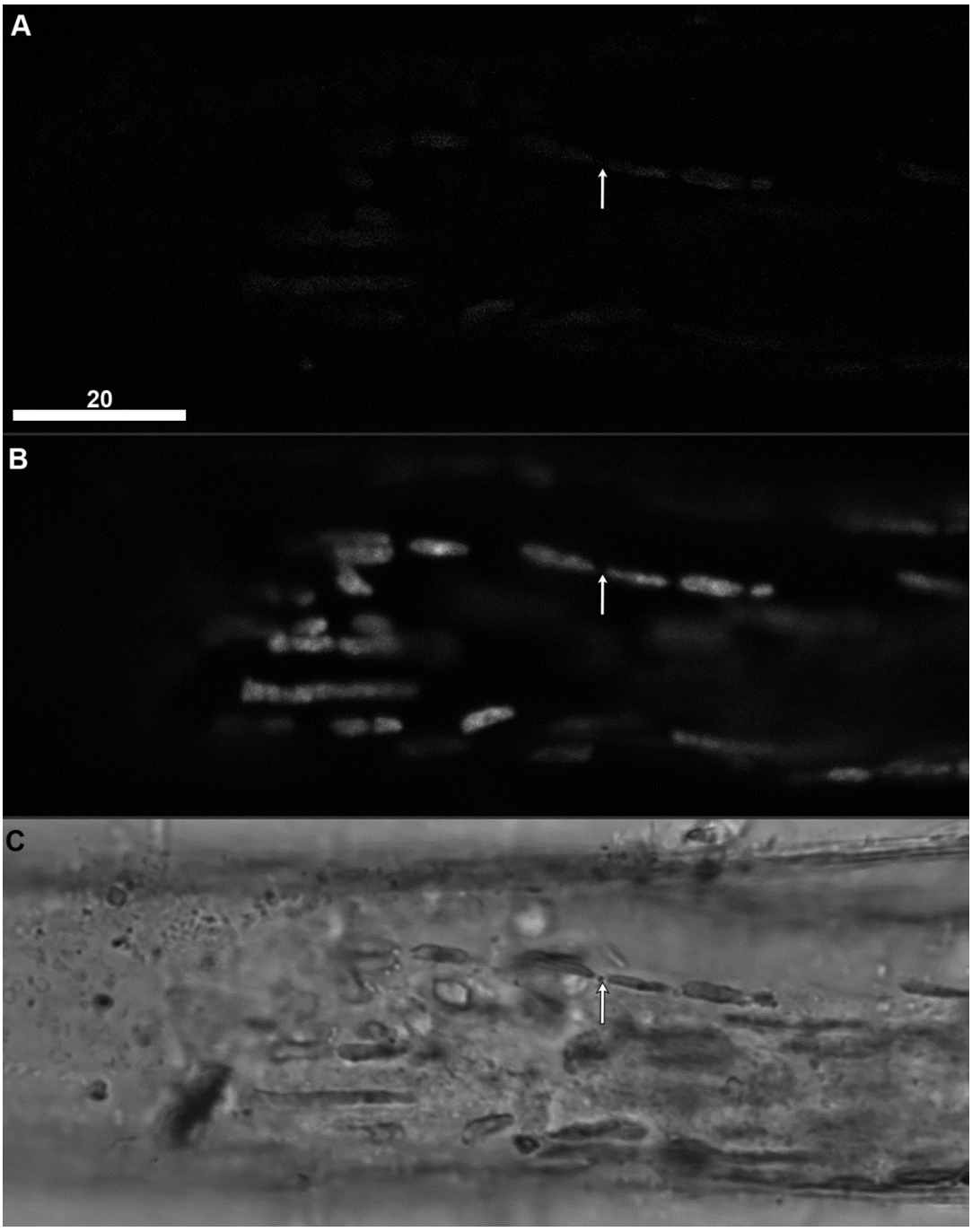

Figure 3.11. Unstained image of an m-rhizoid focused near the periphery of the cell. The m-rhizoids contained sparse chloroplasts that were unusually shaped and still undergoing division. 488+633 nm excitation. Scale bar = 20 µm.

A. 500-550 nm emission. Some chloroplast autofluorescence was present (arrow).

B. 650-700 nm emission. Chloroplast autofluorescence. Some chloroplasts showed clear cleavage points, suggestive of organelle division (arrow).

C. Transmitted light. A chloroplast cleavage point is indicated (arrow).

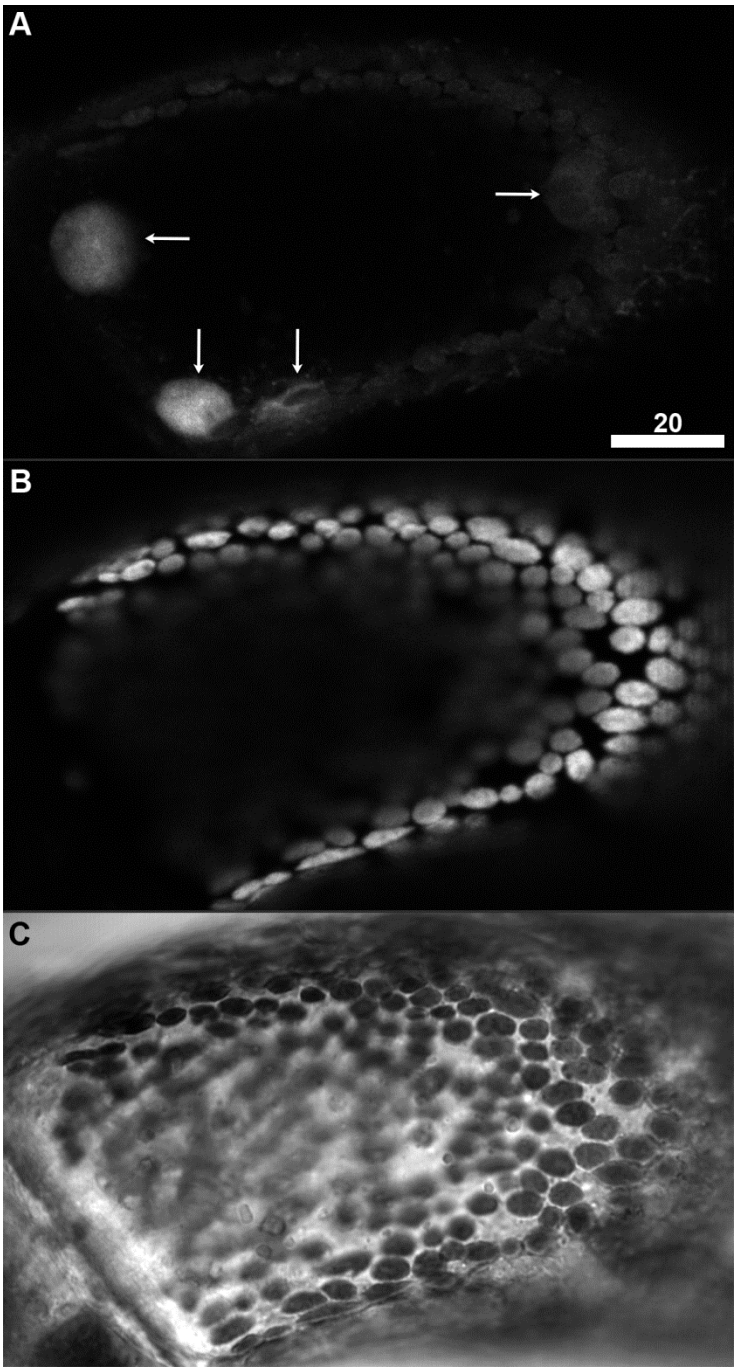

Figure 3.12. Syto-13 imaging of a small secondary branchlet cell, focused on a plane in the endoplasm. 488+633 nm excitation. Scale bar = 20 µm.

A. Syto-13 fluorescence (5 µM, 30 min) from 500-550 nm. Nuclei (arrows) stream around the endoplasm. Some bleed-through from the chloroplasts is present.

B. 650-700 nm emission. Chloroplast autofluorescence.

C. Transmitted light.

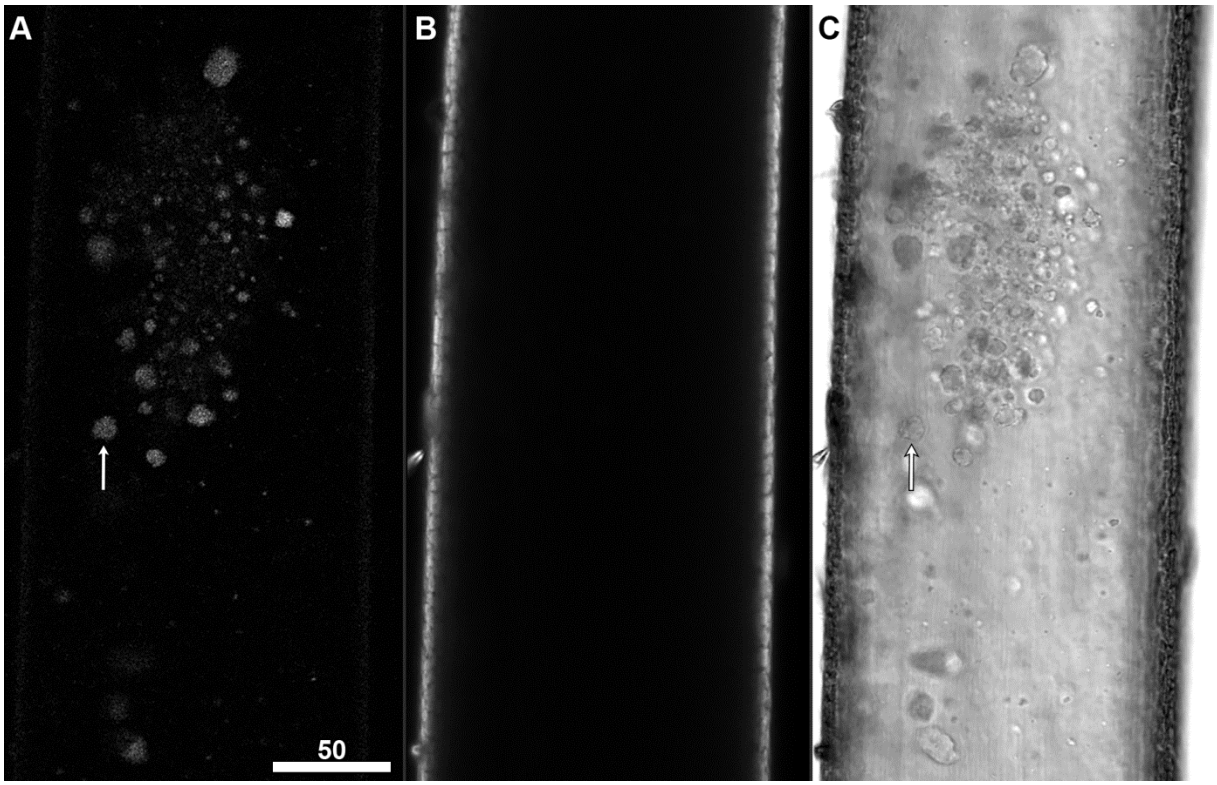

Figure 3.13. Unstained control image of a branchlet cell imaged through the middle of the vacuole. The cell contains a vacuolar mat. These mats would typically display little movement within the cell, but could slowly migrate along the cells length. 561+633 nm excitation. Scale bar = 50 µm.

A. 570-620 nm emission. The vacuolar mats include aggregates of wound plugs whose appearance and autofluorescence were similar to isolated wound plugs (arrow).

B. 650-700 nm emission. Chloroplast autofluorescence.

C. Transmitted light. Many wound plugs were visible, some of which were in the plane of the fluorescence image, and some which were not. The fluorescent wound plug is indicated (arrow).

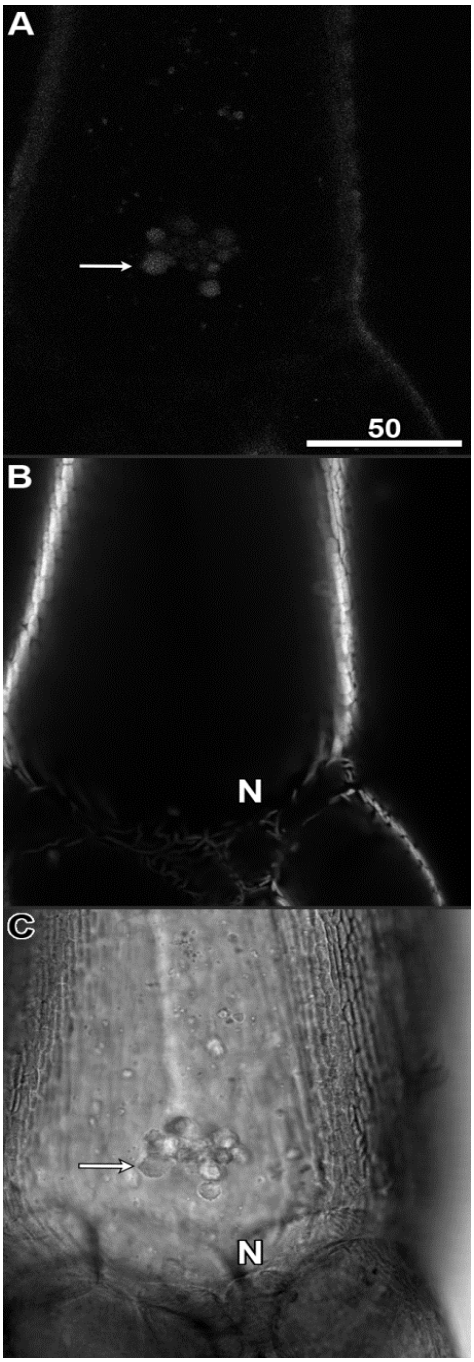

Figure 3.14. Unstained control image of an intermodal cell near the nodal junction focused mid-way through the vacuole, and showing a vacuolar gyre. Unlike vacuolar mats, gyres were generally smaller and could freely rotate along all three axes. 561+633 nm excitation. Scale bar = 50 µm.

A. 570-620 nm emission. The vacuolar gyres had a similar composition to the mats, being composed of a smaller cluster of wound plugs (arrow).

B. 650-700 nm emission. Chloroplast autofluorescence, clearly showing the boundaries between the internodal cell and the multiple, smaller nodal cells (N).

C. Transmitted light. The arrow shows the fluorescent object indicated in panel A. The node junction (N).

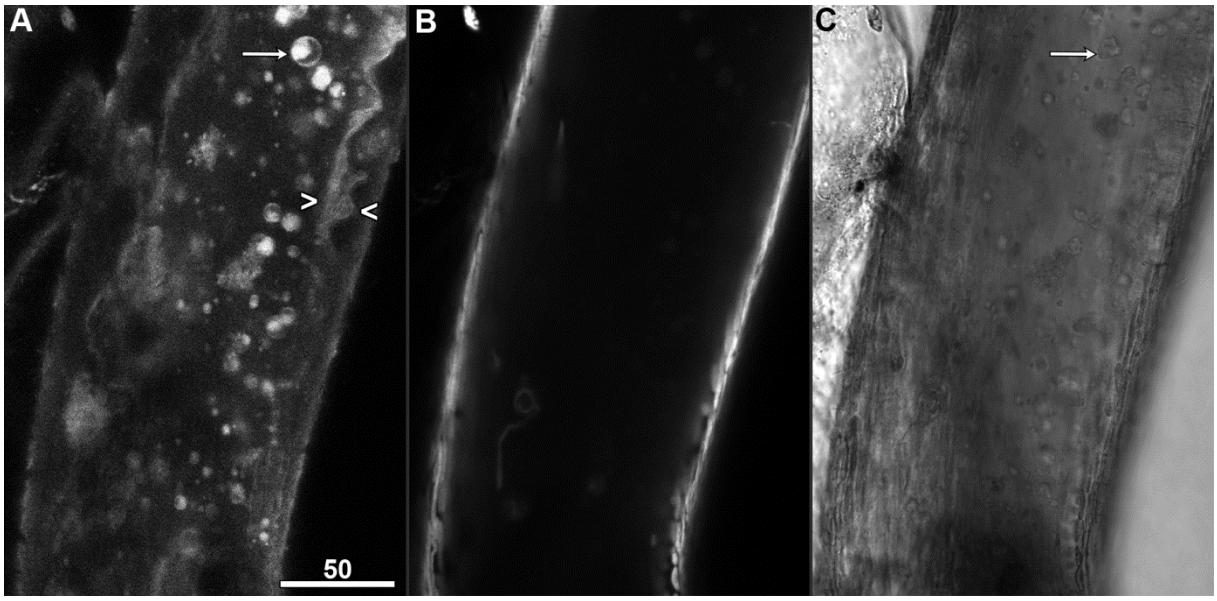

Figure 3.15. Neutral red imaging of a mature primary branchlet cell, showing a cross section through the vacuole. An extensive, undulating network of tubes and membranes was present, as were numerous wound plugs. 561+633 nm excitation. Scale bar = 50 µm.

A. Neutral red (10 µM, 10 min) fluorescence from 550-600 nm. A network of membranes was present (carets) near the tonoplast. Wound plugs and their surrounding membranes fluoresced strongly with neutral red (arrow), even well into the vacuole.

B. 650-700 nm emission. Chloroplast autofluorescence.

C. Transmitted light, with an arrow pointing to the wound plug core from A.

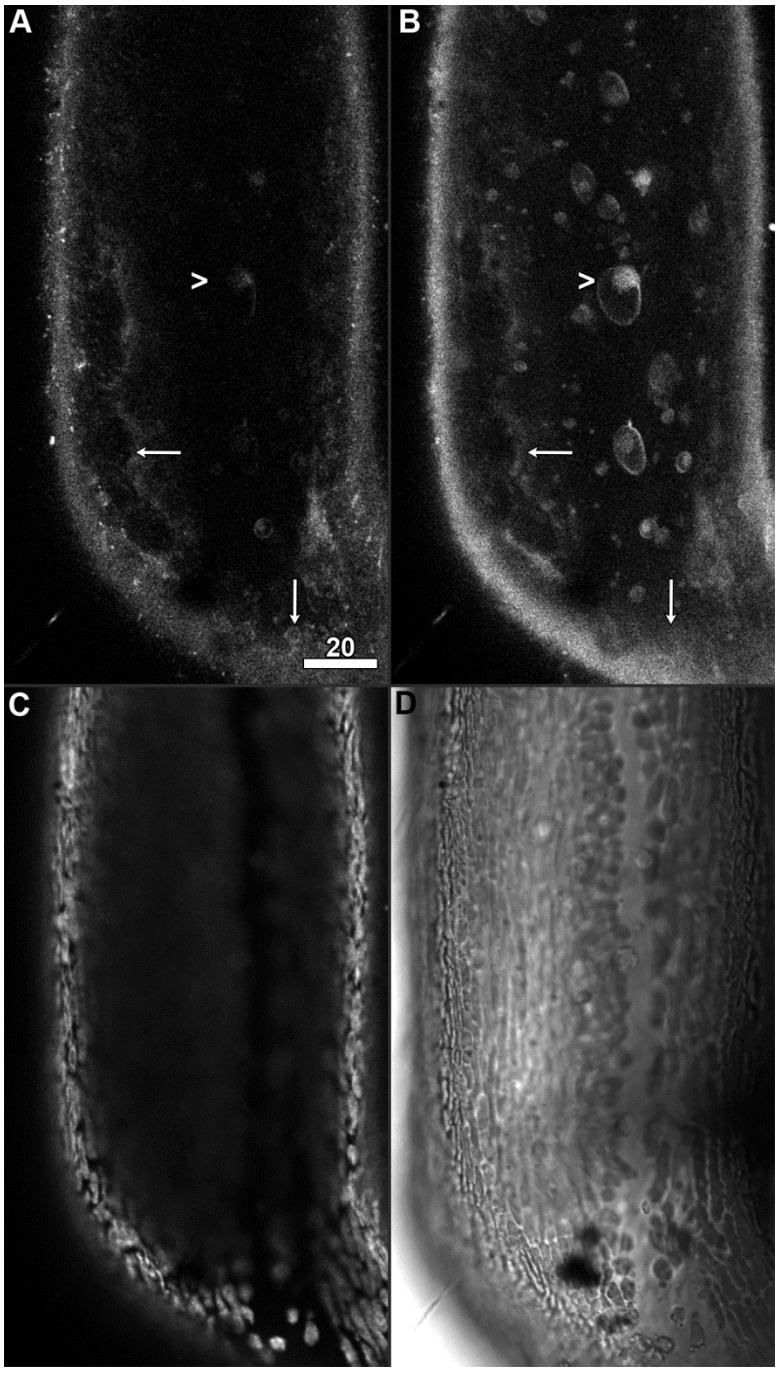

Figure 3.16. A branchlet cell stained with both MDY-64 and neutral red highlighting the differences in staining between the two dyes.

A. MDY-64 (10 µM, 30 min) fluorescence from 470-520 nm. MDY-64 provided sharper imaging of cellular structure than neutral red (arrow), but failed to image objects deeper into the cell, such as vacuolar wound plugs (caret).

B. Neutral red (10 µM, 10 min) fluorescence from 550-600 nm. Neutral red gave hazier staining (arrow), but provided superior penetration into the cell, as evidenced by wound plug imaging (caret).

C. 650-700 nm emission. Chloroplast autofluorescence.

D. Transmitted light.

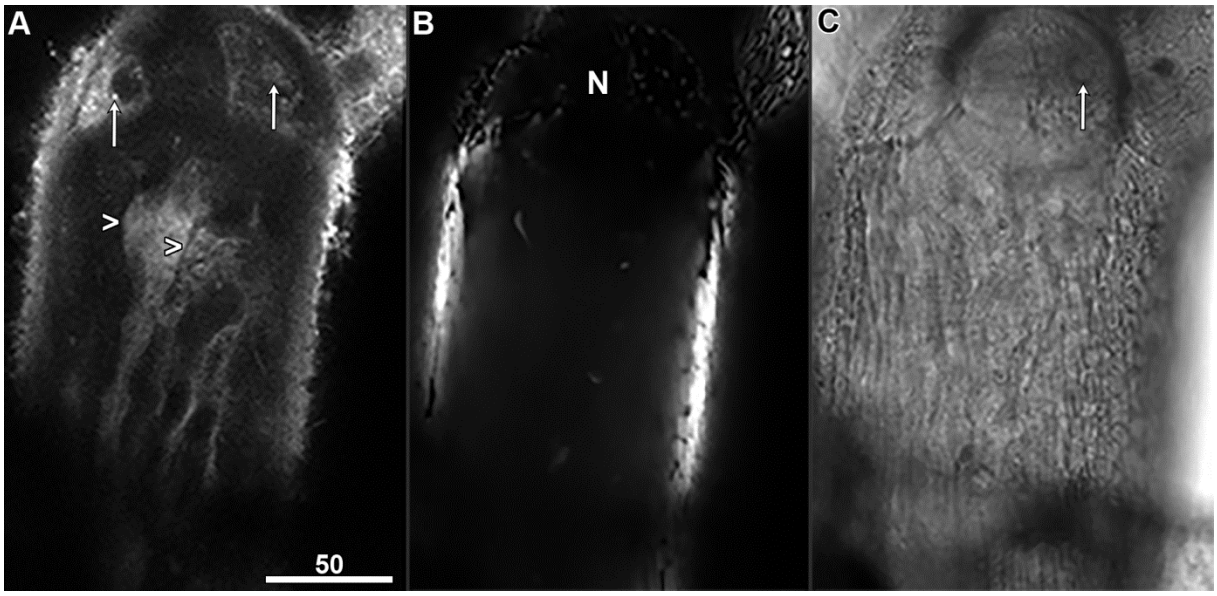

Figure 3.17. Neutral red staining of an internodal cell near the nodal junction focused on the internode's tonoplast . 561+633 nm excitation. Scale bar = 50 µm.

A. Neutral red(10 µM, 10 min) fluorescence from 550-600 nm. The tonoplast appeared to comprise an intricate network of layers and tubes with distinct boundaries (carets). Bright punctate structures were present in the left nodal cell, which features a large dark circle with no fluorescence (left arrow). The right node had a conspicuous circular structure stained (right arrow).

B. 650-700 nm emission. Chloroplast autofluorescence. N = node.

C. Transmitted light, with an arrow pointing to the stained structure in the right node from A.

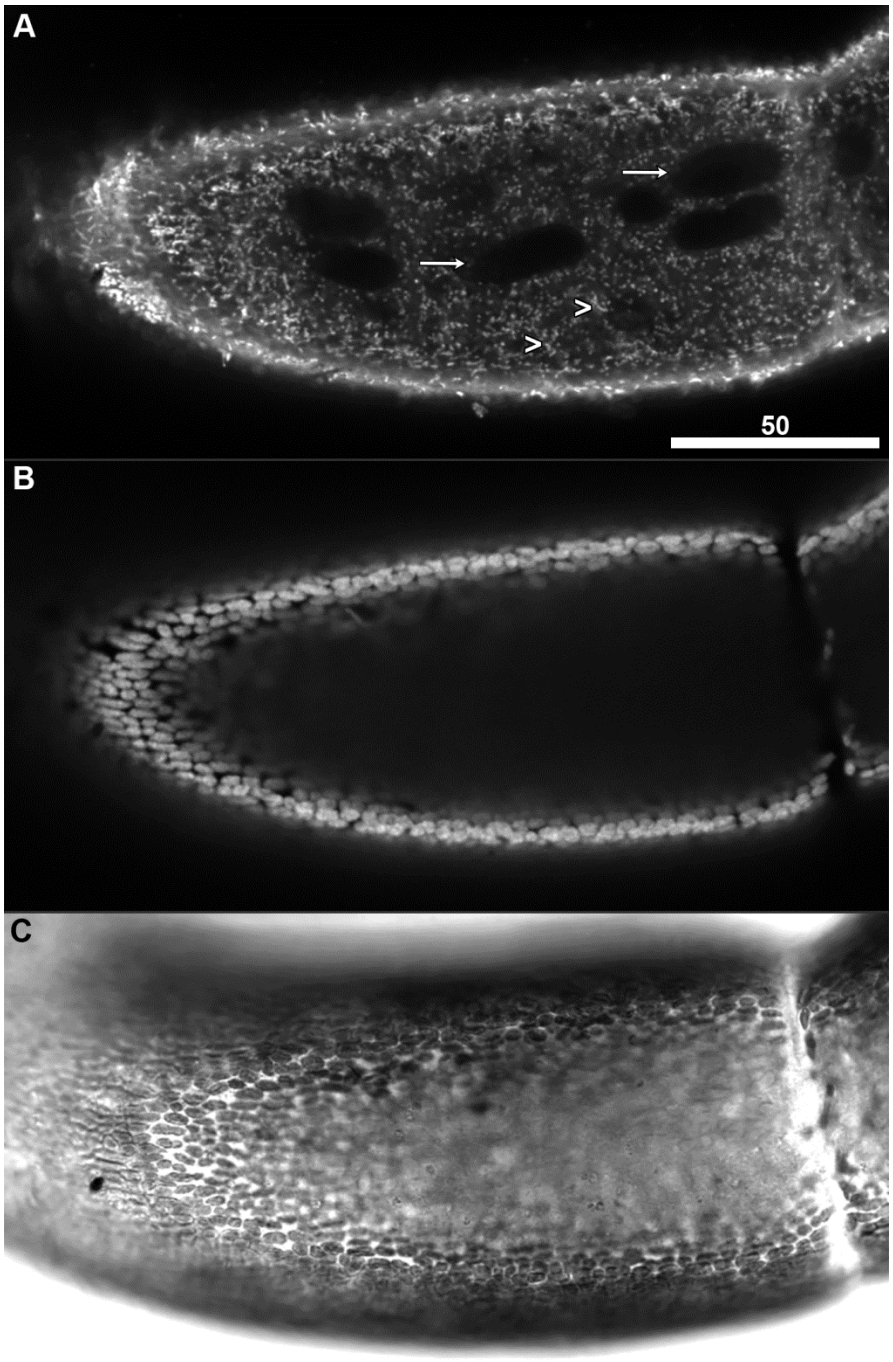

Figure 3.18. $DIOC_6(3)$ imaging of a young primary branchlet cell focussed at the endoplasm layer. 488+633 nm excitation. Scale bar = 50 µm.

A. $DIOC_6(3)$ (10 µM, 20 min) fluorescence from 500-550 nm. The numerous punctate mitochondria form clear outlines around dark disks that are probably nuclei (arrows) that streamed throughout the endoplasm independently of one another.

B. 650-700 nm emission. Chloroplast autofluorescence.

C. Transmitted light.

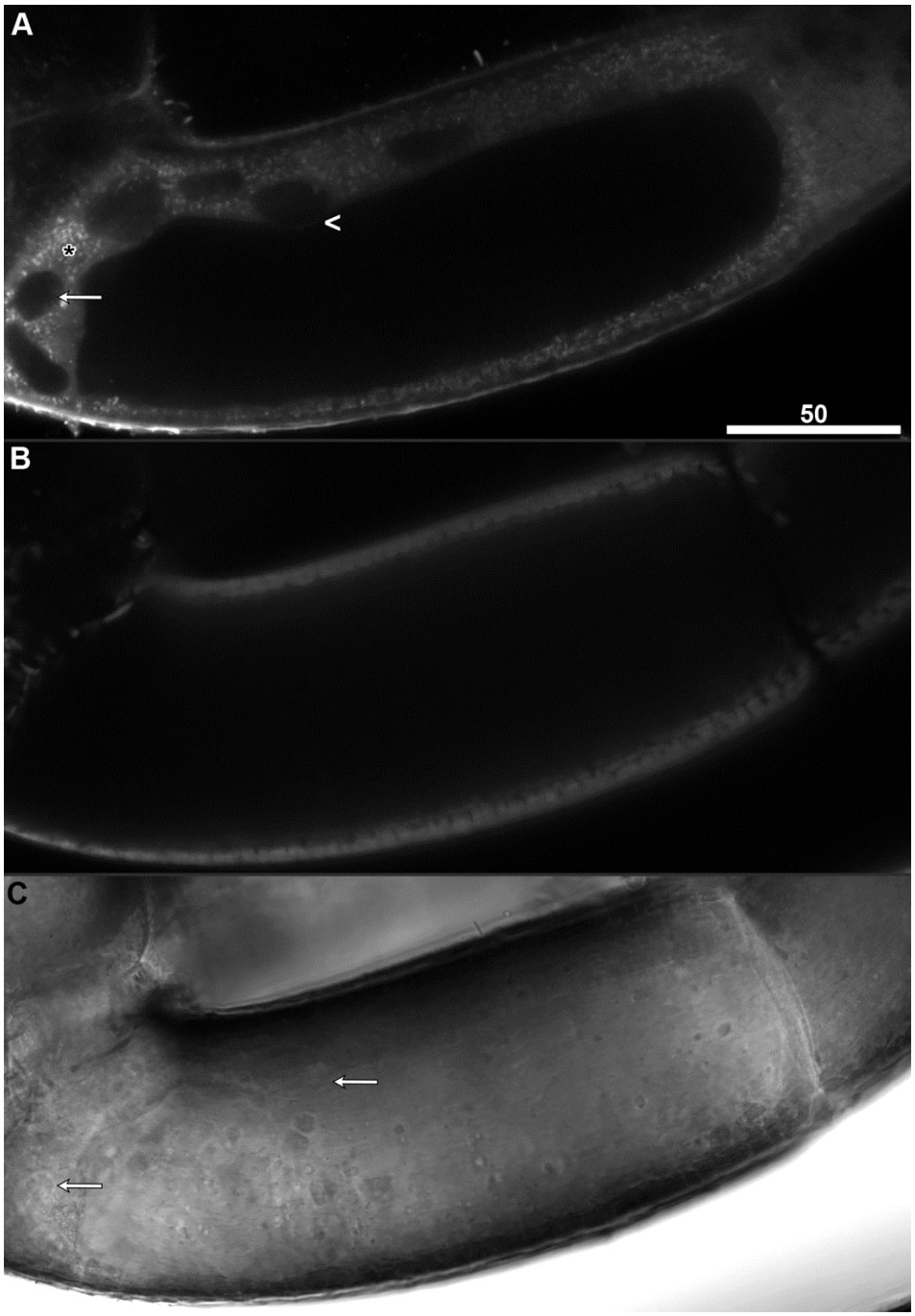

Figure 3.19. $DIOC_6(3)$ imaging of a young primary branchlet cell focused through the middle of the vacuole. This is the same cell from Figure 34 except deeper into the vacuole. 488+633 nm excitation. Scale bar = 50 µm.

A. $DIOC_6(3)$ (10 µM, 20 min) fluorescence from 500-550 nm. The nuclei (arrow) would rotate around the cell, bulging the tonoplast into the unlabelled central vacuole (caret). Mitochondria were numerously present and flowed through the endoplasm (asterisk).

B. 650-700 nm emission. Chloroplast autofluorescence.

C. Transmitted light.

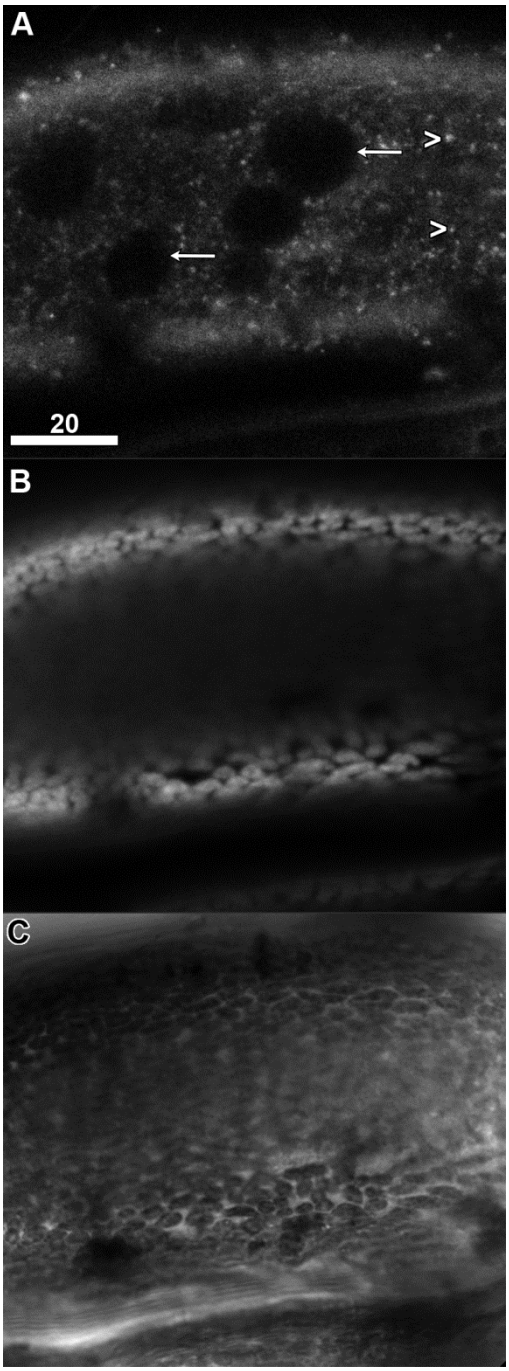

Figure 3.20. MDY-64 imaging of a young branchlet cell near the apical dividing tip, focused on a plane in the endoplasm. 456+633 nm excitation. Scale bar = 20 µm.

A. MDY-64 fluorescence (10 µM, 30 min) from 470-520 nm. Nuclei were negatively stained by the MDY-64 (arrows), which flowed freely through the endoplasm with numerous punctate structures (carets).

B. 650-700 nm emission. Chloroplast autofluorescence.

C. Transmitted light.

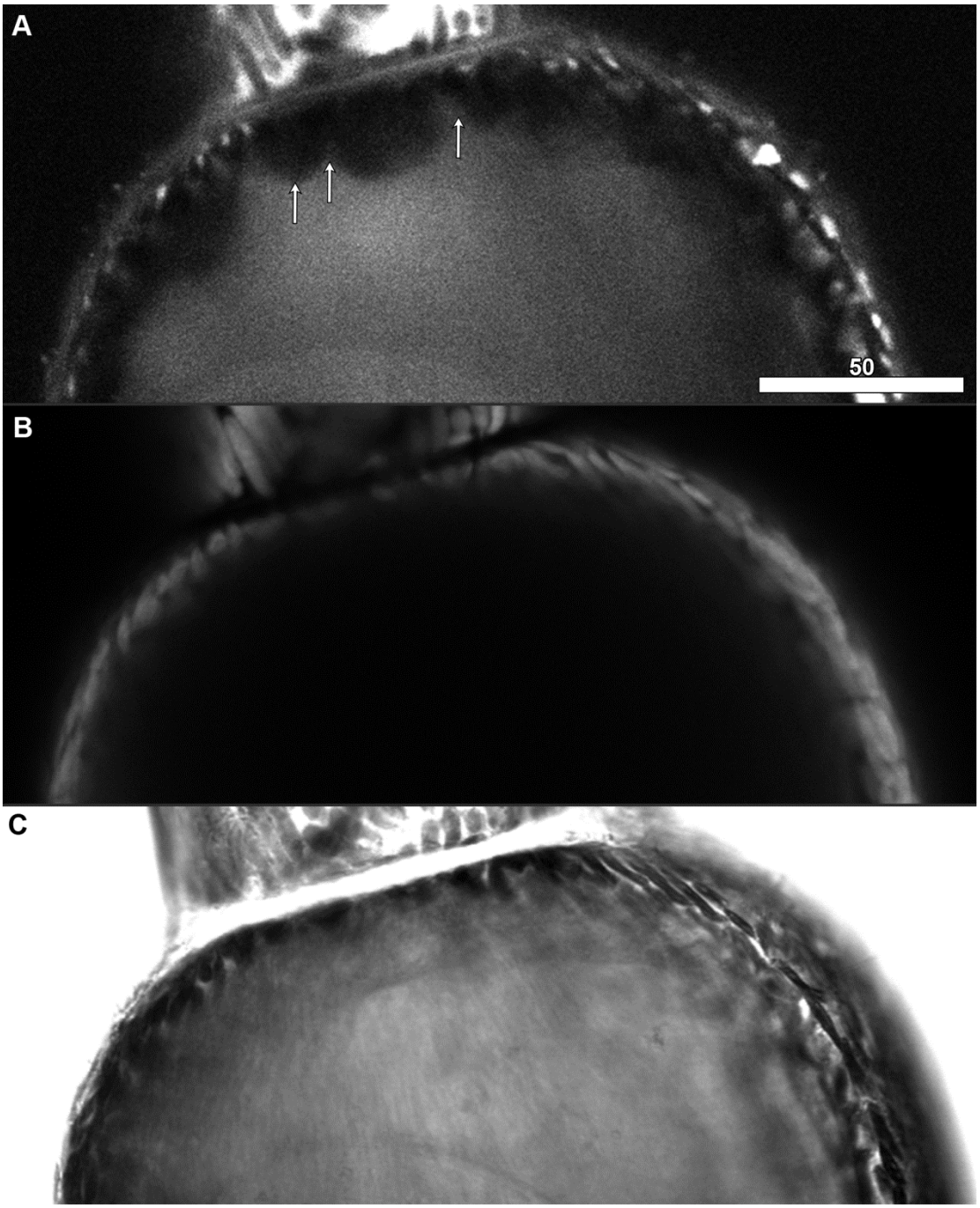

Figure 3.21. Blue CMAC staining of the central vacuole in a branchlet cell, showing a cross section of the cell. 405+633 nm excitation. Scale bar = 50 µm.

A. Blue CMAC fluorescence (100 µM, 30 min) from 415-465. The undulations in the tonoplast (arrows) are clearly seen with Blue CMAC, staining nothing in the endoplasm.

B. 650-700 nm emission. Chloroplast autofluorescence.

C. Transmitted light.

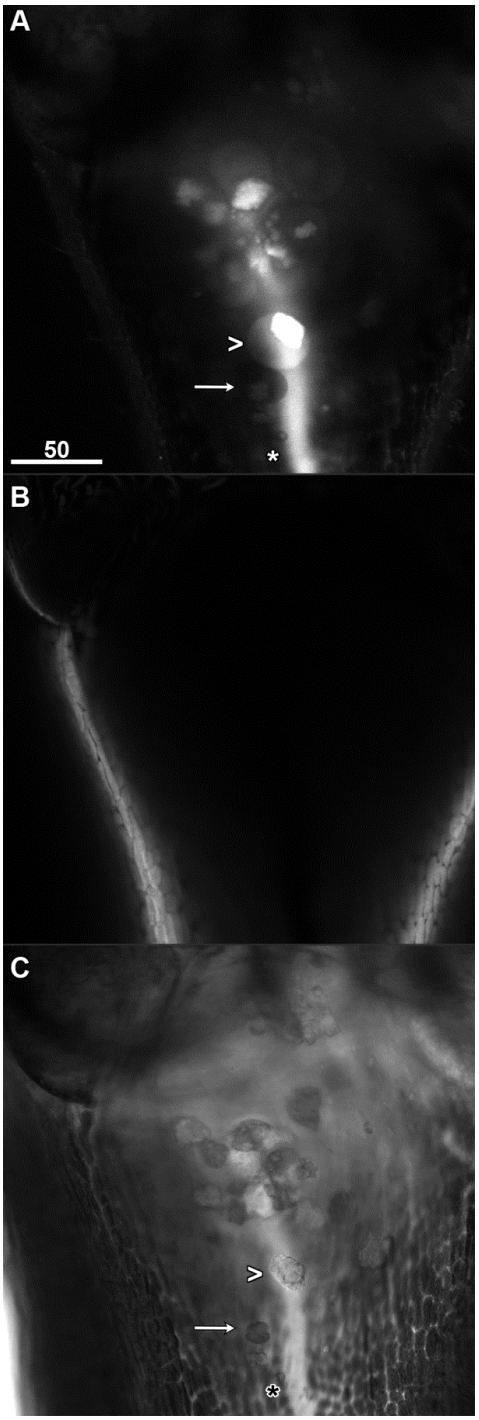

Figure 3.22. Blue CMAC staining of an internodal cell near the junction with the node, focused through the middle of the vacuole. 405+633 nm excitation. Scale bar = 50 µm.

A. Blue CMAC fluorescence (100 µM, 30 min) from 415-465. The neutral line (asterisk) fluoresces strongly, indicating that the chloroplasts are absorbing the excitation and emission light. Wound plugs either fluoresce brightly (caret) or create a shadow (arrow).

B. 650-700 nm emission. Chloroplast autofluorescence.

C. Transmitted light.

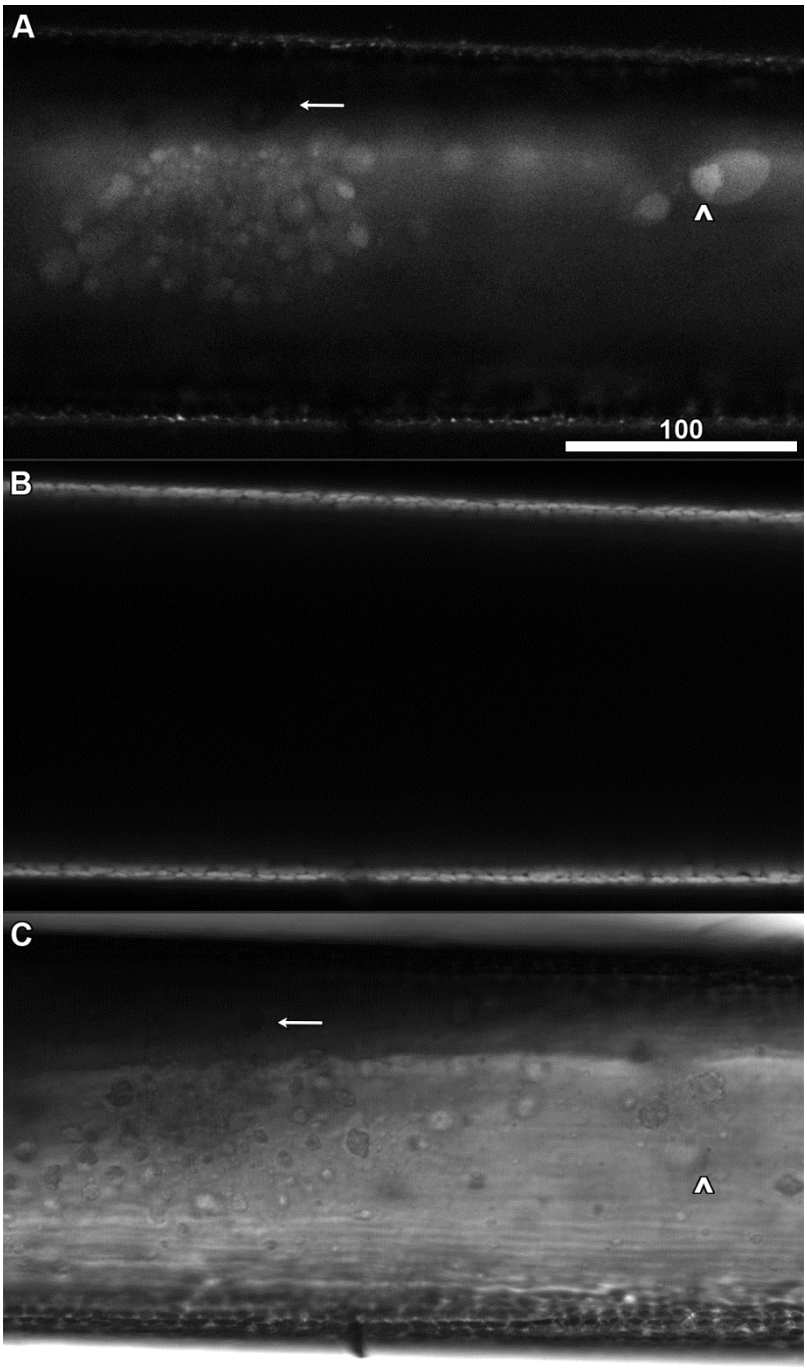

Figure 3.23. Blue CMAC staining of a branchlet cell, focused through the middle of the vacuole on a vacuolar plug. 405+633 nm excitation. Scale bar = 100 µm.

A. Blue CMAC fluorescence (c100 µM, 30 min) from 415-465 nm. Wound plug cores either stain brightly (caret) or create noticeable shadows (arrow). Vacuolar mats are composed of aggregates of wound plugs.

B. 650-700 nm emission. Chloroplast autofluorescence.

C. Transmitted light.

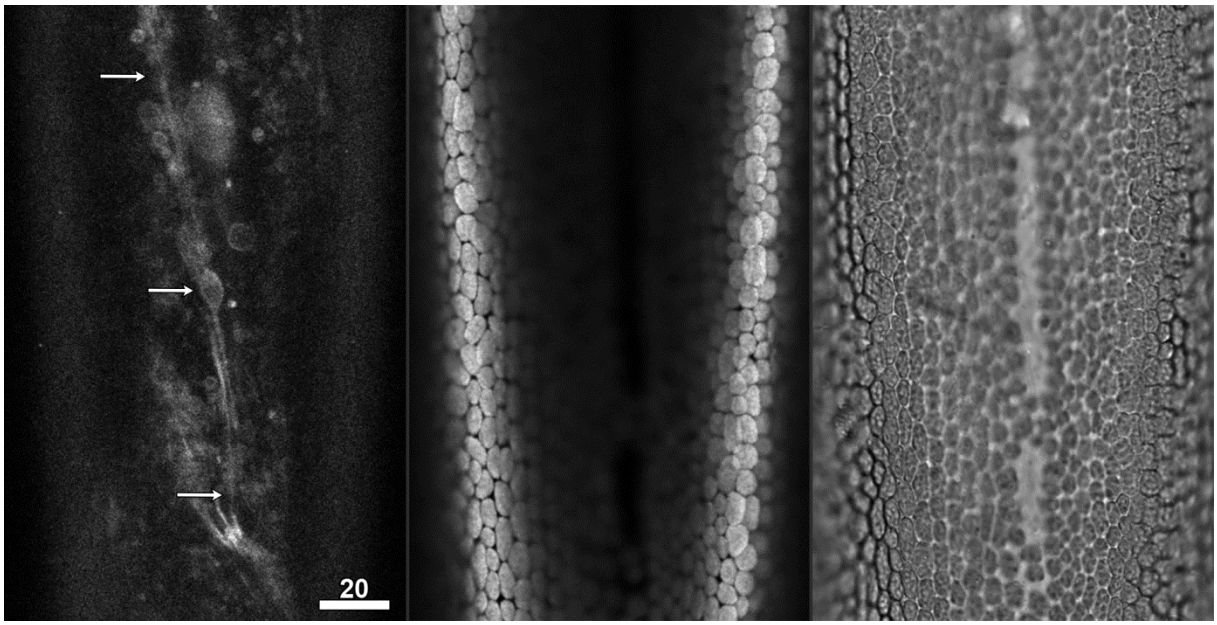

Figure 3.24. Neutral red labeling of an internodal cell, focused in a plane near the outer edge of the vacuole. Vacuolar elements frequently exhibited a stringy nature, as if tethered together. 561+633 nm excitation. Scale bar = 20 µm.

A. Neutral red (10 µM, 10 m) fluorescence from 550-600 nm. In addition to wound plugs, neutral red stained other elements inside of the vacuole, many of which appeared to be tethered together (arrows).

B. 650-700 nm emission. Chloroplast autofluorescence.

C. Transmitted light.

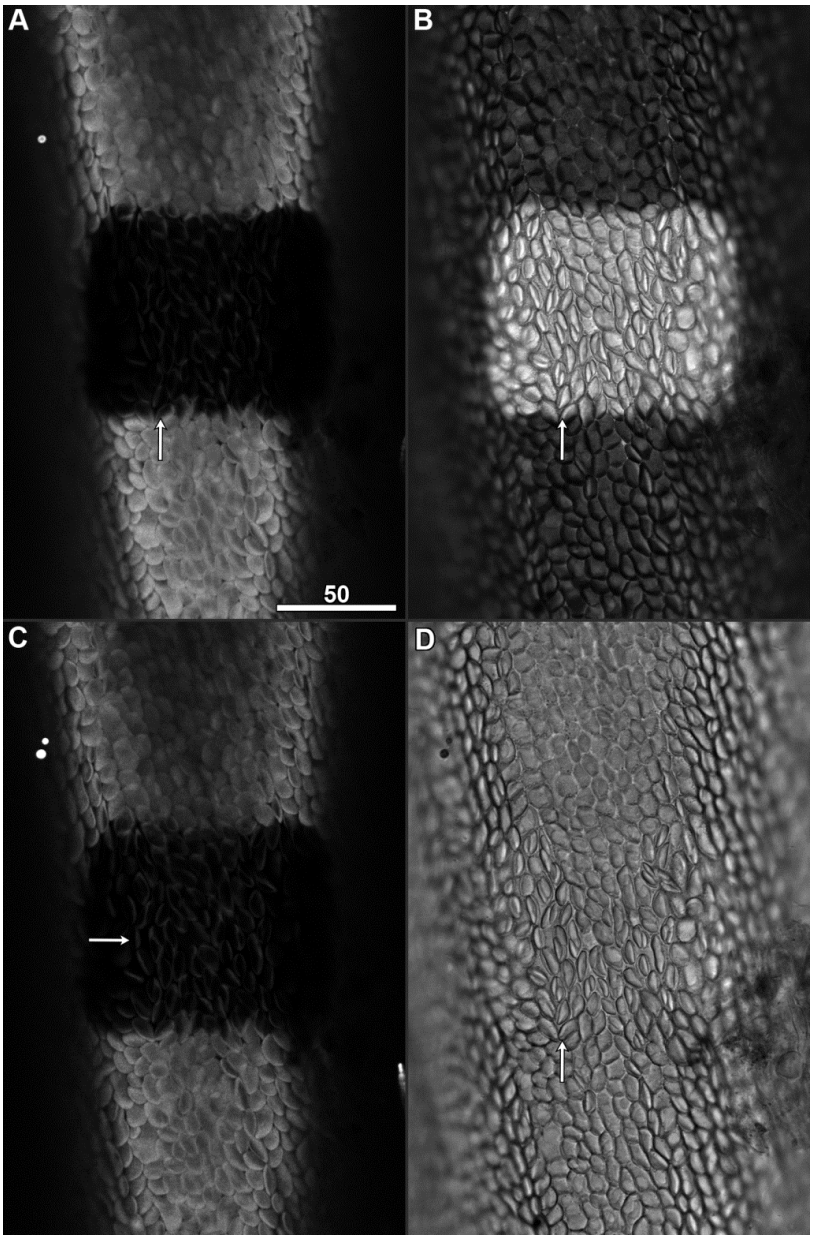

Figure 3.25. Unstained internodal cell focused on the chloroplast layer. The central square region of the cell had been subject to 5 minutes of 405 nm irradiation at 50% laser strength. This region showed rapid radiation damage to the chloroplast layer. Scale bar = 50 µm.

A, B. 456+633 nm excitation, 650-700 nm emission (A), transmitted light (B). The arrows show a clear boundary where the irradiation treatment was performed. Chloroplast autofluorescence disappeared (A), and the transmitted light image gets brighter indicating lower absorption of light and greater transmission (B).

C, D. 561+633 nm excitation, 650-700 nm emission (A), transmitted light (B). A trace “skeleton” of autofluorescence at the boundaries of the chloroplasts remained even after irradiation treatment (arrow) (C). (D) Transmitted light. Compared to B, the arrow in D shows reduced contrast between chloroplasts inside and outside of the treatment area. This is because the 561 nm laser is better at penetrating the chloroplast layer.

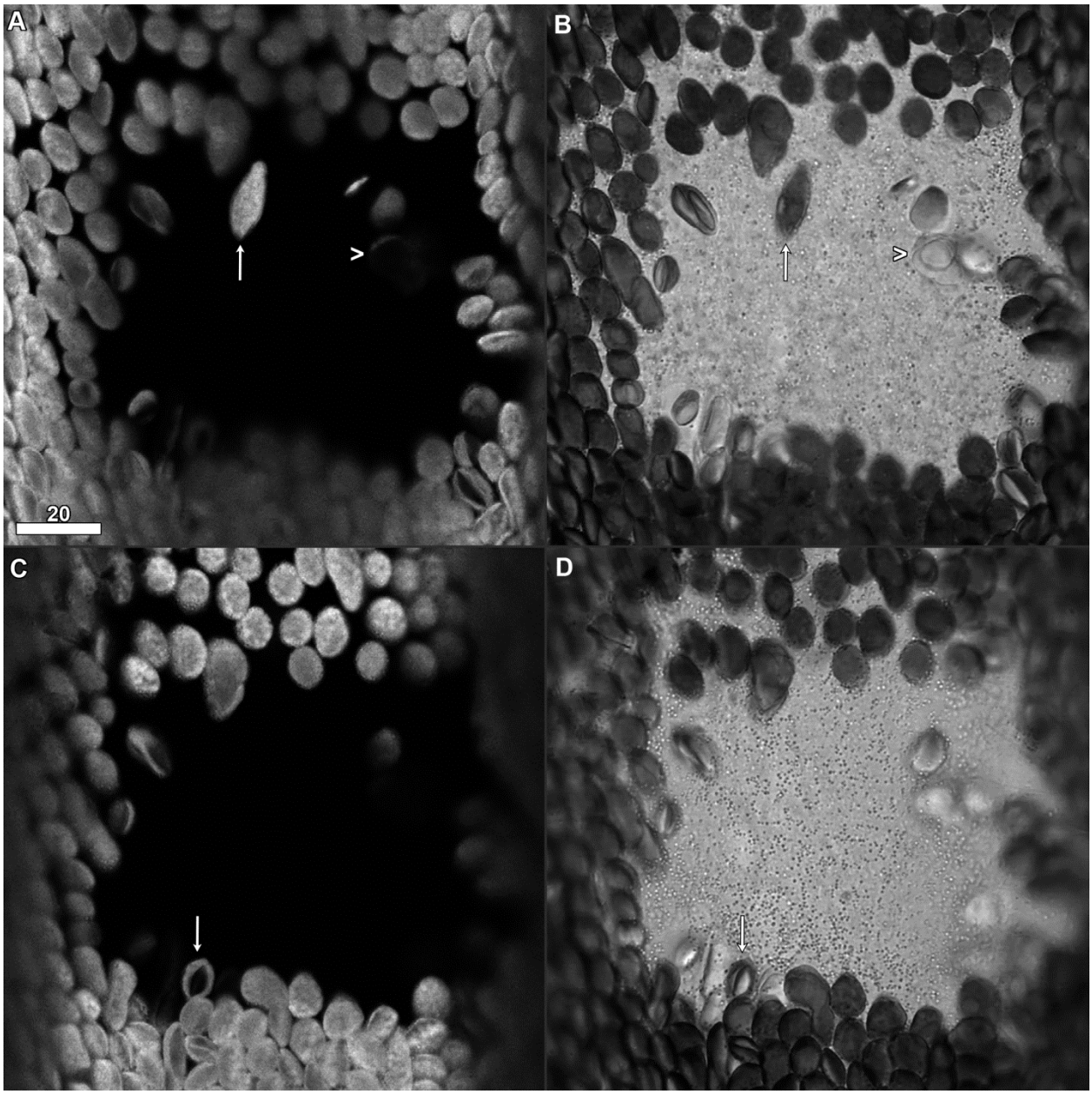

Figure 3.26. The same unstained control cell that had been irradiated as shown in Figure 3.25, after 24 hours. Chloroplasts have completely detached, creating a chloroplast-free "window" into the endoplasm and vacuole. 456+633 nm excitation. Scale bar = 20 μm.

A, B. 650-700 nm emission (A), transmitted light (B). In addition to their location in the chloroplast layer, chloroplasts were also present in the streaming endoplasm (arrows). The structure indicated by the carets appears to be a weakly fluorescent chloroplast surrounded by a membrane.

C, D. 650-700 nm emission (A), transmitted light (B) showing another anomalous chloroplast (arrows).

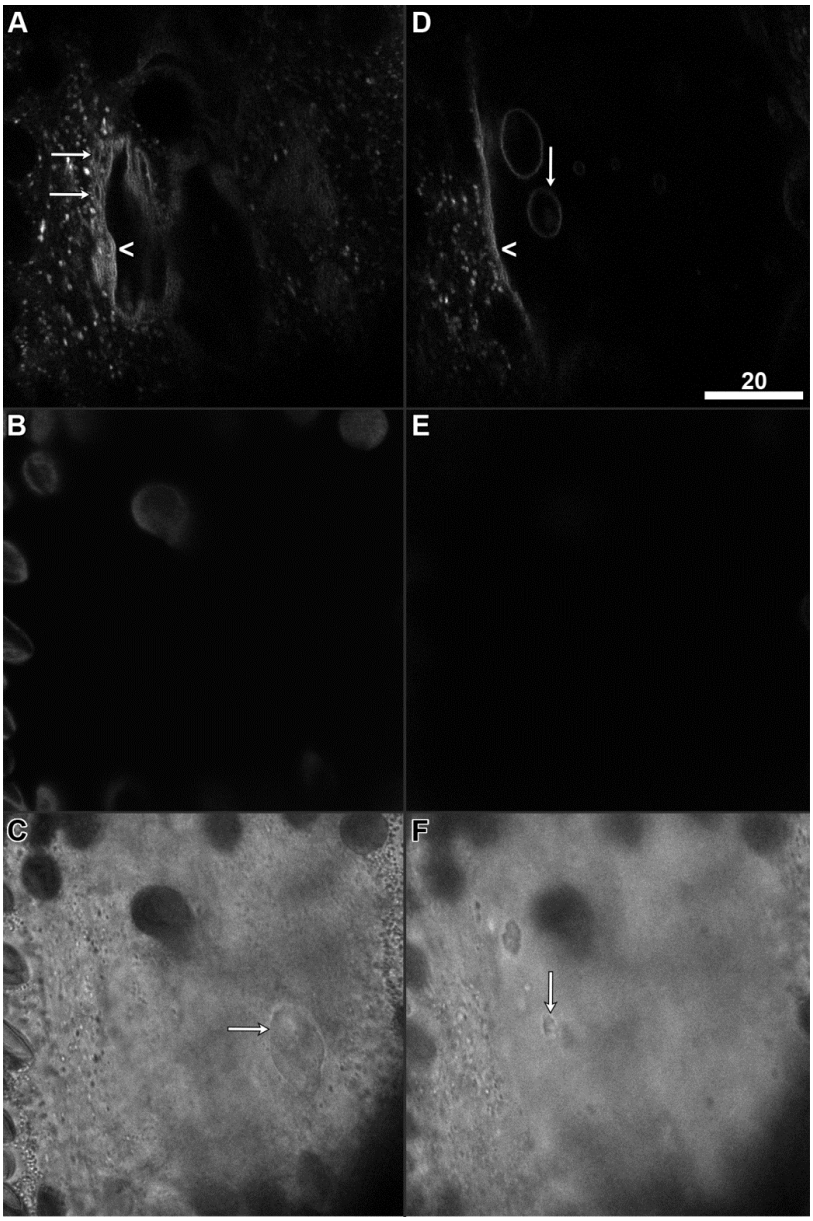

Figure 3.27. MDY-64 imaging of an internode through a chloroplast window, focused at a plane near the tonoplast from the endoplasmic side (A-C) and through the middle of the vacuole (D-F). Scale bar = 20 µm.

A. MDY-64 (10 µM, 30 min) fluorescence from 470-520 nm. Near the tonoplast layer, bulges from the vacuole start appear to create holes in the endoplasm where the tonoplast can be seen (caret). Near such bulges, complex networks of tubules and membranes were present (arrows).

B. 650-700 nm emission. Chloroplast autofluorescence.

C. Transmitted light. Arrows point to an unstained, non-autofluorescing object.

D. MDY-64 (10 µM, 30 min) fluorescence from 470-520 nm. Deep into the vacuole, the tonoplast (caret) and wound plugs (arrow) are brightly labelled.

E. 650-700 nm emission. Chloroplast autofluorescence.

F. Transmitted light, with a wound plug core from A labelled (arrow).

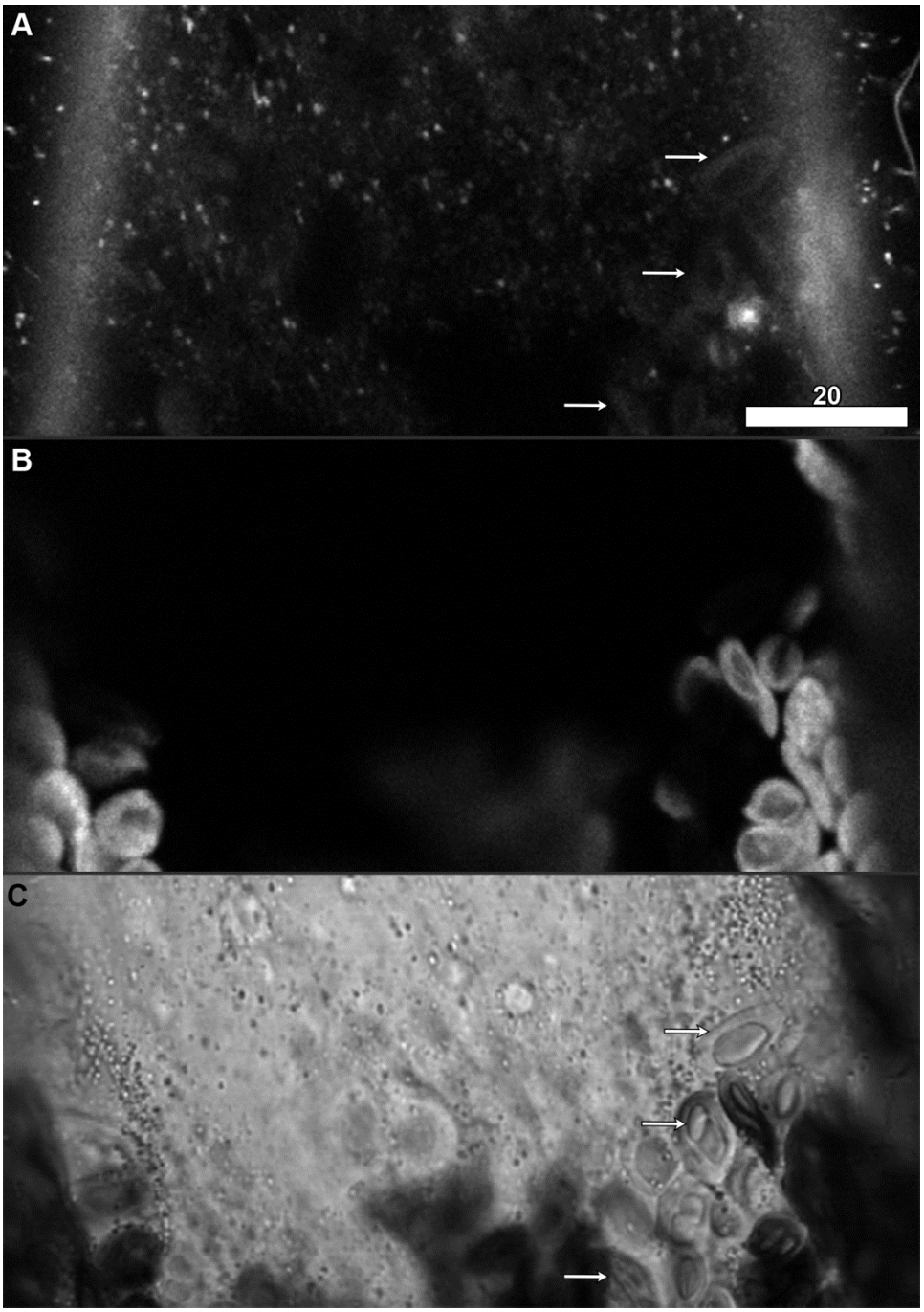

Figure 3.28. MDY-64 imaging of an internode through a chloroplast window, focused at a plane near the chloroplast layer. 456+633 nm excitation. Scale bar = 20 µm.

A. MDY-64 fluorescence (10 µM, 30 min) from 470-520 nm. Numerous membrane-bound structures fluoresced at the periphery of the chloroplast window which did not fluoresce at 650-700 nm like other chloroplasts.

B. 650-700 nm emission. Chloroplast autofluorescence.

C. Transmitted light, with membrane-bound structures (arrows) that did not autofluorescence at the normal chloroplast wavelengths and which contained structures inside that did not fluoresce with the rest of the vesicle.

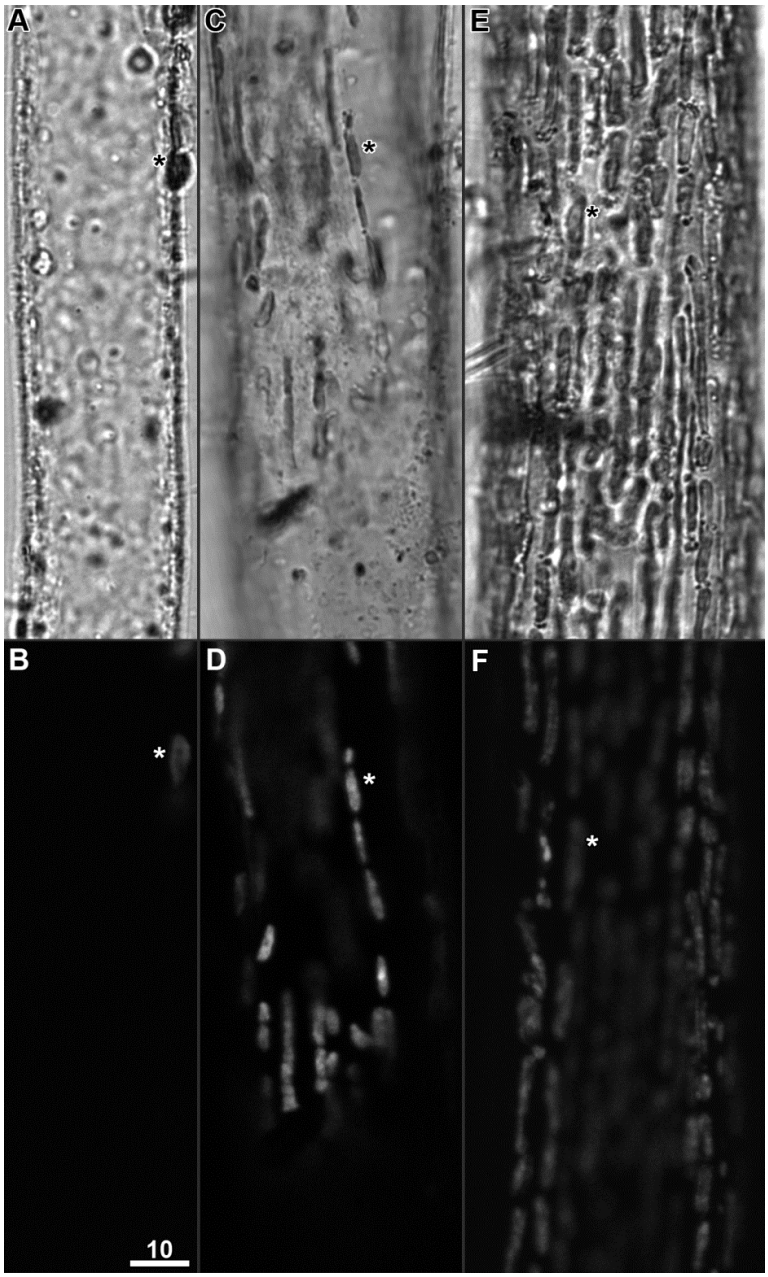

Figure 3.29. Unstained imaging of rhizoids focused on a plane through the middle of the vacuole, showing a direct comparison between s-rhizoids (A, B), m-rhizoids (C, D), and l-rhizoids (E, F). 488+633 nm excitation. Scale = 10 µm.

A. Transmitted light. S-rhizoids were the smallest and lacked any chloroplast coverage. An epiphytic alga is marked (asterisk).

B. 650-700 nm emission. Aside from an epiphytic alga (asterisk), s-rhizoids had no autofluorescence at the chloroplast range.

C. Transmitted light. M-rhizoids begin to increase in size, and have sparse chloroplast coverage (asterisk).

D. 650-700 nm emission. The chloroplasts are labelled (asterisk).

E. Transmitted light. L-rhizoids were the largest, and had thorough chloroplast coverage (asterisk).

F. 650-700 nm emission. The chloroplasts are labelled (asterisk).

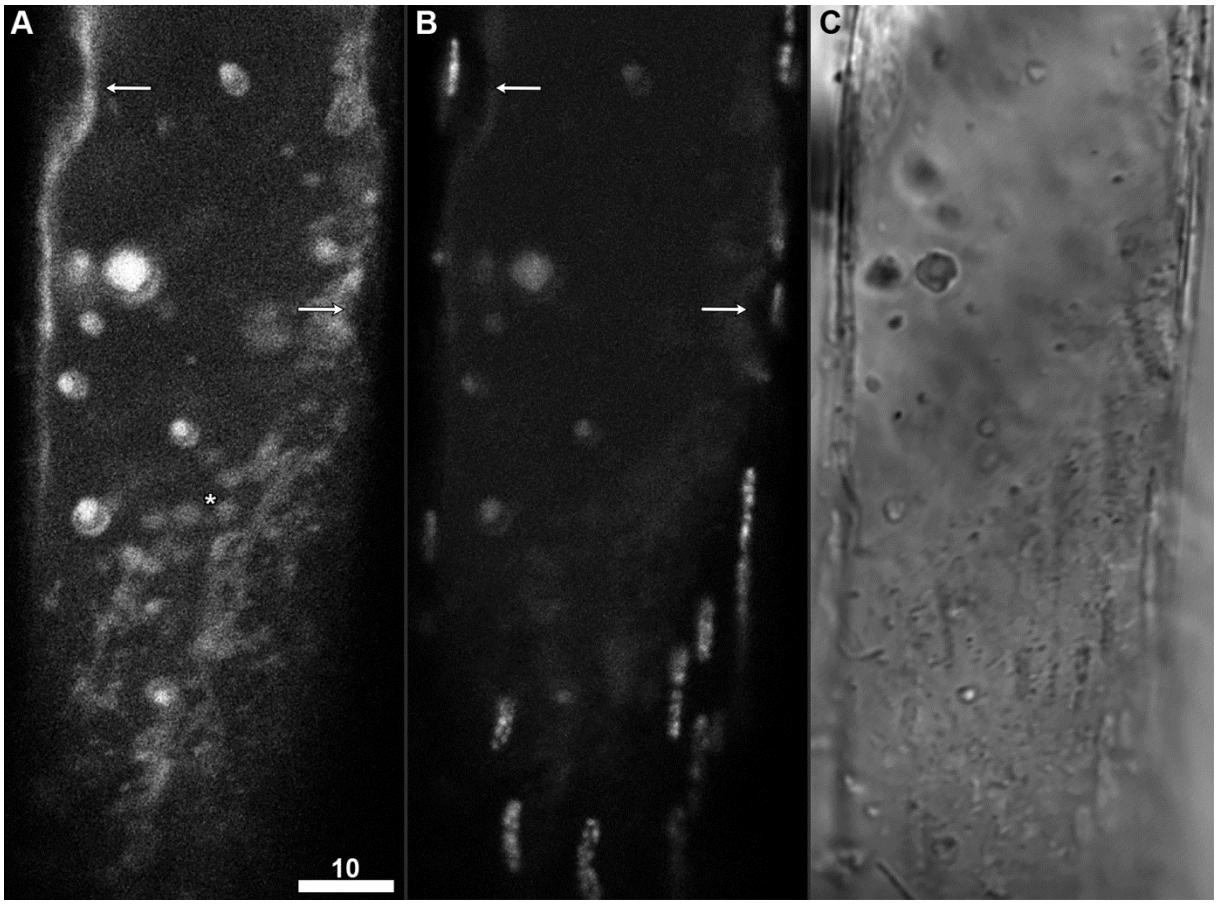

Figure 3.30. Neutral red imaging of an m-rhizoid, showing the similarities and differences in cytoplasmic architecture compared to internodal cells. 561+633 nm excitation. Scale bar = 10 µm.

A. Neutral red (10 µM, 10 min) fluorescence from 550-600 nm. The dynamic tonoplast is clearly labeled and undulating (arrows).

B. 650-700 nm emission. Chloroplast autofluorescence. Note the sparse chloroplast coverage, indicative of an m-rhizoid. Weak emission from the vacuole was present (arrows).

C. Transmitted light.

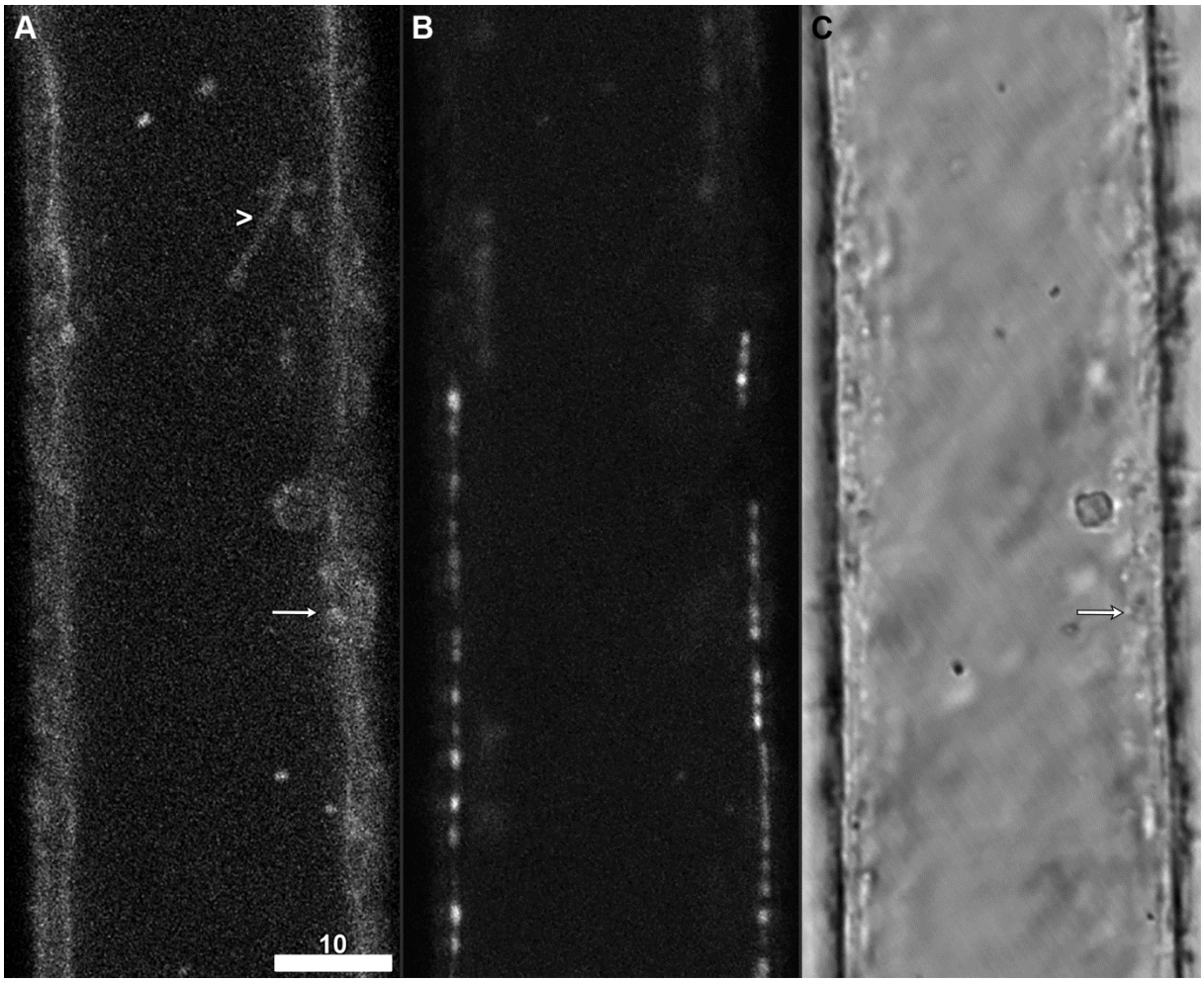

Figure 3.31. Neutral red imaging of an m-rhizoid, showing a cross section through the vacuole. The turbulent tonoplast exhibited the same kind of extensive network of infoldings seen in internodal cells. 561+633 nm excitation. Scale bar = 10 µm.

A. Neutral red (10 µM, 10 min) fluorescence from 550-600 nm. The infolded tonoplast (arrow) was similar to a branchlet cell (Figure 11). Structures that kept a rigid shape also moved through the vacuole (caret).

B. 650-700 nm emission. Chloroplast autofluorescence.

C. Transmitted light. The tonoplast (arrow).

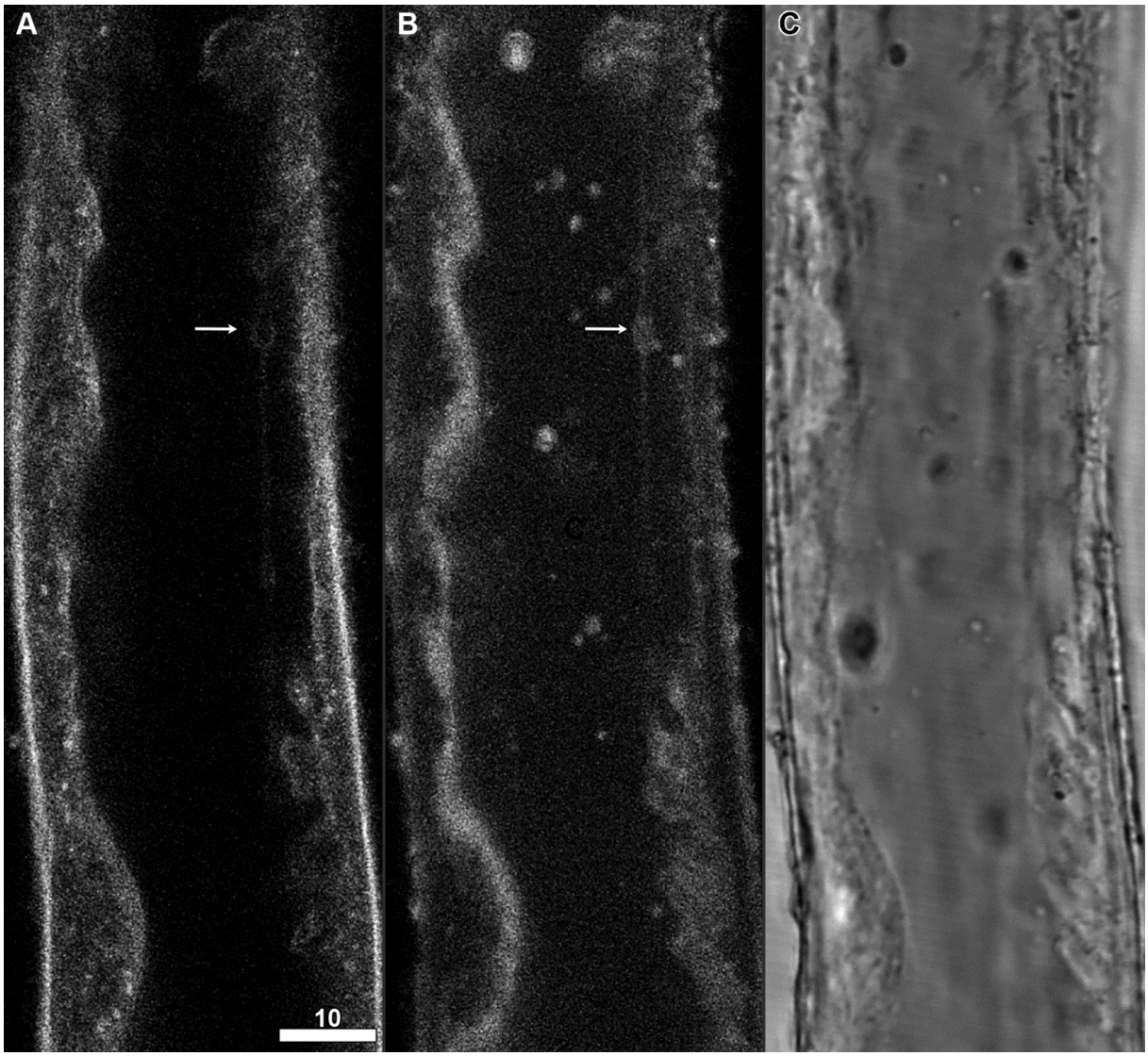

Figure 3.32. An s-rhizoid stained with both MDY-64 and neutral red, showing a cross section through the vacuole. MDY-64 gave brighter and sharper images. 456+561+633 nm excitation. Scale bar = 10 µm.

A. MDY-64 (10 µM, 30 min) fluorescence from 470-520 nm. MDY-64 labeling of the tonoplast was clearer and brighter than neutral red. Stringy elements were also visible (arrow).

B. Neutral red (10 µM, 10 min) fluorescence from 550-600 nm. Note that the vesicle is filled with neutral red, whereas only the membrane was stained by the MDY-64 in A (arrow).

C. Transmitted light.

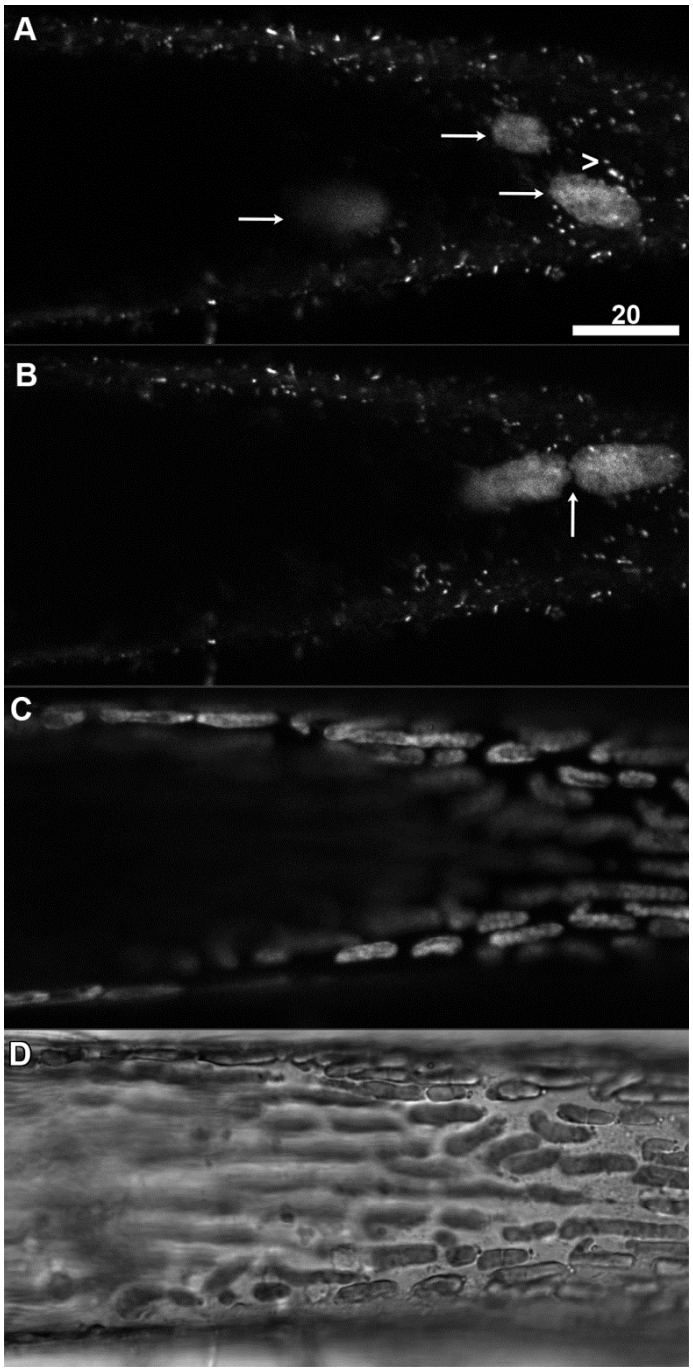

Figure 3.33. Syto-13 imaging of an l-rhizoid, focused on a plane in the endoplasm. 488+633 nm excitation. Scale bar = 20 µm.

A,B Syto-13 fluorescence (5 µM, 30 min) from 500-550 nm. Multiple nuclei (arrows) and mitochondria (caret) stream around the endoplasm. Nuclei sometimes pair, held together at an attachment point (arrow).

C. 650-700 nm emission. Chloroplast autofluorescence showing the extensive coverage of chloroplasts in this L rhizoid.

D. Transmitted light.

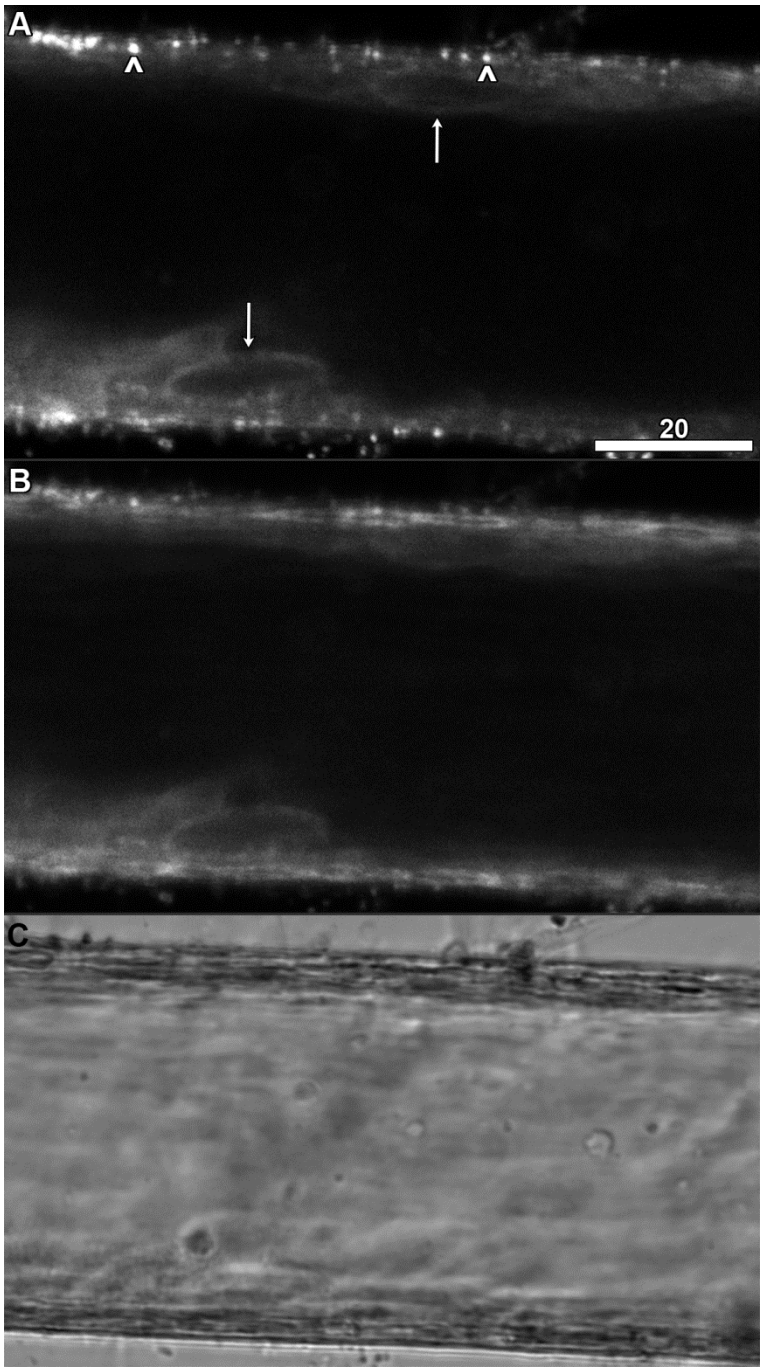

Figure 3.34. Nile red staining of an l-rhizoid, focused on a plane through the middle of the vacuole. 561+633 nm excitation. Scale bar = 20 µm.

A. Nile red fluorescence (50 µM, 30 min) from 570-620 nm. The presence of the dark disks (arrows) in the streaming endoplasm of l-rhizoids suggests their transitioning into a more internode-like state. Lipid droplets were also labelled (carets).

B. 650-700 nm emission. Chloroplast autofluorescence, with significant bleed-through fluorescence from the Nile red.

C. Transmitted light.

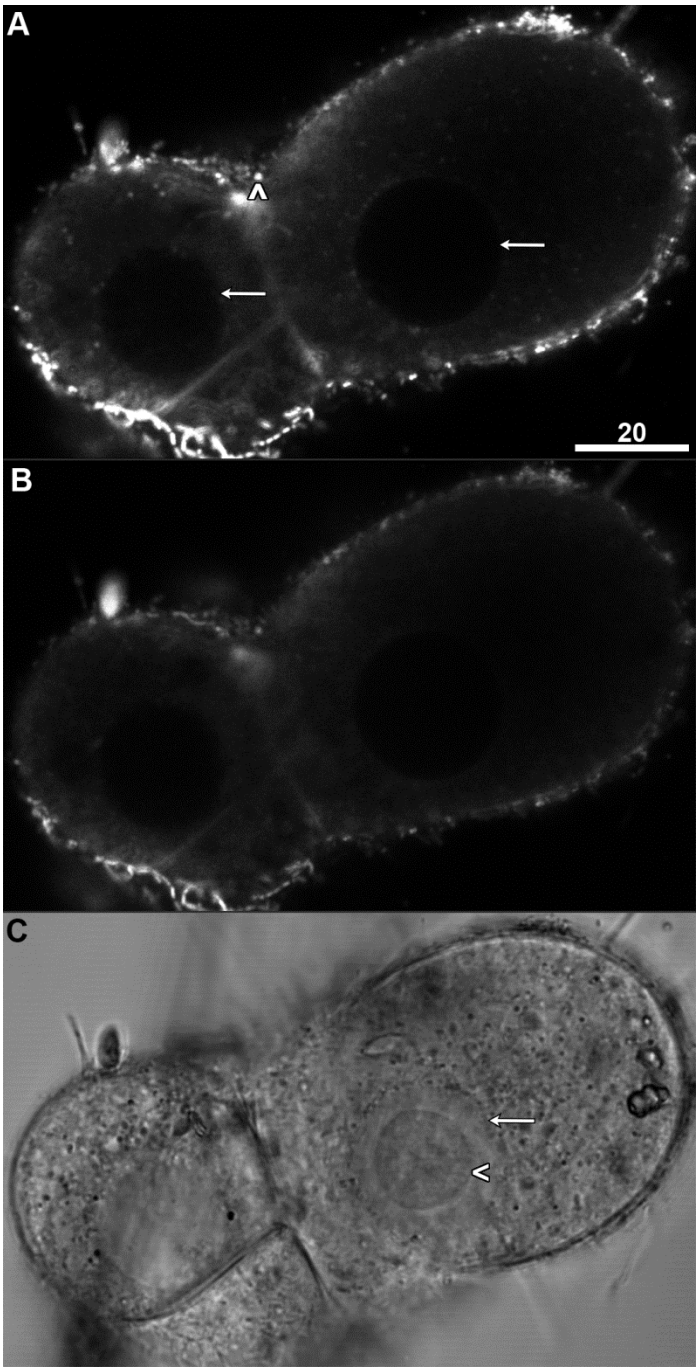

Figure 3.35. Nile red staining of rhizoid junction cells, focused on a plane through the middle of the cell. 561+633 nm excitation. Scale bar = 20 µm.

A. Nile red fluorescence (50 µM, 30 min) from 570-620 nm. Large regions from which dye was excluded (arrows) occur in each of the two nodal cells. Lipid droplets were also labelled (caret).

B. 650-700 nm emission. Chloroplast autofluorescence, with significant bleed-through fluorescence from the Nile red.

C. Transmitted light, with arrows showing the boundary of the dye exclusion (arrow) and a possible nucleolus (caret).

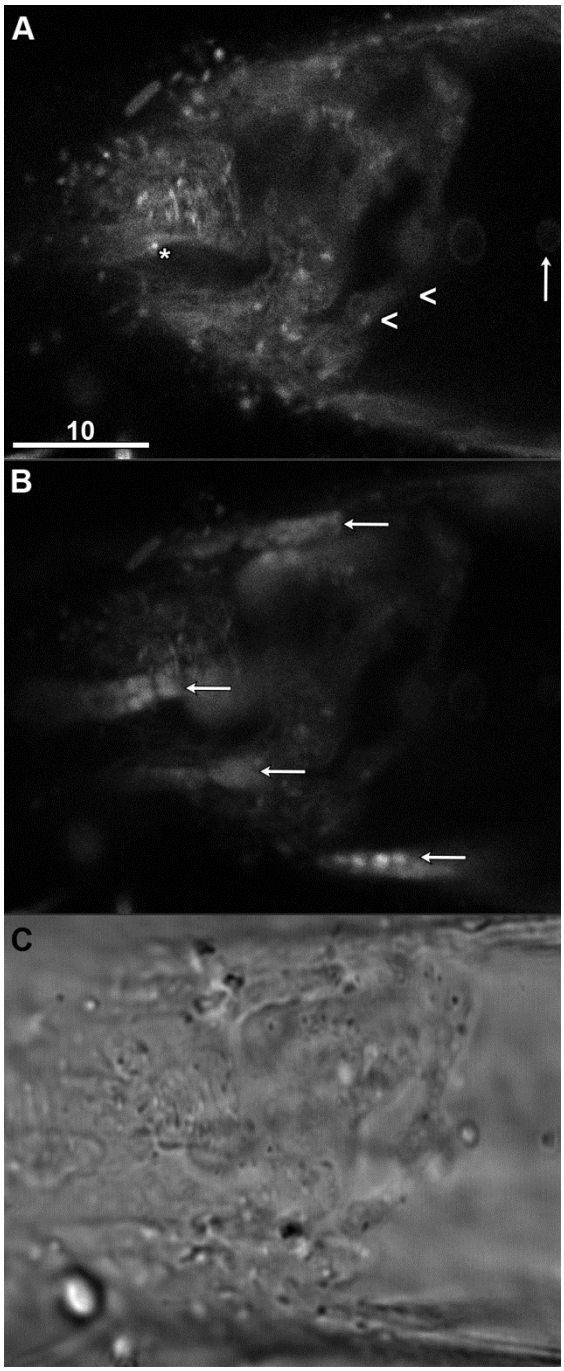

Figure 3.36. Nile red staining of an m-rhizoid, focused on a plane through the endoplasm of a rhizoid that is angled that both the endoplasm and vacuole are within focus. 561+633 nm excitation. Scale bar = 10 µm.

A. Nile red fluorescence (50 µM, 30 min) from 670-620 nm. Bright punctate structures (asterisk) could be seen enmeshed in a complex network of tubules, which extended as 3-dimensional tubules throughout the cell (carets). A wound plug can be seen (arrow).

B. 650-700 nm emission. Chloroplast autofluorescence (arrows), with significant bleed-through fluorescence from the Nile red.

C. Transmitted light.

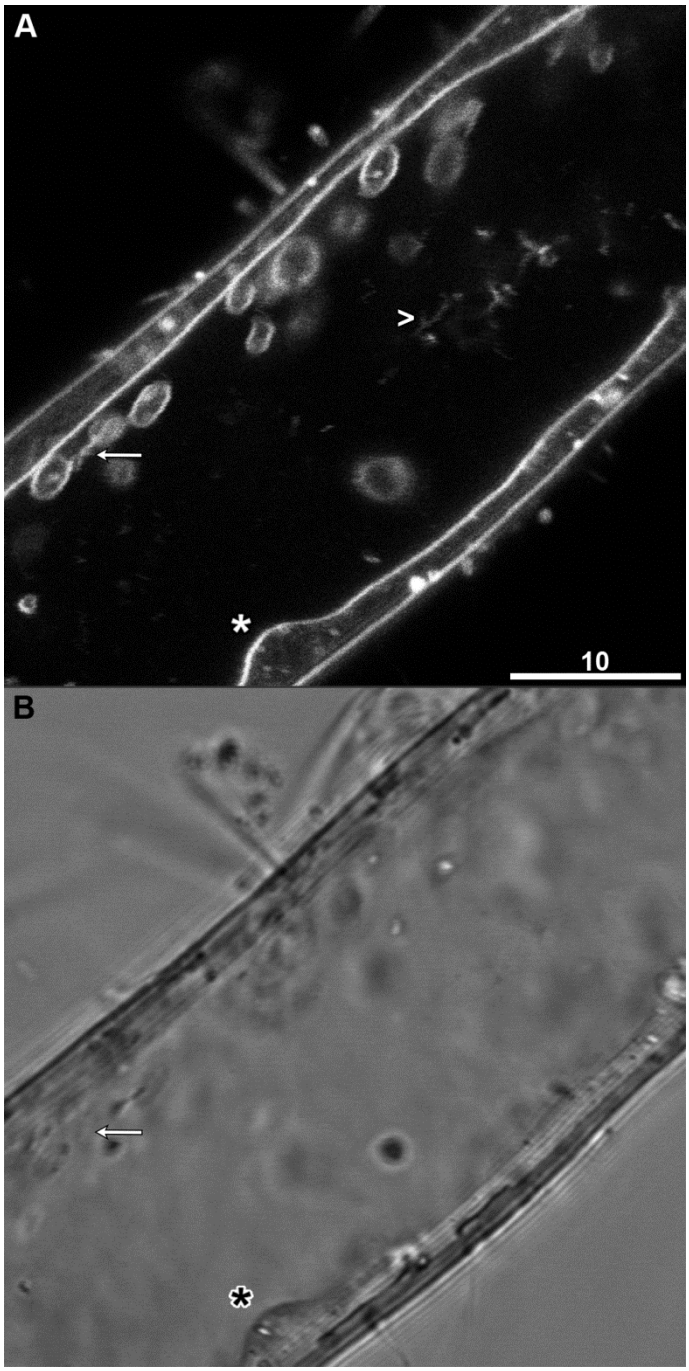

Figure 3.37. MDY-64 imaging of an s-rhizoid showing a cross section through the vacuole, using 63x magnification. 456+633 nm excitation. Scale bar = 20 µm.

A. MDY-64 (10 µM, 30 minutes) fluorescence from 470-520 nm. Brightly-labelled vesicles were connected by a string covered with smaller, bead-like vesicles (arrow). Small, rigid, angular objects (caret) were also present in the middle of the vacuole inside the sharply defined tonoplast (asterisk).

B. Transmitted light.

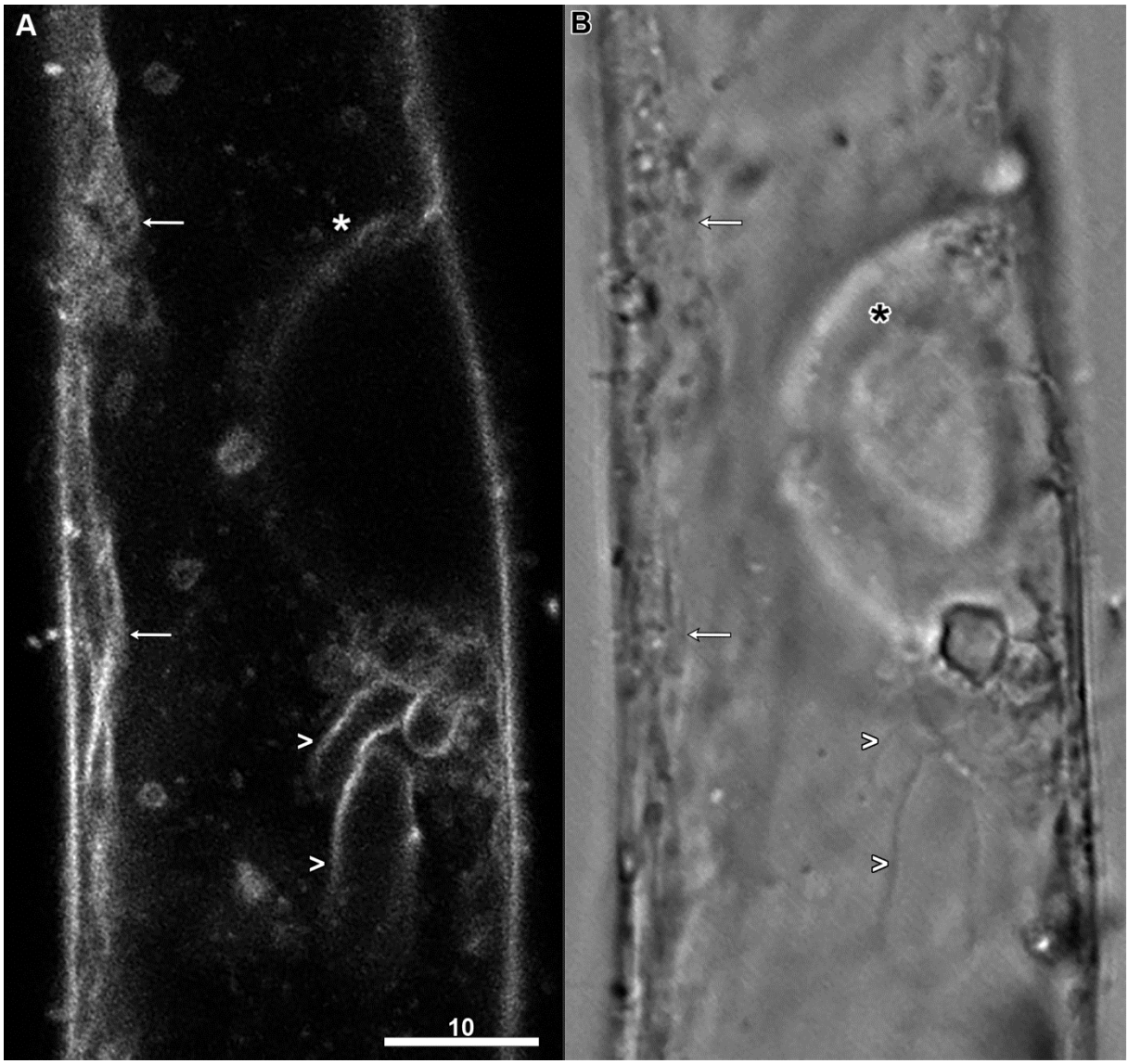

Figure 3.38. MDY-64 imaging of an anomalous nucleus towards the end of an s-rhizoid, showing a cross section through the vacuole. 456+633 nm excitation. Scale bar = 10 µm.

A. MDY-64 (10 µM, 30 min) fluorescence from 470-520 nm. As with larger internodal cells, the tonoplast was highly invaginated and tubular in nature (arrows). The cell contained a nucleus away from the cell apex, with a network of associated membranes (carets). Asterisk marks a conspicuous membrane without any internal staining.

B. Transmitted light. Asterisks indicate an apparent nucleolus.

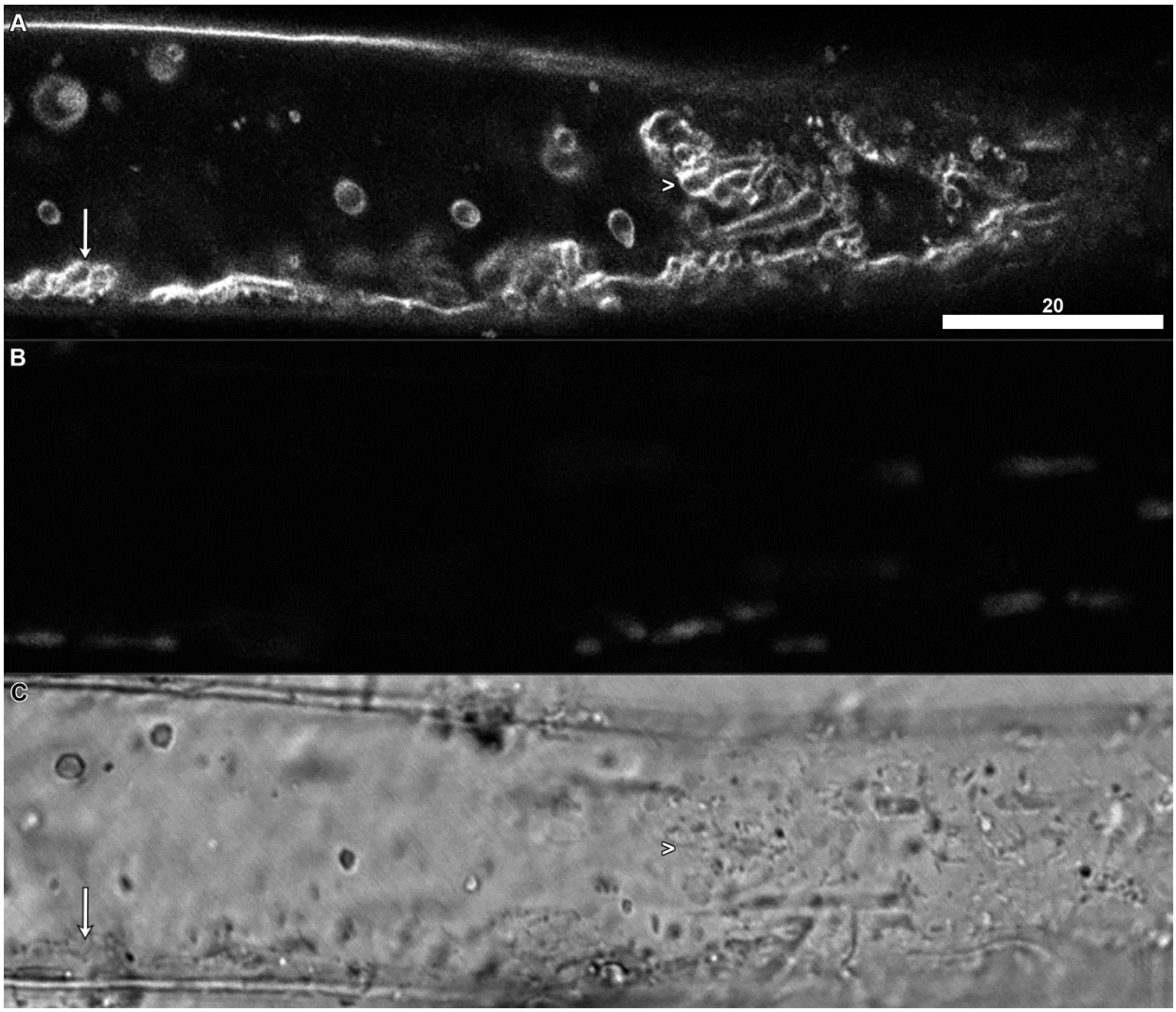

Figure 3.39. MDY-64 imaging of an m-rhizoid, with the plane of section angled from the endoplasm to the vacuole, showing the tonoplast from both the above and in cross section in a single image. Scale bar = 20 µm.

A. MDY-64 (10 µM, 30 minutes) fluorescence from 470-520 nm showed highly complex invaginations and tubules of the tonoplast from the side (arrow) and from the top (caret).

B. 650-700 nm emission. Chloroplast autofluorescence.

C. Transmitted light. Invaginations can be clearly made out in the transmitted light (arrow and caret).

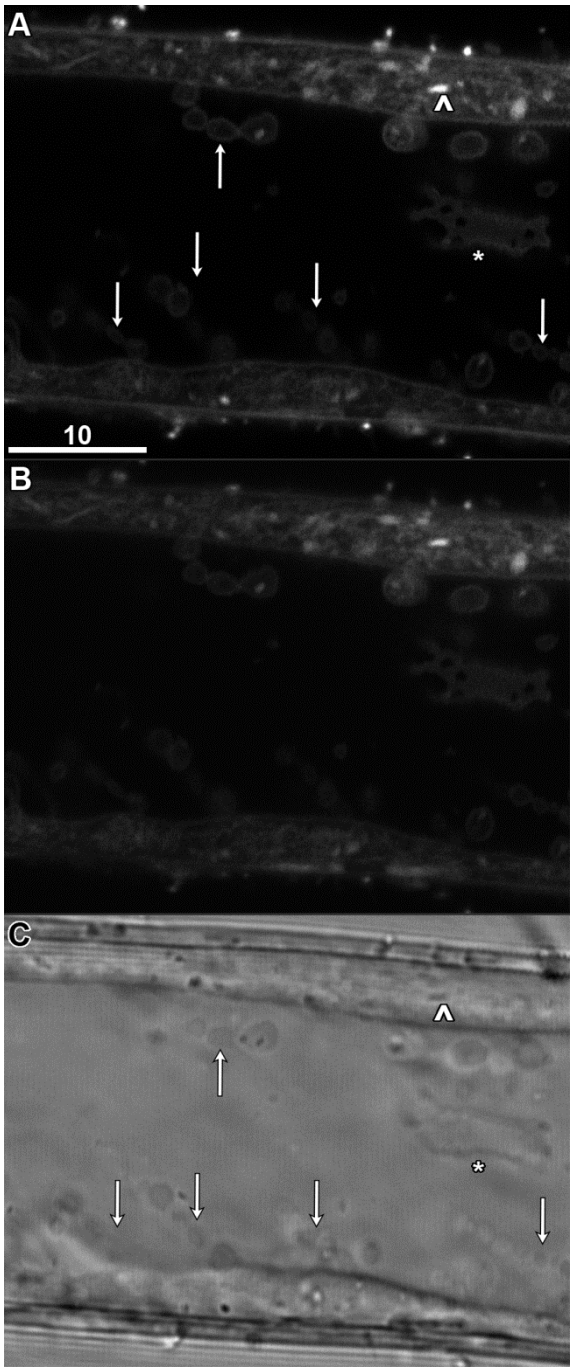

Figure 3.40. Nile red staining of an s-rhizoid, focused on a plane through the middle of the vacuole. 561+633 nm excitation. Scale bar = 30 µm.

A. Nile red fluorescence (50 µM, 30 min) from 570-620 nm. Numerous chains of vesicles anchored to the tonoplast (arrows) stream through the vacuole, and several endoplasmic membranes also fluoresce including rod-like objects (caret). A cytoplasmic inclusion (asterisk) also fluoresces.

B. 650-700 nm emission. Chloroplast autofluorescence (arrows), with significant bleed-through fluorescence from the Nile red.

C. Transmitted light.

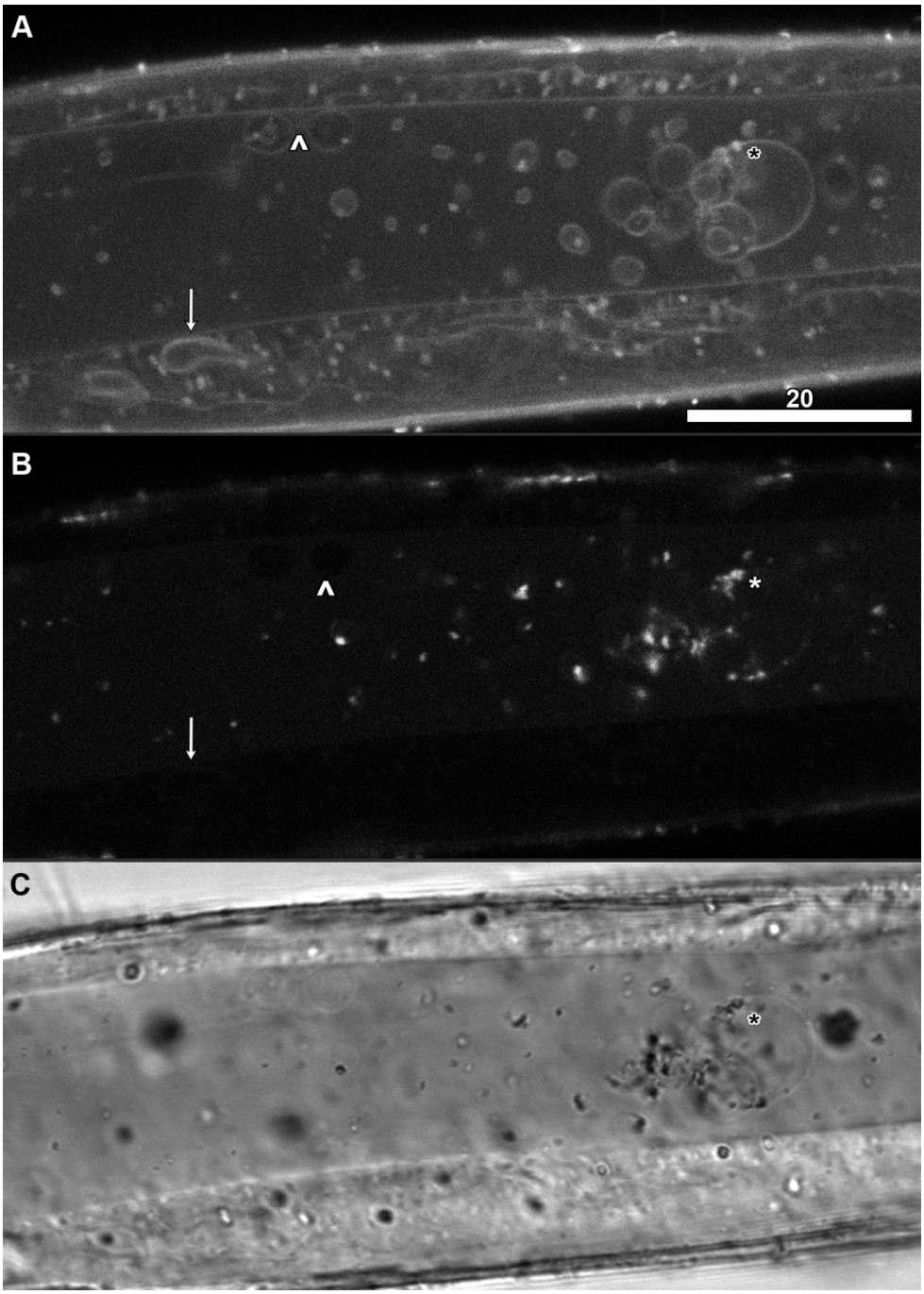

Figure 3.41. Acridine orange imaging of an m-rhizoid, focused on a plane through the middle of the vacuole. 488+633 nm excitation. Scale bar = 20 µm.

A. Acridine orange fluorescence (20 µM, 6 h) from 500-550 nm. The tonoplast (arrow) fluoresced strongly, along with numerous membranes and tubules in the endoplasm. Two vesicles joined along by a string (caret) move with the tonoplast. Numerous wound plugs (asterisk) are present in a vacuolar gyre.

B. 650-700 nm emission. The vacuole faintly fluoresced (arrow), with dark vesicles (caret) fluorescing more like the endoplasm. Wound plugs are labelled (asterisk).

C. Transmitted light.

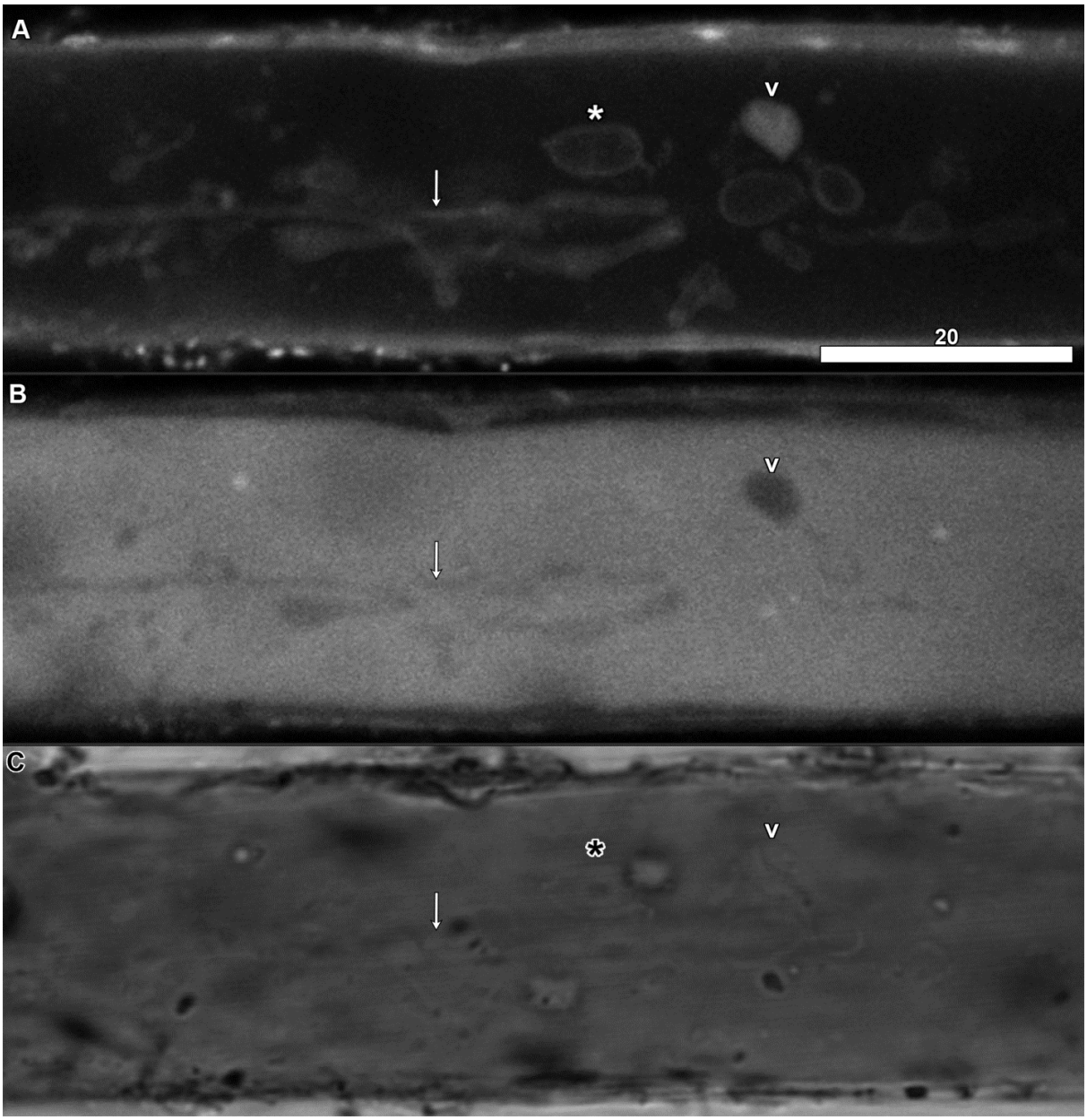

Figure 3.42. Acridine orange staining of an s-rhizoid, focused through the middle of the vacuole. 514+633 nm excitation. Scale bar = 20 µm.

A,B. Acridine orange fluorescence (20 µM, 6 h). The differential staining of acridine orange between the endoplasm and the vacuole reveals the pH dependence of fluorescence.

A. Fluorescence from 525-575 nm. Cytoplasmic inclusions (arrow) fluoresce in a similar to the endoplasm. Two different types of vesicles are present, one endoplasm-like (caret) and one more like the vacuole-like (asterisk).

B. Fluorescence from 650-700 nm. The fluorescence shows the opposite patterns to that at the shorter wavelengths. The endoplasm, inclusion (arrow) and vesicle (caret) are dark while the rest of the vacuole fluoresces brightly.

C. Transmitted light.

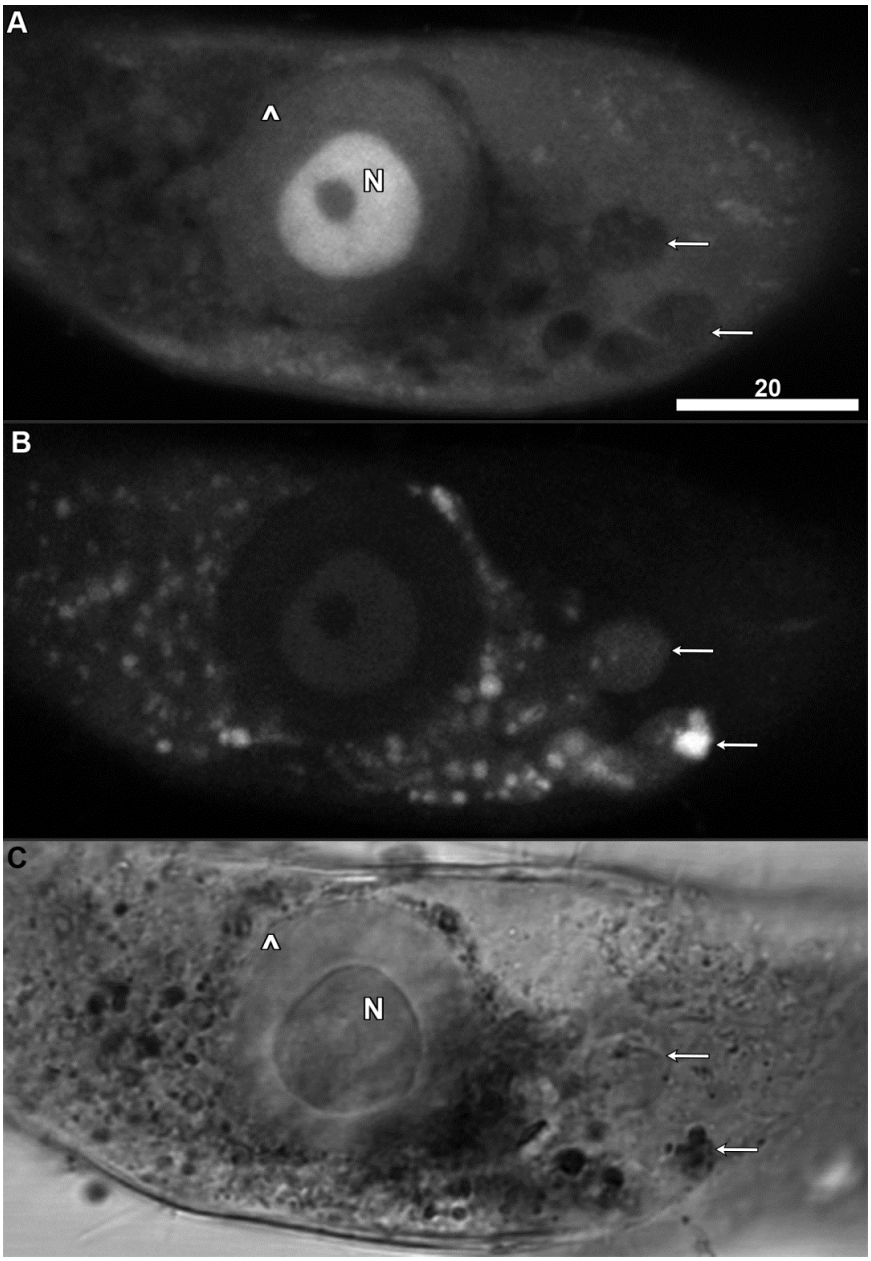

Figure 3.43. Acridine orange imaging of the sub-apical zone of a rhizoid, focused on a plane through the middle of the cell. The nucleus of a rhizoid, as well as various compartments surrounding it in the sub-apical region, is well stained across multiple wavelengths. 488+633 nm excitation. Scale bar = 20 µm.

A,B. Acridine orange (20 µM, 6 h) fluorescence from 500-550 nm (A) and 650-700 nm (B).

A. The nucleolus (N) and nuclear envelope (caret) are visible, but fluorescence is limited from some organelles (arrows).

B. Regions of the cell that were weakly fluorescent at shorter wavelengths (A) fluoresce more brightly at longer wavelengths (arrow), including numerous bright vesicles (asterisk). The nucleolus (N) also had some mild fluorescence.

C. Transmitted light.

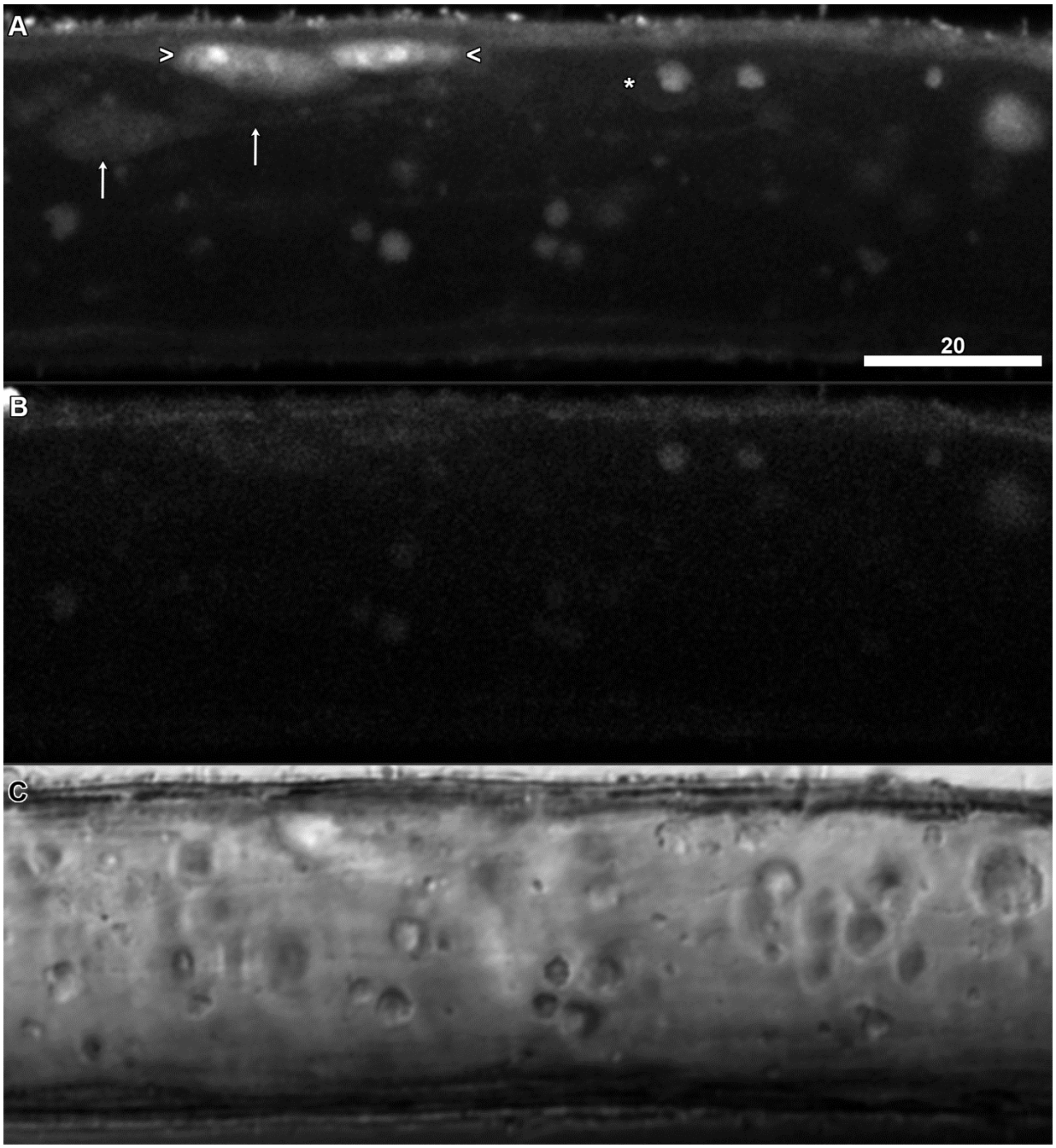

Figure 3.44. Acridine orange imaging of an l-rhizoid, focused on a plane through the middle of the vacuole. 488+633 nm excitation. Scale bar = 20 µm.

A. Acridine orange (20 µM, 6 h) fluorescence from 500-550 nm. Nuclei (carets) are vesicles are labelled. Vesicles in the vacuole seemed to be pulled along by a tubule (arrows).

B. 650-700 nm emission. Chloroplast autofluorescence.

C. Transmitted light.

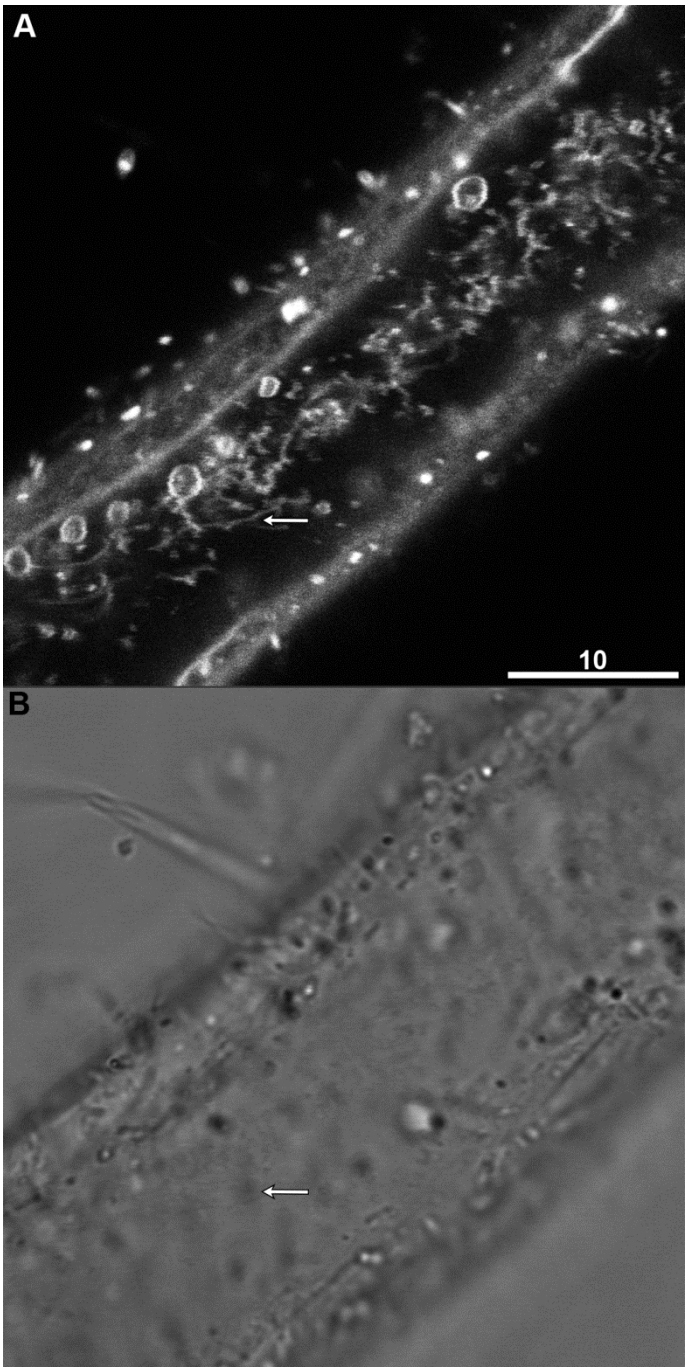

Figure 3.45. MDY-64 imaging of an s-rhizoid showing a cross section through the vacuole, focused on a plane near the tonoplast, using 63x magnification. 456+633 nm excitation. Scale bar = 10 µm.

A. MDY-64 (10 µM, 30 min) fluorescence from 470-520 nm. The upper regions of the vacuole differ from the deeper regions in the relative abundance of structures and infoldings, containing numerous stringy, angular objects (arrow).

B. Transmitted light.

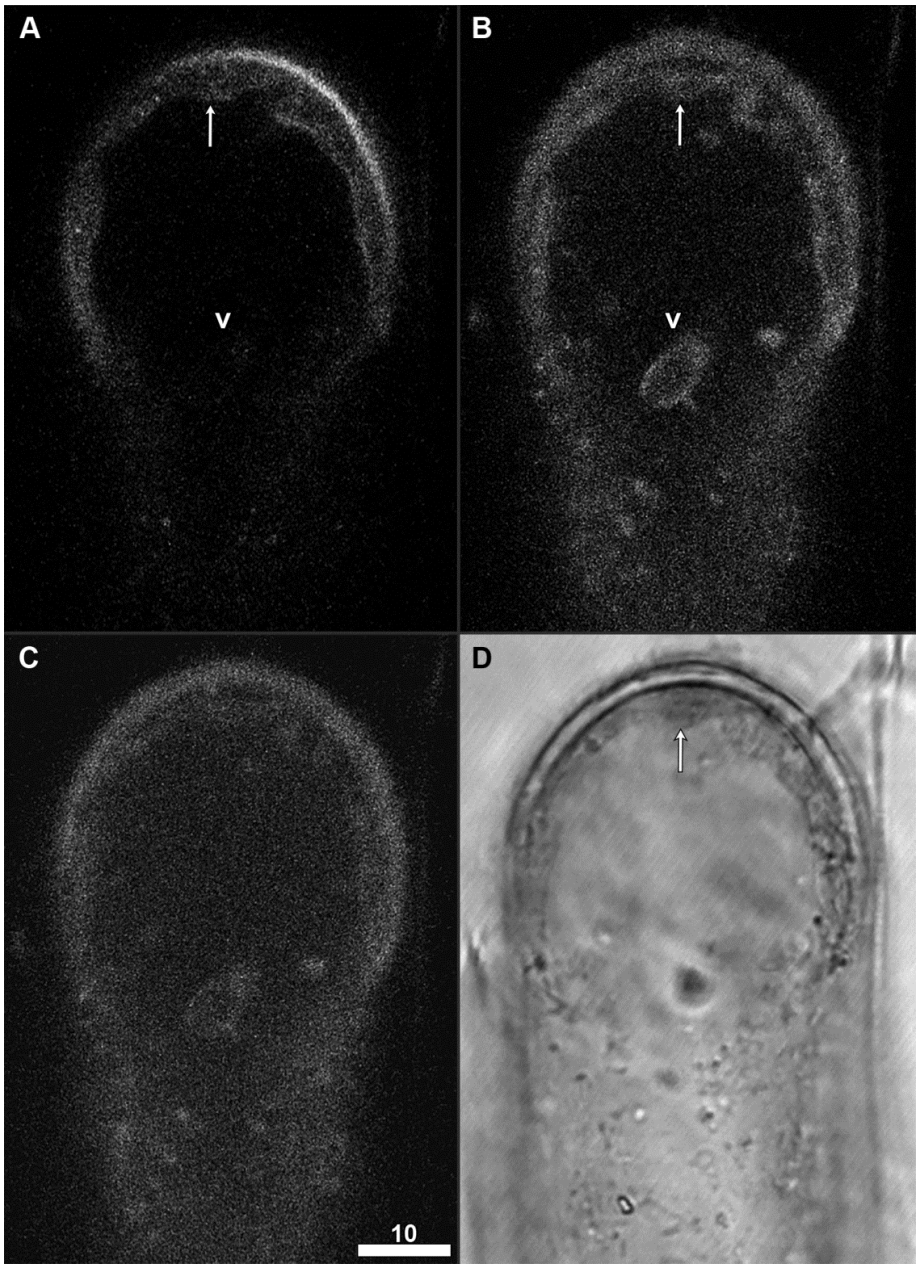

Figure 3.46. An s-rhizoid stained with both MDY-64 and neutral red, showing a cross section through the vacuole. Normally, rhizoids terminate with a nucleus and an extensive, structurally-distinct tip-growing region. Instead, this rhizoid terminated in a semicircle that contained vacuole, suggesting it was no longer actively undergoing tip growth. 456+561+633 nm excitation. Scale bar = 10 µm.

A. MDY-64 (10 µM, 30 min) fluorescence from 470-520 nm. The dynamic tonoplast is sharper in MDY-64 (arrow). The wound plug membranes were not stained (caret).

B. Neutral (10 µM, 10 min) fluorescence from 550-600 nm. The dynamic tonoplast takes on a hazier appearance with neutral red (arrow). Wound plugs labeled better with neutral red (caret).

C. 650-700 nm emission. Chloroplast autofluorescence. The tonoplast is labeled (arrow).

D. Transmitted light.

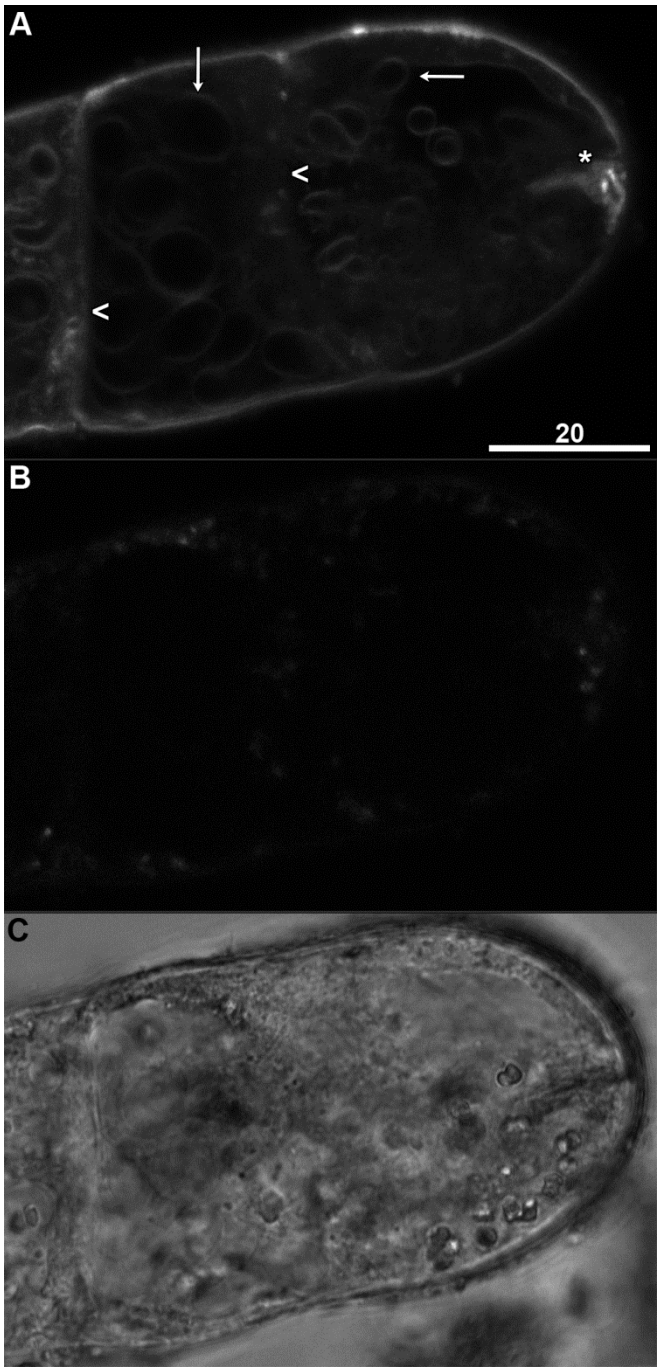

Figure 3.47. MDY-64 imaging of a rhizoid showing anomalous apical tip divisions, focused on a plane half-way through the cell. 456+633 nm excitation. Scale bar = 20 µm.

A. MDY-64 fluorescence (10 µM, 30 min) from 470-520 nm. Numerous membranes pervading the entirety of the intracellular space were present (arrows). At the tip of the end cell existed an area of bright staining with a noticeable tail extending out (asterisk). Boundaries between adjacent cells are marked (caret).

B. 650-700 nm emission. There were no chloroplasts present.

C. Transmitted light.

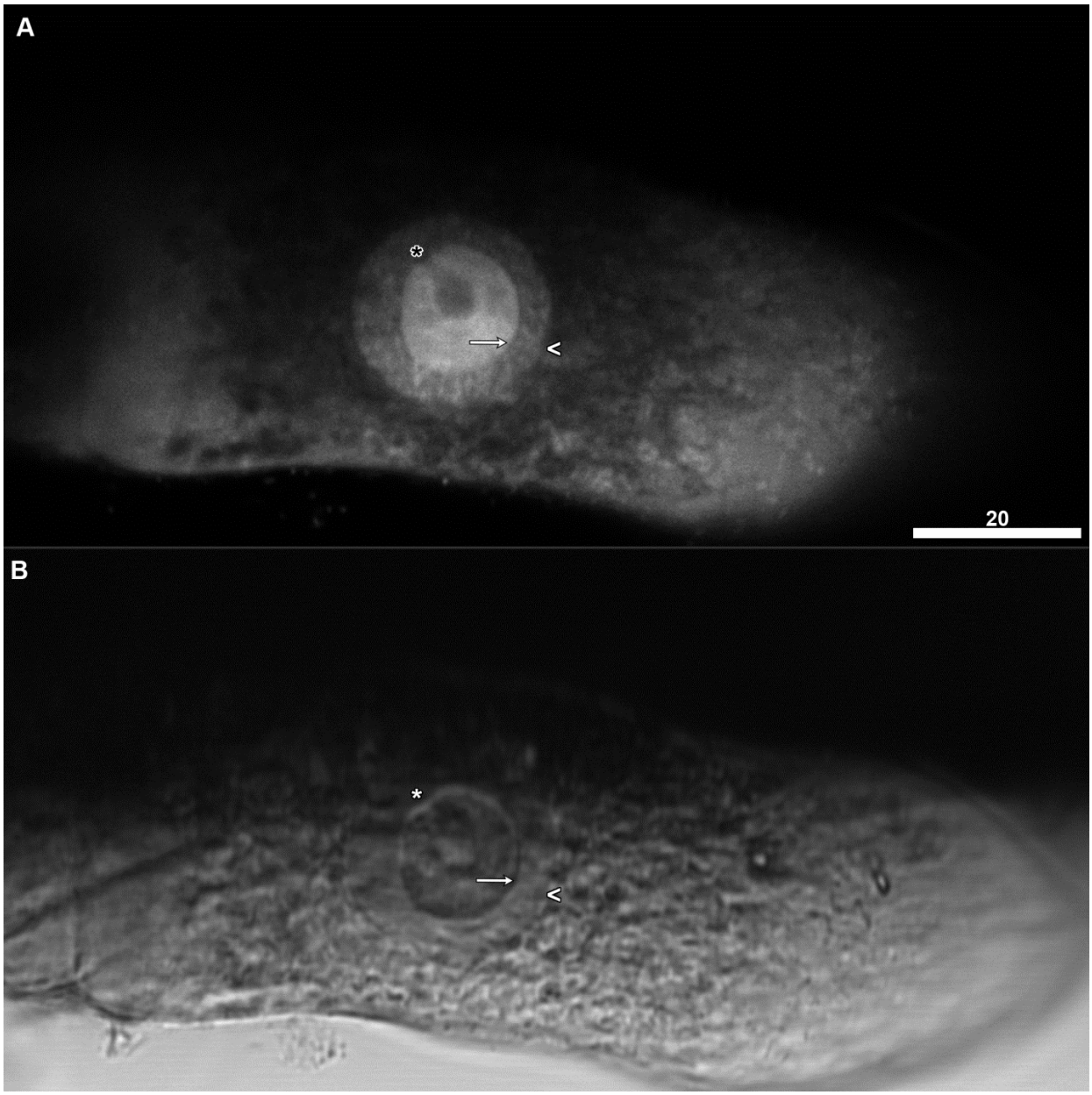

Figure 3.48. Syto-13 imaging of the sub-apical zone of a rhizoid, focused on a plane through the middle of the cell. 488+633 nm excitation. Scale bar = 20 µm.

A. Syto-13 fluorescence (5 µM, 30 min) from 500-550 nm. The nuclear envelope (caret), nucleolus (arrow), and a pocket (asterisk) are all visible.

B. Transmitted light.

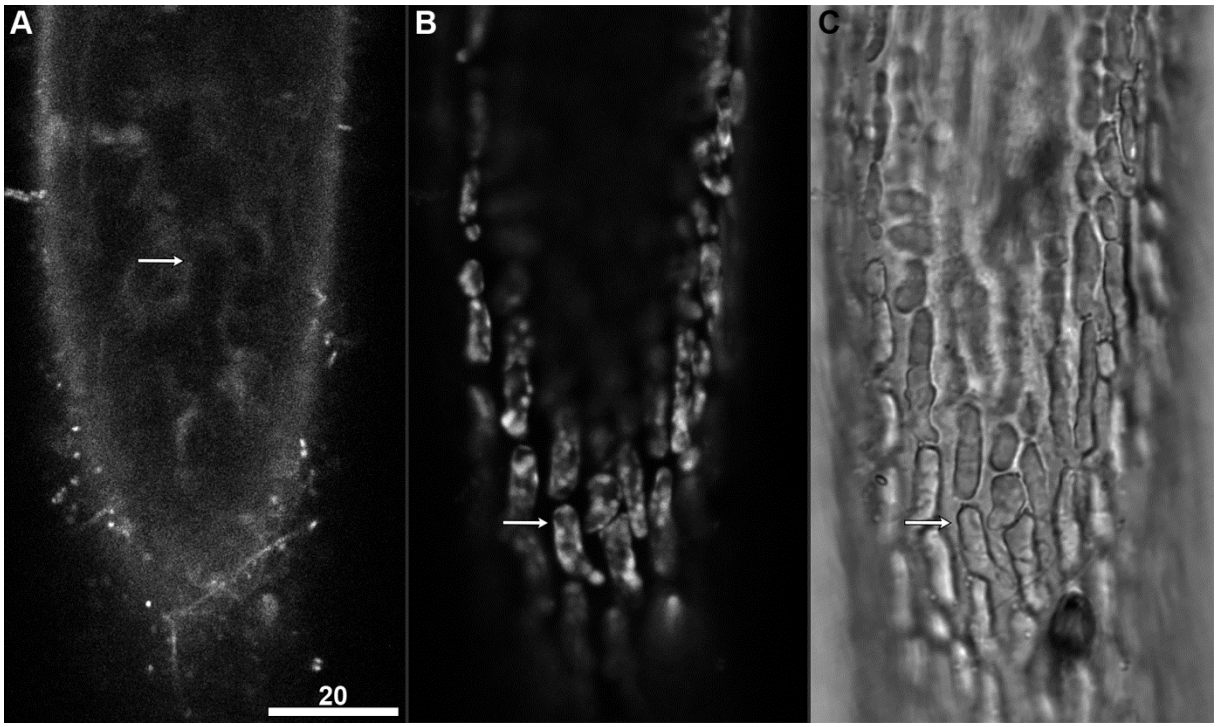

Figure 3.49. Neutral red imaging of an l-rhizoid near the tonoplast, showing their similarity to internodes.

561+633 nm excitation. Scale bar = 20 µm.

A. Neutral red (10 µM, 10 min) fluorescence from 550-600 nm. The staining patterns were similar to internodal cells (Figure 13A).

B. 650-700 nm emission. Chloroplast autofluorescence. Unlike internodes, where chloroplasts were tightly packed and showed even fluorescence, the chloroplast coverage in l-rhizoids was irregular and their fluorescence uneven.

C. Transmitted light.

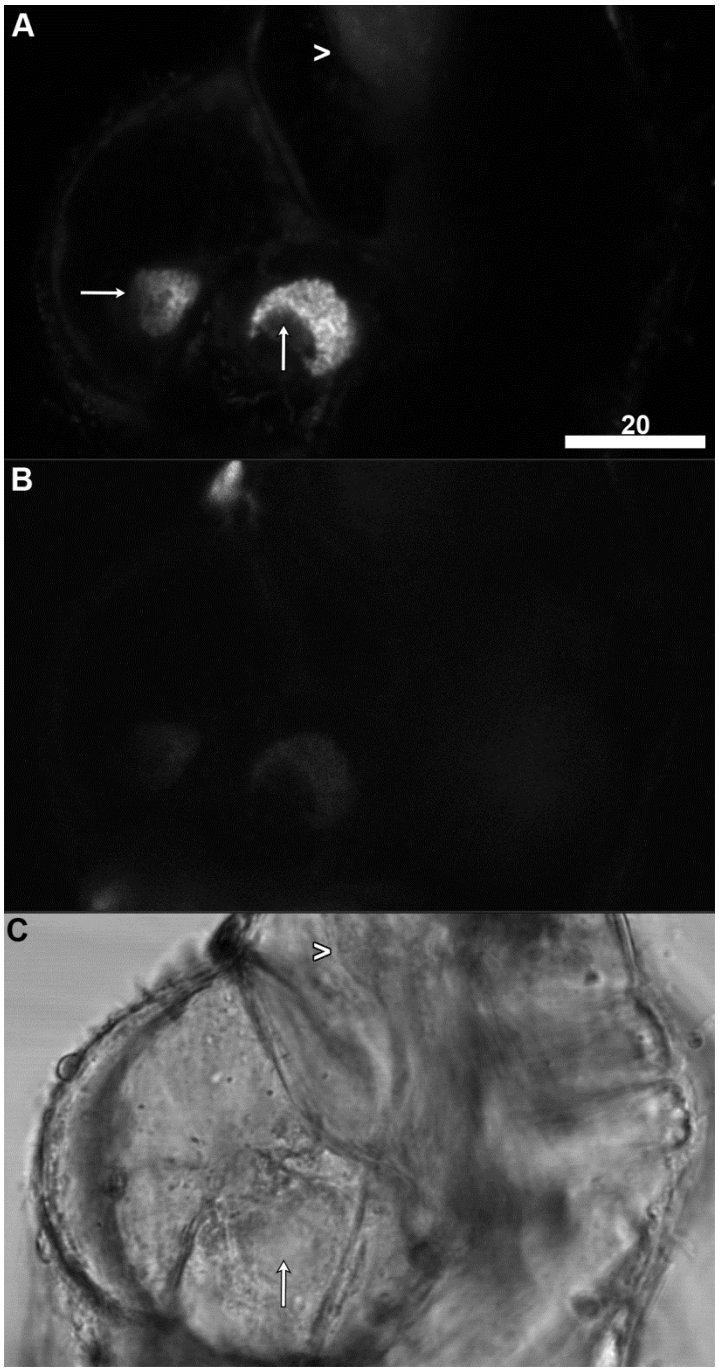

Figure 3.50. Syto-13 imaging of a rhizoid junction cells, focused on a plane through the middle of the cell. 488+633 nm excitation. Scale bar = 20 µm.

A. Syto-13 fluorescence (5 µM, 30 min) from 500-550 nm. The single nuclei (bottom arrows)in the junction cells are sometimes crescent shaped (bottom right arrow). Traces of the streaming endoplasm (caret) from an adjacent rhizoid can be seen.

B. 650-700 nm emission. Chloroplast autofluorescence.

C. Transmitted light, with a nucleus (bottom arrow) and streaming endoplasm (caret).

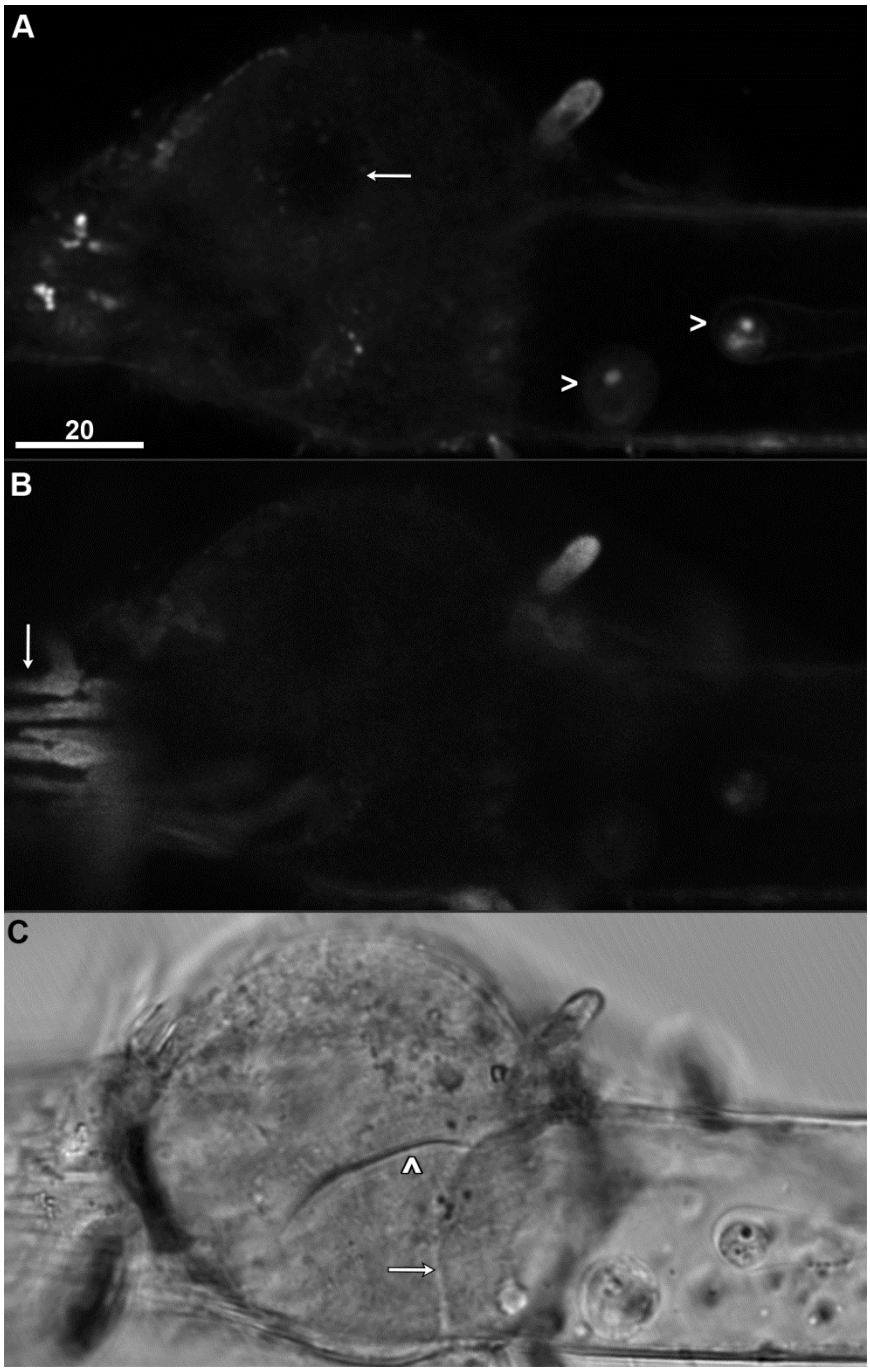

Figure 3.51. Nile red imaging of a rhizoid junction, focused on a plane toward the bottom of the structure where two rhizoids join. 514+633 nm excitation. Scale bar = 20 µm.

A. Nile red fluorescence (50 µM, 30 min) from 525-575 nm. The bottom portion of the nucleus is labelled (arrow). Vacuolar inclusions can be seen in one of the adjoined rhizoids (carets).

B. 650-700 nm emission. One of the adjoining rhizoids was an m-rhizoid with noticeable chloroplast coverage (arrow).

C. Transmitted light. The boundary between two rhizoid node cells (caret) and the boundary between the note cells and the rhizoid (arrow) can be seen.

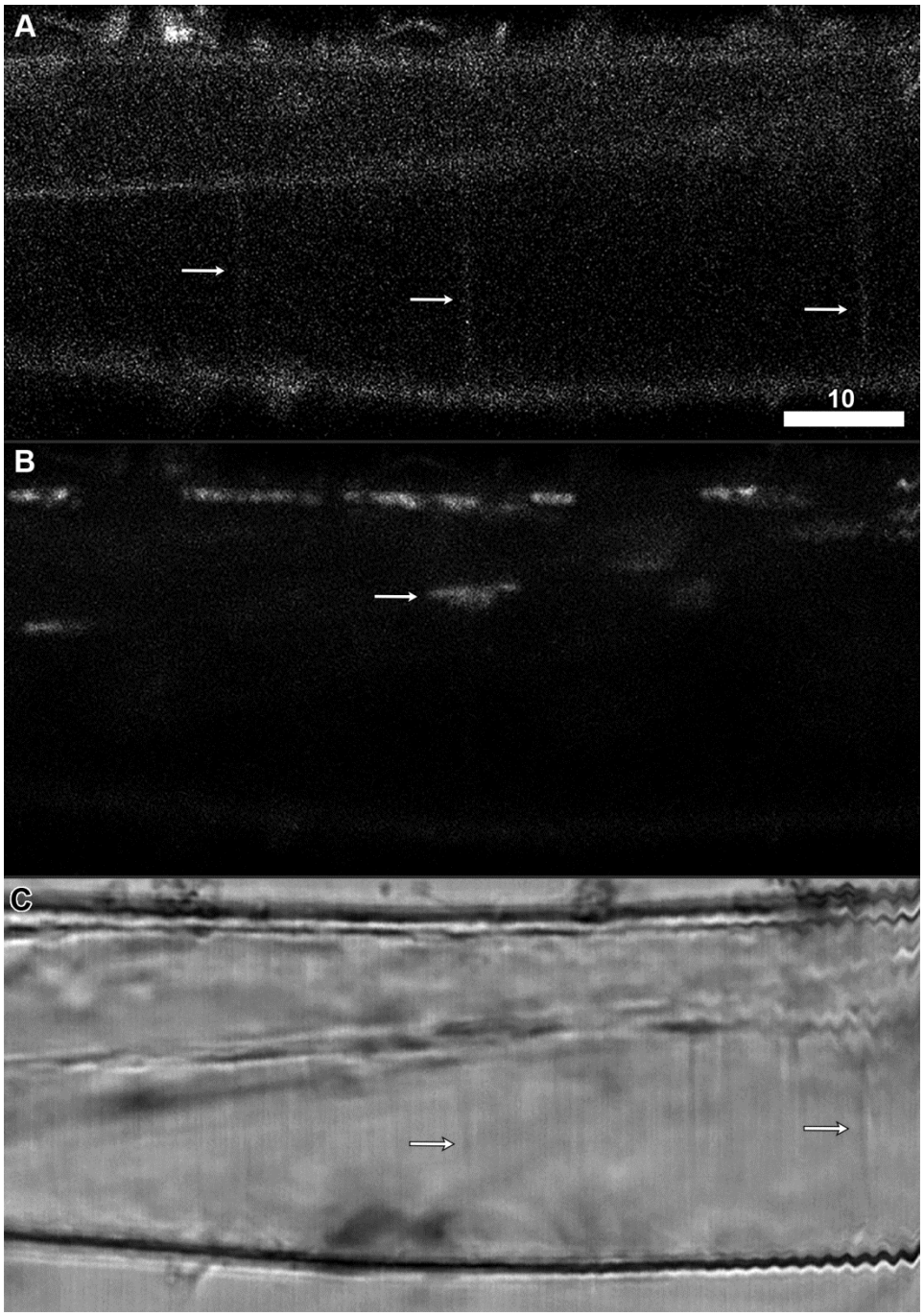

Figure 3.52. Neutral red imaging of a m-rhizoid plasmolyzed with glycerol showing a cross-section through the vacuole. Hechtian strands anchored the plasma membrane to the cell wall. 561+633 nm excitation. Scale bar = 10 µm.

A. Neutral red (10 µM, 10 min) fluorescence from 550-600 nm. Several Hechtian strands anchored strips of plasma membrane to the cell wall (arrows). These structures were ephemeral, and disappeared quickly.

B. 650-700 nm emission. Chloroplast autofluorescence. Note that the developing chloroplast layer (arrow) contracted away from the plasma membrane on the lower side of the cell.

C. Transmitted light. The Hechtian strands were faintly visible with transmitted light (arrows).

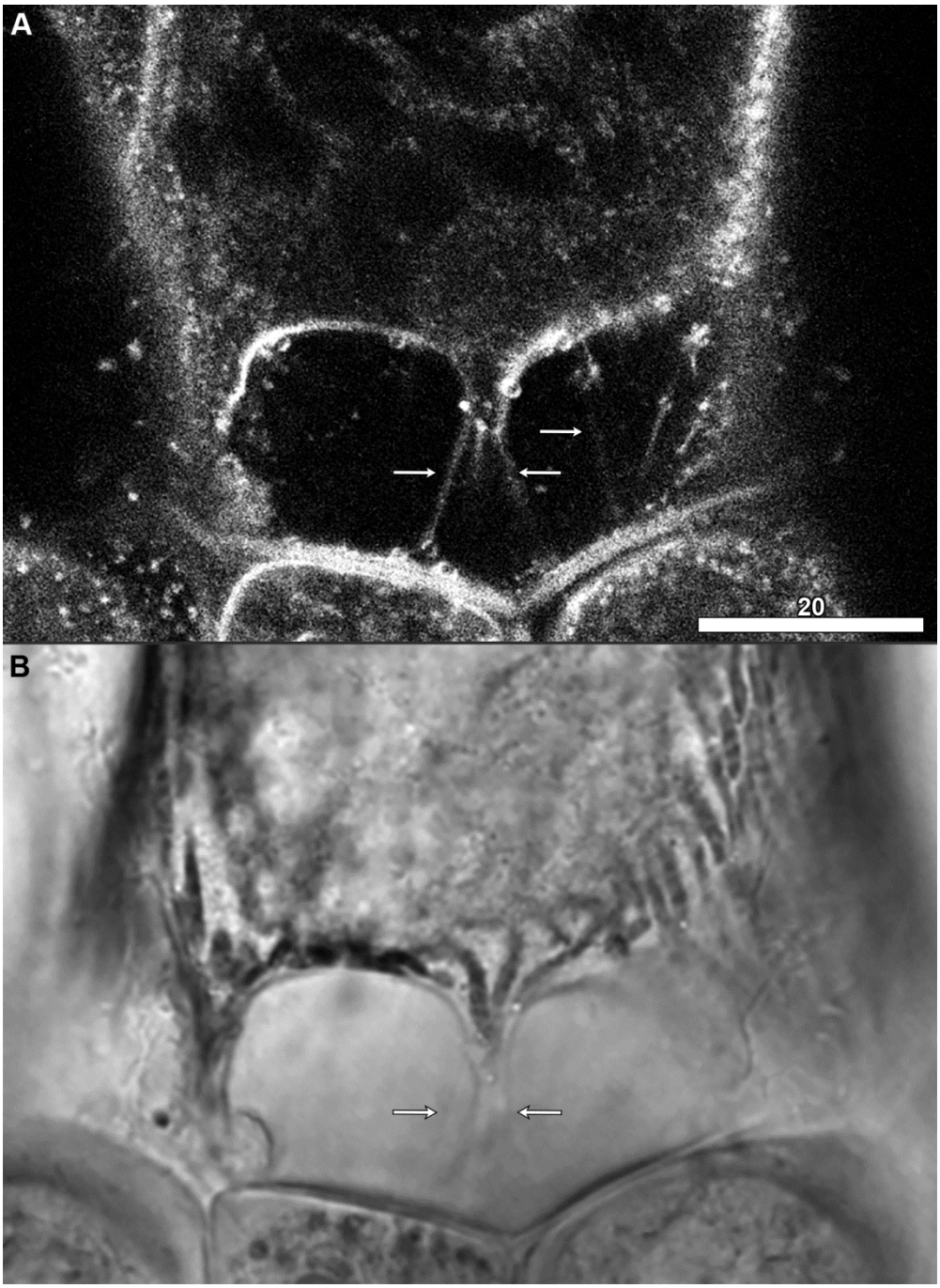

Figure 3.53. MDY-64 imaging of an internodal cell near the nodal junction following plasmolysis with glycerol. As with rhizoids, Hechtian strands were present. 456+633 nm excitation. Scale bar = 20 µm.

A. MDY-64 (10 µM, 30 min) fluorescence from 470-520 nm. Arrows point to Hechtian strands anchoring the plasma membrane to the cell wall, including along the nodal junction.

B. Transmitted light, with Hechtian strands (arrows).

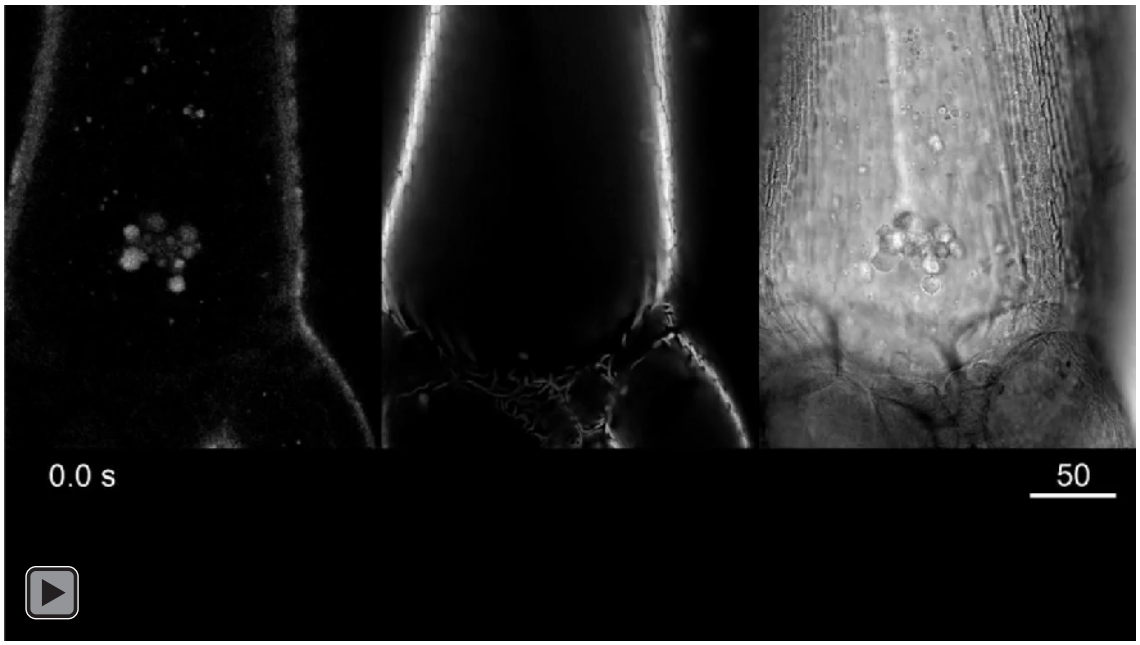

Movie 1. Unstained image sequence of an internode near the nodal junction, focused on a plane through the middle of the vacuole. 561+633 nm excitation. Time in seconds. Scale bar = 50 µm.

Left. Autofluorescence emission from 570-620 nm.

Center. Emission from 650-700 nm. Chloroplast autofluorescence.

Right. Transmitted light.

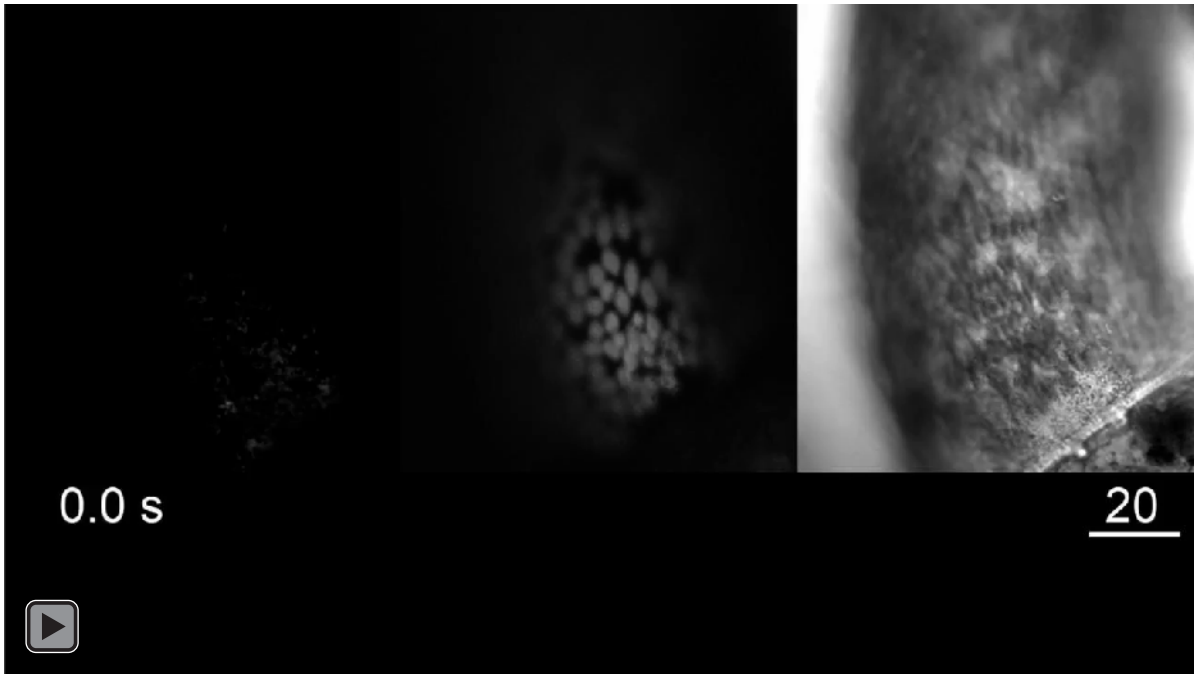

Movie 2. Syto-13 image sequence of a small branchlet cell, changing the focus plane slice-by-slice from the top of the cell through to the bottom. 488+633 nm excitation. Time in seconds. Scale bar = 20 µm.

Left. Syto-13 emission from 500-550 nm. The nuclei come into the plane of view from multiple angles, allowing their discus-like shape to be seen. Mind bleed-through from the chloroplasts can be seen.

Center. 650-700 nm emission. S-rhizoids are lacking in chloroplasts.

Right. Transmitted light.

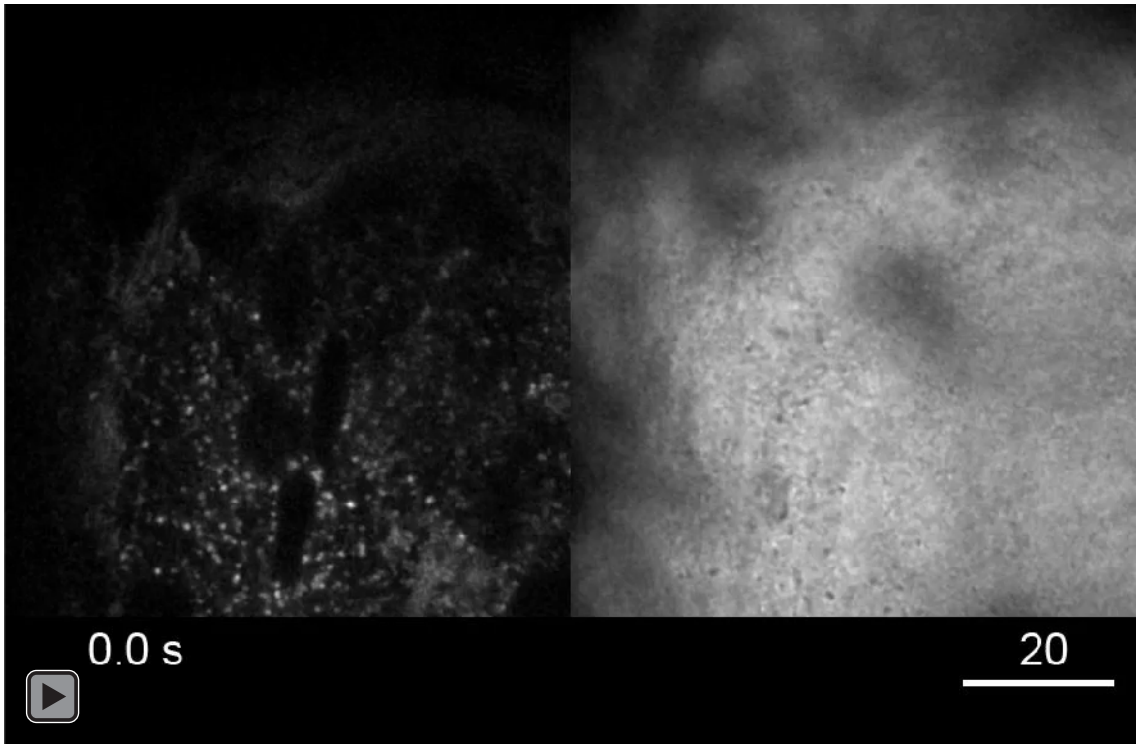

Movie 3. MDY-64 image sequence through a chloroplast-free window, focused on a plane in the endoplasm. 456+633 nm excitation. Time in seconds. Scale bar = 20 µm.

Left. MDY-64 emission from 470-520 nm. As with rhizoids, prolonged irradiation with the chloroplast shielding quickly results in a breakdown of cytoplasmic architecture.

Right. Transmitted light.

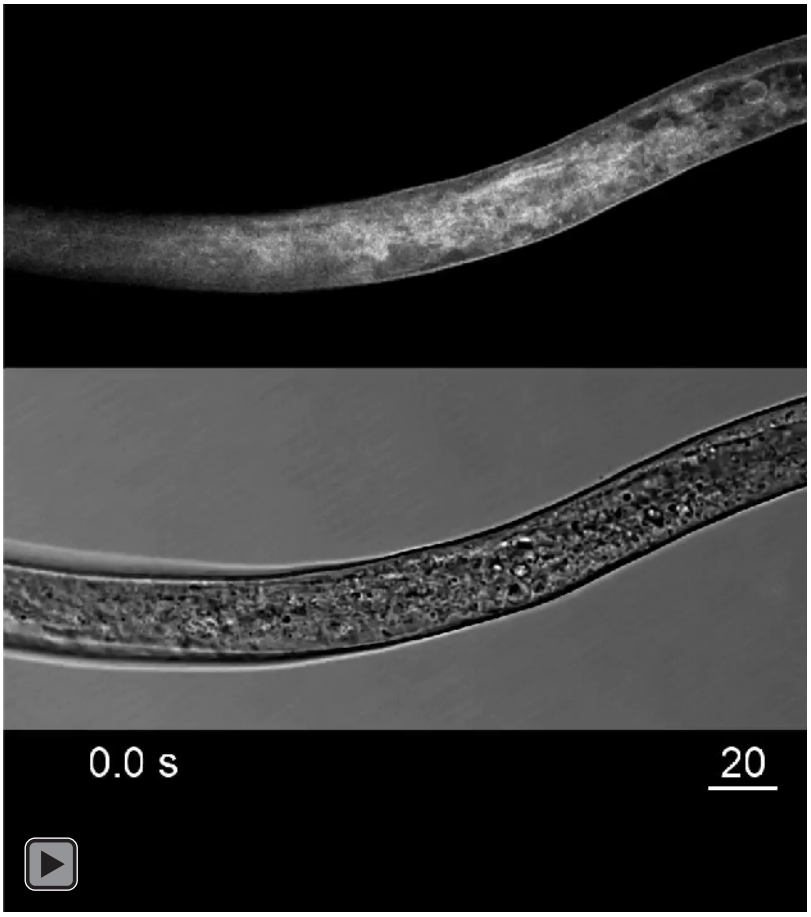

Movie 4. Neutral red image sequence of an s-rhizoid, focused on a plane through the middle of the vacuole, and showing the effects of photodamage due to prolonged irradiation. 561+633 nm excitation. Time in seconds. Scale bar = 20 µm.

Top. Neutral red emission from 570-620 nm. The cytoplasmic architecture, including the vacuole breaks down and becomes comparatively homogenized.

Bottom. Transmitted light.

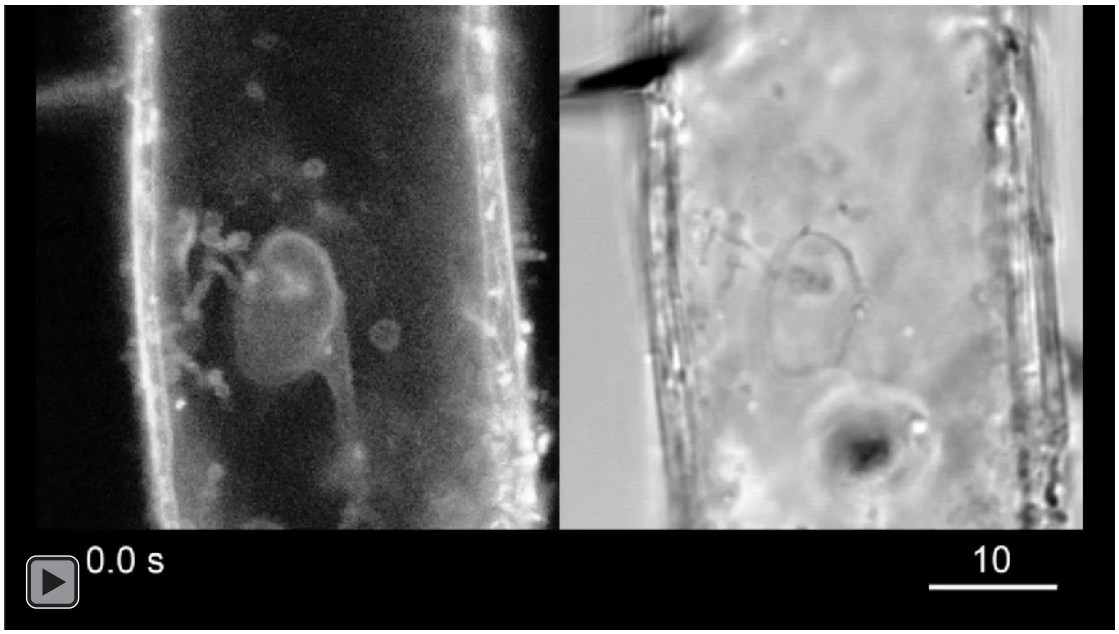

Movie 5. Nile red imaging in an s-rhizoid. 561+633 nm excitation. Time in seconds. Scale bar = 10 µm.

Left. Nile red emission from 570-620 nm. Numerous objects can be seen interacting inside of the vacuole. Of note is a somewhat large, stationary vesicle with significant internal fluorescence, with which numerous other objects flowing near the tonoplast appear to briefly interact. Vesicles attached along a string near the tonoplast on the left side of the vacuole perform striking zig-zag motions as they flow with the rest of the tonoplast.

Right. Transmitted light. Numerous structures from A can be clearly discerned in the transmitted light images as well.

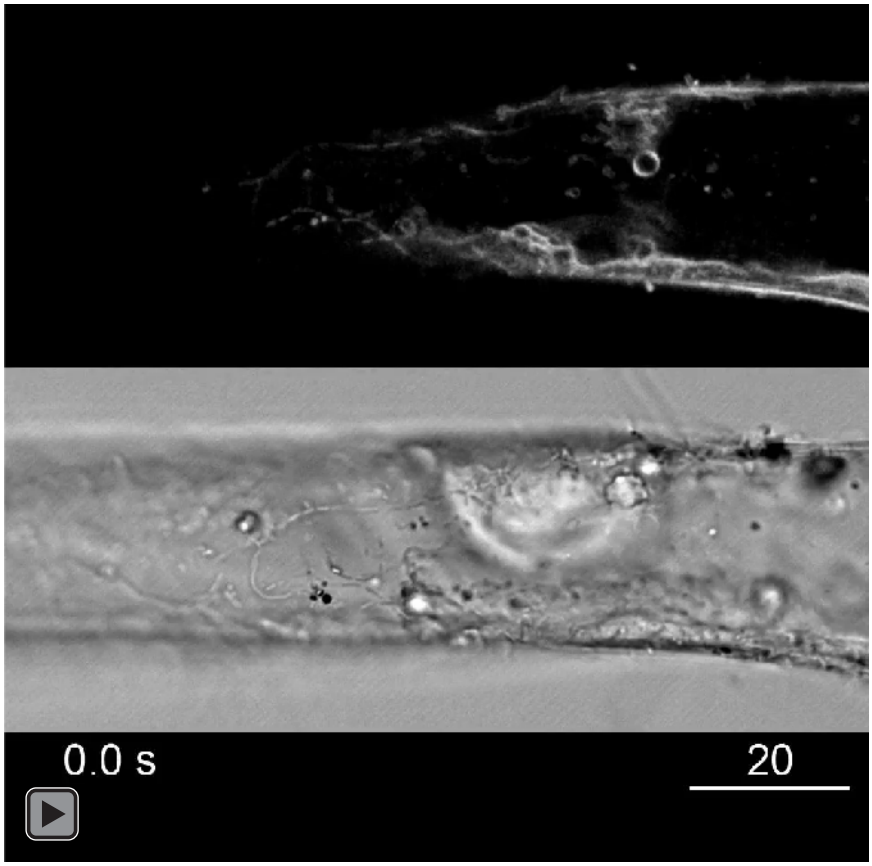

Movie 6. MDY-64 image sequence of an s-rhizoid, changing the focal plane slice-by-slice from the top of the cell through to the bottom. 456+633 nm excitation. Time in seconds. Scale bar = 20 µm.

Top. MDY-64 emission from 470-520 nm. The three-dimensional structure of the membranes surrounding the nucleus are revealed in detail.

Bottom. Transmitted light.

4: Discussion

4.1: Imaging Approaches

In this section, I consider some of the technological and methodological challenges met in the live cell imaging of the streaming endoplasm and vacuole of *Nitella hookeri*. The formidable nature of some of these challenges explains why there is little information in the literature concerning the organization of these aspects of the Characean internode.

4.1:1: Autofluorescence

The results show that apart from chlorophyll autofluorescence from the well-defined and well-located chloroplast layer, generated by most excitation wavelengths and present over a broad range of emissions, none of the cell types in *Nitella* generate much autofluorescence. The cores present at the center of the wound plugs in vacuolar inclusions were autofluorescent, but this was not nearly as bright as the fluorescence from these structures when stained with a range of dyes such as MDY-64 and acridine orange. This was also true of the cores found in rhizoids. Thus, autofluorescence posed little difficulty during the experiments. Furthermore, as Characean cells are extremely large, it can be difficult to orientate oneself when looking at images of the internal cell. The chlorophyll autofluorescence from 650 - 700 nm, well away from the emission of most live cell imaging dyes and readily generated by the 633 nm red laser, serves as a valuable spatial indicator.

4.1:2: Variability In Fluorescence From Live Cell Imaging Dyes

A major problem encountered in this study was that labelling with a variety of different dyes was highly variable. Not only were the structures observed with any one dye variable between cells, but the fluorescence intensity when staining the different cell types with any one dye was also highly variable. Sometimes, staining with dyes such as MDY-64 and, less commonly, $DIOC_6(3)$ would result in rather brilliant fluorescence in internodal cells. This was, however, uncommon, and as staining of internodes with these dyes was typically poor, it was inefficient in terms of microscope time and dye usage. Even neutral red could exhibit considerable variability in the intensity of fluorescence between cells. Several dyes were more reliable in internodal cells. Acridine orange and Blue CMAC were surprisingly effective at imaging internodal cells, generally performing quite well, although imaging with acridine orange using 488 nm excitation was difficult because of the string absorbance of this wavelength by chlorophyll. Blue CMAC, excited at 405 nm, suffered less from this problem. Rhizoids were also found to be variable in their ability to stain, even between rhizoids of the same class. M-Rhizoids, which generally were difficult to image because of their developing chloroplast layer, would occasionally image well.

The reasons for this variability between cells remain unknown. The variability might, perhaps, relate to the ease of imaging. In some cases, it may be that sections of the cell with less chloroplast coverage simply afforded the chance for more light to penetrate, for example at the ends of the cells where chloroplast coverage is reduced. Some observations also indicated that younger cells, towards the apical end of the thallus, imaged better.

Variability may also relate to the effectiveness with which the different cells absorbed the dyes. These differences might relate to the health of the cells, or to more specific effects. One example of problems with dye loading concerned preliminary attempts to stain internodal cells with fluorescein diacetate (FDA) and carboxyfluorescein diacetate (CFDA). These dyes rely on the enzymatic cleavage of an acetate moiety by esterase enzymes, normally found within the cytoplasm, to become fluorescent. In *Nitella*, however, it was observed that overnight incubations in FDA and CFDA resulted in a fluorescent solution surrounding the cells, and no fluorescence within the cells, suggesting the presence of esterases within the cell wall that block the loading of dyes of this type. This observation was different to previous studies in which esterase based dyes have been used to stain vacuolar inclusions in *Lamprothamnium* (Beilby et al., 1999).

Variations in internal dye concentrations between cells might also be a possible reason for variations in imaging. For rhizoids, this might be particularly important, because the s-rhizoids have a higher surface-area-to-volume ratio compared to the m- and l-rhizoids, and a much higher ratio than internodes. This would help the cells absorb the dye more quickly. As the cells seem to be able to concentrate the dye rather effectively, as demonstrated by the ability of cells to accumulate neutral red in the vacuole (Hitchcock 1919, Shimmen and MacRobbie, 1987, Beilby and Shepherd, 1989), and because a finite amount of molecules of dye were applied to each sample, this could result in the smaller cells absorbing most of the dye before larger cells have a chance to accumulate much. These results suggest that it might be prudent to use larger volumes of dye for staining reactions, and to prune away un-needed cells prior to dye incubations, or even trying to isolate single cells.

4.1.3: The Difficulties in Imaging A Fast-Streaming Cell

A second major problem encountered within this study was the high rate of cytoplasmic streaming, not just in the internodes but also in the rhizoids. In this study, attempts were made to overcome the rate of streaming through the use of a variety of technological approaches including increased imaging speed, bidirectional scanning and reduced averaging. All of these come at the cost of reduced image quality.

The problems of streaming-induced image degradation when imaging the contents of the endoplasm and the vacuole might be overcome in two ways. One approach would be to reduce the rate of

cytoplasmic streaming. The mechanical induction of an action potential, which can sometimes be achieved by gently tapping on the coverslip, transiently stopping streaming before streaming recovers. This allows one to observe the gradual change in cell dynamics as speed steadily increases over the course of about a minute, with the cell remaining stationary for about 20 seconds before initial recovery. This might be handy for observing cytoplasmic architecture, but was not easy to reproduce. Further, by stopping streaming, one loses the very cytoplasmic dynamics that make the internode so interesting. Alternatively, streaming might be disrupted through compounds that target the actin microfilaments, including cytochalasin D. Cytochalasin treatments cause a rapid, dose-dependent blockage of streaming that is readily reversible when the drug is washed out. Interestingly, older cells are more susceptible to cytochalasin D, and very young cells can actually recover some streaming even in the presence of cytochalasin (Collings et al., 1996), a process which might relate to the variability in efficacy of dye uptake experiments. However, while these experiments would allow a better view of the endoplasm and vacuole, removing the cytoplasmic streaming would change the structures present there. Thus, drug experiments were not attempted in this study.

The other class of ways to overcome the fast streaming rates is to increase the imaging speed. In this study, this was achieved by using a combination of bi-directional scanning, reducing the imaging area, reducing the resolution, and reducing the number of times each line is scanned. Each of these approaches introduced compromises. Bi-directional scanning doubles scan speed but introduces scan lines into the image. These scan lines, however, do not always meaningfully distort the image, and the scan phase was carefully monitored. Having a smaller area allows for more scans per minute, which allows capture of smaller portions of the cell at a time without issue, but is problematic when imaging larger internodal and branchlet cells. Reducing the resolution increases pixel size, allowing for faster imaging but this produces lower quality images with less fine details. Lastly, one can reduce the number of times each line is scanned, however this produces noisier images due to image noise unique to each image not being averaged out.

The second way to observe the structures within the vacuole and streaming endoplasm would be to use imaging systems that are faster than the Leica SP5 confocal that was available for this study. Such systems, which would still need the confocals ability to generate optical sections, include:

~ the newer generation of conventional confocal microscopes in which “resonant scanning” is used, allowing the excitation light to be scanned across the sample much faster (Jonkman and Brown, 2015).

~ spinning disc confocal microscopy, in which the sample is not scanned by a single light point, but instead by many separate light points concurrently, each generating fluorescence that passes through a separate pinhole (Domozych, 2012, Jonkman and Brown, 2015).

~ light sheet microscopy, in which an entire optical section is rapidly imaged with a sheet of light directed into the system from the side (Truong et al., 2011, Pampaloni et al., 2015).

Unfortunately, these technologies were not available for this study. However, the understanding of the various fluorescent dyes, and the methodological approaches (windows and rhizoids) developed in this study, could be applied to these more advanced imaging systems.

4.1.4: The Threat of Artefacts

Work done by Kamitsubo (1972) is ultimately the foundation of the window technique. Even then, Kamitsubo recognized the value of the windows for improving the ability to view into the endoplasm and vacuole. However, a lack of confocal technology and suitable fluorescent dyes at that time precluded detailed studies of the endoplasm and vacuole. By the time these technologies had been developed, much of plant cell biology had become focussed on model higher plants such as *Arabidopsis thaliana*, and the use of GFP constructs - Characean internodes have somewhat fallen into obscurity. However, with these techniques now available, a *window of opportunity* is now available for probing further into the secrets of the Characean cell. The use of chloroplast-free windows, however, makes the assumption that their generation does not modify structure further inside the cell, and that observations made through them reflect the natural state of the live, healthy cell.

In this study, a 5-minute irradiation with the 405 nm laser running at 50% was found to be sufficient to generate a chlorolast-free window after 24 h recovery -shorter irradiation times did not result in complete loss of chloroplasts by the next day. In other studies, (Williamson et al., 1984), it has been determined that as long as irradiation times are minimised, the sub-cortical actin bundles regenerate, parallel to the direction of streaming, indicating that cells simply extended actin filaments from non-irradiated areas. Window generation results in changes to the cell cortex: Cortical actin microfilaments disappear (Foissner et al., 1996), and randomly-orientated microtubules that normally exist in the cortex align parallel to the direction of streaming (Foissner and Wasteneys, 1999). This confirms that significant changes to the organization of the cell occur after the irradiation treatment and subsequent detachment of chloroplasts. The question, then, is whether irradiation also causes changes in the fast-flowing endoplasm. However, actin immunofluorescence microscopy has confirmed that the actin bundles do regenerate across the chloroplast-free window (Williamson et al., 1984) suggesting that

little change to endoplasmic architecture and dynamics should occur. Similarly, because of the fast streaming rates, anything in the endoplasm or vacuole would flow through the irradiated area in less than a second.

4.1.5: A Gestalt Approach

Nonetheless, it would be foolhardy to simply assume these things without checking them. This created the need for comparison data. The first source of this came from imaging internodes without irradiation treatment. However, getting vivid imaging from internodes is an arduous, inefficient task. Nonetheless, it can be done, and the writer's suspicion is that young internodes and branchlets near the apical nodes of the cell were the cells that achieved the best imaging. However, as this was not noticed until analysis of the images later, this was not systematically investigated. It is being noted as a possible avenue of inquiry, as nearly every case that MDY-64 and $DIOC_6(3)$ imaged vividly in non-rhizoids was in small branchlet cells.

The second source came from imaging the rhizoids, which similar to the internodes, have a fast-streaming endoplasm and a large central vacuole occupying most of the volume of the cell. They are, however, much smaller in size and have little if any chloroplast coverage, facilitating the imaging of their internal contents as light has less material through which to travel to reach the innermost regions of the cell, and little to no chloroplasts to absorb excitation and emission light. This makes them a good source of comparative data, as you can image them much easier and use a far greater variety of dyes on them. However, there are numerous differences as well. For example, there are multiple nuclei streaming throughout the endoplasm of internodal cells. Rhizoids, on the other hand, typically have a single nucleus near the tip of the cell within the sub-apical region. Because of this, rhizoids cannot always serve in a comparative fashion for certain aspects of cytoplasmic architecture and dynamics.

A possibly interesting development here, however, could be the l-rhizoids, which unlike the s and m-rhizoids, had nuclei flowing through the endoplasm. If it turns out that the l-rhizoids have developed in such a way as to more closely resemble the internodes in turns of cytoplasmic architecture and dynamics, they may very well be able to serve as a model in areas where s and m-rhizoids cannot, as experiments showed that while l-rhizoids have extensive chloroplast coverage, it was easier to penetrate through the sparser, non-overlapping chloroplasts of the l-rhizoids, in addition to still having a much smaller volume through which to penetrate excitation light than branchlet or internodal cells.

It seems as if imaging in non-irradiated internodes, chloroplast-free windows, and rhizoids has lined up well enough to create confidence that the observations shown through the chloroplast-free windows reflect the state of a healthy cell, beyond any changes the presence of the dye itself may have caused. However, the chloroplast-free windows and rhizoids have a noticeable weakness that needs to be

considered. Any scientist that has done much imaging of Characean internodes with confocal laser scanning microscopy can tell you how resilient the cells are with regard to being irradiated via laser scanning. An internode can be scanned for up to a minute or more without very noticeable effects. This disappears entirely, however, once the chloroplast layer is stripped away. Both chloroplast-free windows and rhizoids experience significant disruption of cytoplasmic organization if irradiation is prolonged and/or too strong. While the cells can apparently recover from this in time (Own observations), it is best to keep scan times to less than 15-20 seconds. After this, noticeable disruption begins to become evident (Movies 3, 4), starting with an apparent thinning of the vacuole and bulging of the endoplasm, and an arrest of streaming and breakdown of the central vacuole being the end result.

4.2: Imaging Dyes

A total of 7 different fluorescent labels were successfully used for live cell imaging in this study, while labelling with several more dyes such as FDA, CFDA, MitoTracker red and LysoTracker red was attempted unsuccessfully. In this section, I review the results obtained with each of the successful dyes, and note that some of the labelling patterns observed were perplexing.

4.2.1: Neutral Red

Neutral red was the most successful at imaging non-irradiated internodal cells, and generated relatively consistent labelling patterns, unlike dyes such as MDY-64 and $DIOC_6(3)$. Neutral red, therefore, was very valuable for comparison purposes due to its ability to readily image in both rhizoids and internodes. Nonetheless, it still imaged more reliably in rhizoids, and its fluorescence in internodes was noticeably brighter along the neutral line.

The most curious observation with neutral red, however, was the near-complete lack of fluorescence from the central vacuole. Neutral red is a weak acid that accumulates in acidic organelles, and has been used to stain the central vacuole of Characean algae a vibrant red colour (Hitchcock 1919, Shimmen and MacRobbie, 1987, Beilby and Shepherd, 1989). It has also been extensively used as a fluorescence label for the higher plant vacuole (di Sansebastiano et al., 2001, Dubrovsky et al., 2006). In this study, neutral red visibly loaded into the vacuole and stained many things within it, rapidly giving it a red colour at high concentrations, yet little fluorescence emerged. The reason for this lack of fluorescence is unknown. Several possibilities were considered, including that the active fluorophore within commercially-supplied neutral red is not the same as the coloured dye that accumulates in the vacuole. A similar effect has been observed for aniline blue, a chromogenic dye that also binds to callose where it generates fluorescence. In that case, the actual fluorophore within the chemical is a by-product of its

manufacture, contaminating the aniline blue, and not the aniline blue *per se* (Stone et al., 1984). This possibility was tested by comparing the labelling patterns generated by a crude neutral red sample, and a high purity neutral red sample from Molecular Probes. As both gave identical labelling of membranes, and not the central vacuole, it does not appear that contamination of the dye is an issue.

It is also possible that chemical changes to the neutral red inside the central vacuole prevent it from fluorescing. Aggregates can also form at high enough concentrations, which can shift spectral properties further still (see Chapter 1.3.2). Further experiments with neutral red exploring the specifics of how its absorbance and emission spectra change as it protonates and forms into aggregates could shed some more light on this.

4.2.2: MDY-64

MDY-64 is a relatively new fluorescence dye that was introduced as a stain for the fungal tonoplast (Cole et al., 1998, Fratti et al., 2004), and which has recently been used successfully to label the plant tonoplast (Wiltshire and Collings, 2009, Collings, 2013). Given its success in plants, it is not surprising that it effectively imaged the often highly complex tonoplast in internodes (via chloroplast-free windows) and rhizoids. However, while MDY-64 would sometimes image well in un-irradiated internodes, it was a laborious task to find cells that would image bright enough to image. MDY-64, in particular, seems to image the tonoplast in a highly infolded, dynamic state when imaging rhizoids. However, it is possible that the tonoplast is not always in such a state, as other occasions would reveal the tonoplast to be a simple, if undulating, membrane. This staining was extraordinarily bright, producing some of the brightest and most vivid imaging of all dyes.

4.2.3: Acridine orange

Acirdine orange is a traditional fluorescent molecule, in that its use extends back more than several decades. It binds to nucleic acids, and as a weak acid, also loads into the central vacuole. Moreover, acridine orange exhibited highly divergent spectral properties throughout the course of these experiments. On some occasions, acridine orange was excited more strongly with the 488 nm laser line, whereas in other experiments, better excitation was achieved with the weaker 514 nm laser line. Further, the emission wavelengths for acridine orange were also variable, emitting from 500-550 or 525-575 in the cytoplasm and 650 - 700 nm in the vacuole. These shifts in spectra are not surprising as, similar to neutral red, the properties of acridine orange can change based on factors such as pH and concentration through protonation and the formation of aggregates (see Appendix A1.1).

4.2.4: Blue CMAC

Blue CMAC, 7-amino-4-chloromethylcoumarin, is a cell-tracer dye from Molecular Probes that reacts with thiols to produce a fluorescently-tagged molecule that is then pumped into the vacuole. Although this dye has not previously been used with plant cells, unpublished data show it to label the central vacuole in a range of higher plant cells (D. Collings, *personal communication*). In *Nitella*, it proved to be the most reliable dye for staining the central vacuole of internodal cells. Significantly, this provided a convenient negative stain to the endoplasm. In comparison to acridine orange and neutral red, which also loads into the vacuole, Blue CMAC proved superior. Its fluorescence was more reliable, unlike neutral red which did not fluorescence, and occurred at a constant wavelength unlike acridine orange. Moreover, it did not stain the various objects both inside the vacuole and the endoplasm that these dyes did. It is most likely that Blue CMAC would perform well in rhizoids. Unfortunately, however, this could not be tested as no rhizoids were growing and available for study when Blue CMAC was being experimented with.

4.2.5: Other Dyes

The remaining three dyes that were used in this study (Syto-13, Nile red and DIOC6(3)) all behaved in the manner that might be expected of them (in contrast to some of the other dyes used). Syto-13 is highly-specific, membrane-permeant DNA stain. Being membrane permeant, it is more suitable for live cell imaging of nuclei than conventional DNA stains such as propidium iodide and DAPI (diaminophenylindole), and allowed the streaming and rotating nuclei of internodes to be imaged, and on occasions also labelled the mitochondrial nucloid. Similarly, Nile red also acted as expected labelling lipid droplets in both internodes and rhizoids, as has been demonstrated in *Chara corallina* (Foissner 2009). $DIOC_6(3)$, which in plants and animal cells labels mitochondria at low concentrations stains and the endoplasmic reticulum at higher concentrations, was only observed to label mitochondria in this study, although on some occasions a tubular network was also observed (Figure 3.7A, arrow). This did not appear to show classical organization of the endoplasmic reticulum, and the nature of what was being stained remains unknown.

4.3: Vacuolar Imaging

Labelling of the tonoplast with numerous dyes showed that it is nothing like the clean, static structure typically depicted in schematic diagrams of *Nitella* and other Characean algae (Figure 1.1). Instead, it is a complex and highly dynamic structure that is subjected to an extremely turbulent environment, often distorted by the passage of organelles such as nuclei and often highly infolded and tubular. This was confirmed with fluorescent dyes that labelled the tonoplast, notably MDY-64, but also by other dyes such as neutral red which appeared to label the membrane adjacent to the tonoplast, if not the tonoplast itself. A highly complex tonoplast is not necessarily surprising in such dynamic cells. Increased rates of cytoplasmic streaming were observed on confocal imaging of onion epidermal cells, possibly due to laser absorption warming the cells. This increased streaming was accompanied by the development a more complex tonoplast, complete with tubules, infoldings and vacuolar inclusions (Wiltshire and Collings, 2009).

Within the vacuole, various labelling patterns were observed in this study. The wound plug cores and membranes were labelled by a variety of dyes, including MDY-64, neutral red, Nile red, and acridine orange (Figure 3.46A, B, caret) (Figure 3.36A, arrow, Figure 3.44A, asterisk). In their review, Foissner and Wasteneys (2014) suggest that because $DIOC_3(6)$ stains the membranes surrounding the wound plug cores, and because they can be seen within the cisternae of endoplasmic ER, that their membranes may be in turn derived from the ER. However, it is now clear that numerous other dyes will stain them as well without unmistakably staining the ER, having possible implications with regard to this hypothesis. The cores would fluoresce brighter than their normal autofluorescence, which can be seen faintly autofluorescing in unstained cells, particularly with 561 nm excitation (Figure 3.10B, arrow). Also labelled were various other vesicles which lacked cores, which would sometimes appear tethered together anchored to the tonoplast (Figure 3.40A, arrows) or flowing unanchored in the vacuole (Figure 3.44A, arrows). Various types of other inclusions would also appear inside of the vacuole (Figure 3.40A, asterisk). Staining with acridine orange of such inclusions fluorescing at the same wavelength as the endoplasm (Figure 3.42A, B) appears to reinforce the idea that some have an endoplasmic origin, or at least have a similar pH, as per acridine orange's pH-dependent fluorescence. Inclusions were of highly variable size, stain intensity, and stain patterning, and some often had a jagged-like appearance to them (Figure 3.45A, arrow) or would move with striking, zigzag motions (Movie 5).

This all suggests that in *Nitella*, the vacuole is a far more intricate and dynamic organelle than previously realized, as can be indicated by the latest review on Characean cell biology (Foissner and Wasteneys, 2014, section 2.1). There, discussion on inclusions within the vacuole largely pertains to the

wound plugs, and cytoplasmic inclusions resulting from arrested streaming and subsequent bulging and pinching via uneven recovery. Nothing of tethered inclusions, anchored or free-floating, is indicated.

Further adding to this are the vacuolar inclusions and wound plugs present within the vacuole, which often grouped together into structures that the writer refers to as mats and gyres. Both the mats are large accumulations of vacuolar structures that move *en masse* within the cell, with the gyres being smaller and typically showing rotational movements. These gyres are of variable size (taking up to the entirety of the volume of the vacuole to the point where they noticeably bulge into the endoplasm). There appears to be little if any mention of such gyres in the primary literature, and they appear even inside of unstained cells and rhizoids. At this stage, it is uncertain if they are simply an undescribed aspect of cell architecture. It is also unclear how they develop or what purpose they may serve.

There are a few possibilities as to the function of the vacuolar inclusions and wound plugs. The wound plug cores themselves are not believed to function as reserve material as demonstrated by Härtel (1951), who saw no reduction in their size and number after prolonged darkness. In that capacity, it seems unlikely that the gyres and mats serve as any kind of material reserves. Rather, the wound plugs are believed to function in plugging punctures to the cell. The gyres then might simply function as larger wound plugs to help the cell survive even more traumatic puncture events. They may also simply be incidental accumulations of vacuolar material, or deliberately accumulated waste material. High concentrations of certain dyes such as neutral red appeared to increase the prevalence of gyres, although this was not confirmed rigorously. In the case of incidental accumulation, it may be that the apparent increase in gyres from high concentrations of neutral red could be caused by an increase in the viscosity of the vacuole. In the case of deliberate accumulation, it may be an effort by the cell to contain excess dye or cellular material damaged by the excess dye.

4.4: Endoplasm

In the current literature, images of organelles from the endoplasm and vacuole have been obtained for both internodes (Foissner and Wasteneys, 2014, Figures 7.6-7) and for rhizoids (Braun et al., 1999, Figures 2-9). However, most of these images use electron microscopy techniques that employ methods such as cryo-substitution, chemical fixing, and immunogold labelling. Each of these inevitably kill the cells, although efforts are taken to minimize disruptions to cellular structure. Even if these methods are good representations of live cellular structure, such techniques can never capture the dynamics of a live cell, and can never create the certainty of imaging live cells. In this thesis, not only are these organelles imaged vividly in live, healthy cells, each figure was created from images obtained via an image stack composed of a series of images scanned fast enough such that movies capturing these organelles in

motion can be created from them. While only 6 movies are included in this thesis, every single figure could be theoretically replaced with its own movie.

Additionally, the research on rhizoids is largely focused on the apical and sub-apical regions, with comparatively little attention paid to the basal streaming region, a result of research being largely focused around the tip-growing region of the cell (Gerber et al., 1991, Braun et al., 1999), and particularly the cytoskeleton (Sievers et al., 1991, Braun and Wasteneys, 1998). This thesis provides, to the writer's knowledge, the first comprehensive effort to obtain image data focused mostly on this region of the rhizoids.

4.5: Junction Cells and Hechtian Strands.

Rhizoids often form junctions that sit far from the growing apical region. At these junctions, roughly spherical cells, which the writer calls junction cells, can be located, and from which secondary rhizoid formation can occur (Fritsch 1948). Information about the internal structure and development of these cells is sparse in the scientific literature, as are any pictures, of which only one could be found in a recent paper (Gerber et al., 1995, Figure 2), itself citing a figure from Fritsch (1948) which is only a drawing and not an actual image of a rhizoid junction. Because of this, imaging of these junction cells was done whenever possible in order to provide the first modern imaging of these begin providing a body of image data on these fascinating structures.

Hechtian strands have previously reported in *Chara* (Foissner 2009) following plasmolysis with 300 mM sucrose and staining with Bodipy PC. In higher plants, strands of ER are known to extend into the Hechtian strands (Oparka 1994) (Lang-Pauluzzi 2000). A simple and likely explanation is that the MDY-64 partially stained the plasma membrane. It may be possible that the vacuole was present within the Hechtian strands, as evidenced by staining with MDY-64 and neutral red. If it turns out these dyes also stain the ER in the endoplasm, this may be responsible for the fluorescence as well.

4.6: Conclusions

While the techniques presented in this paper were a success, this is only the beginning. A window has been opened, literally and metaphorically, into the endoplasm and vacuole of Characean cells, but these experiments were only cursory. The exact nature of the tonoplast dynamics seen here warrant further investigation, especially to clarify uncertainties with regards to why the tonoplast appears infolded and entubuled at some times, and other times a simple undulating membrane. In addition to this, there is the variance associated with the network of membranes and tubules frequently seen adjacent to the tonoplast. Further investigations are also needed to fully explore the nature of rhizoid

greening and the extent to which it causes changes in cellular organization, so that scientists can better select a class of rhizoids for their experiments. Current evidence suggests that rhizoids are capable of transitioning into an internode-like state in order to give rise to new thalli, as has been observed at least once (Gerber et al., 1995), which is bolstered by the demonstration of endoplasmic nuclei within l-rhizoids here. There are also the reasons and mechanisms behind why some rhizoids, even s-rhizoids, seem to lack a nucleus or in some cases the typical apical and sub-apical regions surrounding the nucleus. Lastly, experiments are needed to ascertain whether or not a 405 nm laser (or 353 nm, as per recommended by Molecular Probes) would be too disruptive to delicate rhizoids and the unshielded endoplasm.

References

Ackers, D., Buchen, B., Hejnowicz, Z., & Sievers, A. (2000). The pattern of acropetal and basipetal cytoplasmic streaming velocities in *Chara* rhizoids and protonemata, and gravity effect on the pattern as measured by laser-Doppler-velocimetry. *Planta, 211(1),* 133-143. DOI: 10.1007/s004250000273

Allen, N.S., & Brown, D.T. (1988). Dynamics of the endoplasmic reticulum in living onion epidermal cells in relation to microtubules, microfilaments and intracellular particle movement. *Cell Motility and the Cytoskeleton, 10(1-2)*, 153-163. doi: 10.1002/cm.970100120

Andrews, M. (1987). Phosphate uptake by the component parts of *Chara hispida*. *British Phycological Journal, 22(1),* 49-53. doi: 10.1080/00071618700650061

Andrews, K., Reed, S. M., & Masta, S. E. (2007). Spiders fluoresce variably across many taxa. *Biology Letters, 3*(3), 265-267. doi: 10.1098/rsbl.2007.0016

Appelgren, K., & Mattila, J. (2005). Variation in vegetation communities in shallow bays of the northern Baltic Sea*. Aquatic Botany, 83(1),* 1-13. doi: 10.1016/j.aquabot.2005.05.001

Bauhin, C. 1623. Pinax theatri botanici, 219.

Beilby, M. J. (2016). Multi-scale Characean experimental system: From electrophysiology of membrane transporters to cell-to-cell connectivity, cytoplasmic streaming and auxin metabolism. *Frontiers in Plant Science, 7*, 1052. doi: 10.3389/fpls.2016.01052

Beilby, M. J., & Casanova, M. T. (2014). *The Physiology of Characean Cells.* Springer-Verlag, Heidelberg.

Beilby, M.J., Cherry, C.A., & Shepherd, V.A. (1999) Dual turgor regulation response to hypotonic stress in *Lamprothamnium papulosum. Plant Cell and Environment, 22(4),* 347-359. doi: 10.1046/j.1365-3040.1999.00406.x

Beilby, M. J., & Shepherd, V. A. (1989). Cytoplasm-enriched fragments of *Chara*: Structure and electrophysiology. *Protoplasma, 148(2-3),* 150-163. doi: 10.1007/BF02079334

Bharathan, S., & Sundralingam, V. (1984). Developmental morphology of *Lamprothamnium papulosum* (Wallr.) J. Groves and *Lamprothamnium succinctum* (A. Br.) RD Wood. *Journal of the Indian Botanical Society, 63*, 97-107.

Blindow, I. (2000). Distribution of charophytes along the Swedish coast in relation to salinity and eutrophication. *International Review of Hydrobiology, 85(5-6)*, 707-717. doi: 10.1002/1522-2632(200011)85:5/6<707::AID-IROH707>3.0.CO;2-W

Boot, K. J. M., Libbenga, K. R., Hille, S. C., Offringa, R., & van Duijn, B. (2012). Polar auxin transport: an early invention. *Journal of Experimental Botany, 63*(11), 4213-4218. doi: 10.1093/jxb/ers106

Bornette, G., & Arens, M.-F. (2002). Charophyte communities in cut-off river channels: The role of connectivity. *Aquatic Botany, 73(2),* 149-162. doi: 10.1016/S0304-3770(02)00017-7

Braun, M., & Wasteneys, G. O. (1998). Reorganization of the actin and microtubule cytoskeleton throughout blue-light-induced differentiation of characean protonemata into multicellular thalli. *Protoplasma, 202(1)*, 38-53. doi: 10.1007/bf01280873

Braun, M., Buchen, B., & Sievers, A. (1999). Electron microscopic analysis of gravisensing *Chara* rhizoids developed under microgravity conditions. *The FASEB Journal, 13(9001),* S113-S120.

Broady, P., Flint, E., Nelson, W., Cassie Coope, V., De Winton, M., & Novis, P. (2012). Phylum Chlorophyta and Charophyta: Green Algae. New Zealand Inventory of Biodiversity. Volume Three. Kingdoms Bacteria, Protozoa, Chromista, Plantae, Fungi. Canterbury University Press, Christchurch, 347-381.

Casanova, M. (1991). An SEM study of developmental variation in oospore wall ornamentation of three *Nitella* species (Charophyta) in Australia. *Phycologia, 30(3),* 237-242. doi: 10.2216/i0031-8884-30-3-237.1

Casanova, M. T. (1994). Vegetative and reproductive responses of charophytes to water-level fluctuations in permanent and temporary wetlands in Australia. *Marine and Freshwater Research, 45(8),* 1409-1419. doi: 10.1071/MF9941409

Casanova, M. T., & Brock, M. A. (1990). Charophyte germination and establishment from the seed bank of an Australian temporary lake. *Aquatic Botany, 36(3),* 247-254. doi: 10.1016/0304-3770(90)90038-M

Casanova, M. T., & Brock, M. A. (1999). Life histories of Charophytes from permanent and temporary wetlands in eastern Australia. *Australian Journal of Botany, 47*(3), 383-397. doi: 10.1071/BT97086

Casanova, M. T., & Brock, M. A. (1999a). Charophyte occurrence, seed banks and establishment in farm dams in New South Wales. *Australian Journal of Botany, 47(3),* 437-444. doi:10.1071/BT97099

Casanova, M. T., de Winton, M. D., Karol, K. G., & Clayton, J. S. (2007). *Nitella hookeri* A. Braun (Characeae, Charophyceae) in New Zealand and Australia: Implications for endemism, speciation and biogeography. *Charophytes, 1*, 2-18. doi: 10.13140/2.1.4989.7604

Collings, D.A., Wasteneys, G.O., & Williamson, R.E. (1995) Cytochalasin rearranges cortical actin of the alga *Nitella* into short, stable rods. *Plant and Cell Physiology*, *36(5),* 765-772.

Collings, D.A., Wasteneys, G.O., & Williamson, R.E. (1996) Microtubule / actin interactions in the alga *Nitella*: analysis of the mechanism by which microtubule depolymerization potentiates cytochalasin's effects on streaming. *Protoplasma, 191(3),* 178-190. doi: 10.1007/BF01281816

Cole, L., Orlovich, D.A., & Ashford, A.E. (1998) Structure, function, and motility of vacuoles in filamentous fungi. *Fungal Genetics and Biology 24(1-2)*, 86–100. doi: 10.1006/fgbi.1998.1051

Cook, M. E., Graham, L. E., Botha, C. E. J., & Lavin, C. A. (1997). Comparative ultrastructure of plasmodesmata of *Chara* and selected bryophytes: Toward an elucidation of the evolutionary origin of plant plasmodesmata. *American Journal of Botany, 84*(9), 1169-1178. doi: 10.2307/2446040

Corti, B. (1774) *Osservazioni Microscopiche Sulla Tremella E Sulla Circolazione Del Fluido in Una Pianta Acquajuola*. G. Rocchi, Lucca.

de Winton, M. D., Casanova, M. T., & Clayton, J. S. (2004). Charophyte germination and establishment under low irradiance. *Aquatic Botany, 79(2),* 175-187. doi: 10.1016/j.aquabot.2004.01.013

di Sansebastiano, G. P., Paris, N., Marc-Martin, S., & Neuhaus, J.-M. (2001). Regeneration of a lytic central vacuole and of neutral peripheral vacuoles can be visualized by green fluorescent proteins targeted to either type of vacuoles. *Plant Physiology, 126(1),* 78-86. doi: 10.1104/pp.126.1.78

Delaux, P.-M., Xie, X., Timme, R. E., Puech-Pages, V., Dunand, C., Lecompte, E., Delwiche, C. F., Yoneyama, K., Bécard, G., Séjalon-Delmas, N. (2012). Origin of strigolactones in the green lineage. *New Phytologist, 195*(4), 857-871. doi: 10.1111/j.1469-8137.2012.04209.x

Domozych, D.S. (2012) The quest for four-dimensional imaging in plant cell biology: it's just a matter of time. *Annals of Botany, 110(2)*, 461-474. doi: 10.1093/aob/mcs107

Dubrovsky, J.G., Guttenberger, M., Saralegui, A., Napsucially-Mendivil, S., Voigt, B., Baluska, F., & Menzel, D. (2006) Neutral red as a probe for confocal laser scanning microscopy studies of plant roots. *Annals of Botany, 97(6),* 1127-1128. doi: 10.1093/aob/mcl045

Dugdale, T. M., de Winton, M. D., & Clayton, J. S. (2001). Burial limits to the emergence of aquatic plant propagules. *New Zealand Journal of Marine and Freshwater Research, 35(1),* 147-153. doi: 10.1080/00288330.2001.9516984

Foissner, I. (2004). Microfilaments and microtubules control the shape, motility, and subcellular distribution of cortical mitochondria in Characean internodal cells. *Protoplasma, 224(3-4),* 145-157. doi: 10.1007/s00709-004-0075-1

Foissner, I., & Wasteneys, O. G. (1999). Microtubules at wound sites of *Nitella* internodal cells passively co-align with actin bundles when exposed to hydrodynamic forces generated by cytoplasmic streaming. *Planta, 208(4),* 480-490. doi: 10.1007/s004250050585

Foissner, I., & Wasteneys, G. O. (2014). Characean internodal cells as a model system for the study of cell organization. *International Review of Cell and Molecular Biology, 311,* 307-364. doi: 10.1016/B978-0-12-800179-0.00006-4

Foissner, I., Lichtscheidl, I. K., & Wasteneys, G. O. (1996). Actin-based vesicle dynamics and exocytosis during wound wall formation in Characean internodal cells. *Cell Motility and the Cytoskeleton, 35(1)*, 35-48. doi: 10.1002/(SICI)1097-0169(1996)35:1<35::AID-CM3>3.0.CO;2-H

Foissner, I., Menzel, D., & Wasteneys, G. O. (2009). Microtubule-dependent motility and orientation of the cortical endoplasmic reticulum in elongating Characean internodal cells. *Cell Motility and the Cytoskeleton, 66(3),* 142-155. doi: 10.1002/cm.20337

Fotopoulos, V. (2012). Never say dye. *Plant Signaling & Behavior, 7(3),* 342-344. doi: 10.4161/psb.19236

Fratti, R.A., Jun, Y., Merz, A.J., Margolis, N., & Wickner, W. (2004) Interdependent assembly of specific regulatory lipids and membrane fusion proteins into the vertex ring domain of docked vacuoles. *Journal of Cell Biology, 167(6),* 1087-1098. doi: 10.1083/jcb.200409068

Galbraith, C.G., & Galbraith, J.A. (2011) Super-resolution microscopy at a glance. *Journal of Cell Science, 124(10),* 1607-1611. doi: 10.1242/jcs.080085

Gerber, N., Bisson, M., & Chau, R. (1995). Anomalous differentiation in *Chara* rhizoids: Effect of gravity vector. *International Journal of Plant Sciences, 156(6),* 747-755. doi: 10.1086/297298

Greenspan, P., Mayer, E. P., & Fowler, S. D. (1985). Nile red: A selective fluorescent stain for intracellular lipid droplets. *Journal of Cell Biology, 100(3),* 965-973. doi: 10.1083/jcb.100.3.965

Grolig, F., Williamson, R., Parke, J., Miller, C., & Anderton, B. (1988). Myosin and Ca^{2+}-sensitive streaming in the alga *Chara*: detection of two polypeptides reacting with a monoclonal anti-myosin and their localization in the streaming endoplasm. *European Journal of Cell Biology, 47*(1), 22-31.

Han, J., & Burgess, K. (2010). Fluorescent indicators for intracellular pH. *Chemical Reviews, 110(5),* 2709-2728. doi: 10.1021/cr900249z

Johnson, I., & Spence, M.T.Z. (2010). *The Molecular Probes Handbook—A Guide to Fluorescent Probes and Labeling Technologies*. 11th edition, Life technologies, Carlsbad.

Härtel, O. (1951). Die Stachelkugeln von *Nitella*. *Protoplasma, 40(3),* 526-540. doi: 10.1007/bf01247669

Hitchcock, R. (1919). Preliminary note on a differential staining of the cytoplasm of Characeae. *Bulletin of the Torrey Botanical Club, 46(9),* 375-379.

Hodick, D., & Sievers, A. (1998). Hypergravity can reduce but not enhance the gravitropic response of *Chara globularis* protonemata. *Protoplasma, 204*(3), 145-154. doi: 10.1007/bf01280321

Höfte, H., Peaucelle, A., & Braybrook, S. (2012). Cell wall mechanics and growth control in plants: the role of pectins revisited. *Frontiers in Plant Science, 3*, 121. doi: 10.3389/fpls.2012.00121

Hope, A. B., & Walker, N. A. (1975). The physiology of giant algal cells: Taylor & Francis, New York.

Jensen, M. S., & Bainton, D. F. (1973). Temporal changes in pH within the phagocytic vacuole of the polymorphonuclear neutrophilic leukocyte. *Journal of Cell Biology, 56(2),* 379-388. doi: 10.1083/jcb.56.2.379

Jin, Q., Scherp, P., Heimann, K., & Hasenstein, K. H. (2008). Auxin and cytoskeletal organization in algae. *Cell Biology International, 32*(5), 542-545. doi: 10.1016/j.cellbi.2007.11.005

Johannes, E., & Felle, H. (1990). Proton gradient across the tonoplast of *Riccia fluitans* as a result of the joint action of two electroenzymes. *Plant Physiology, 93*(2), 412-417. doi: 10.1104/pp.93.2.412

John, D. M., & Moore, J. A. (1987). An SEM study of the oospore of some *Nitella* species (Charales, Chlorophyta) with descriptions of wall ornamentation and an assessment of its taxonomic importance. *Phycologia, 26(3),* 334-355. doi: 10.2216/i0031-8884-26-3-334.1

Jonkman, J., & Brown, C.M. (2015) Any way you slice it—A comparison of confocal microscopy techniques. *Journal of Biomolecular Techniques, 26(2)*, 54–65. doi: 10.7171/jbt.15-2602-003

Kamitsubo, E. (1972). A 'window technique' for detailed observation of characean cytoplasmic streaming. *Experimental Cell Research, 74(2),* 613-616. doi: 10.1016/0014-4827(72)90430-2

Karol, K. G., McCourt, R. M., Cimino, M. T., & Delwiche, C. F. (2001). The closest living relatives of land plants. *Science, 294(5550)*, 2351-2353. doi: 10.1126/science.1065156

Kaźmierczak, A., & Stępiński, D. (2005). GA_3 content in young and mature antheridia of *Chara tomentosa* estimated by capillary electrophoresis. *Folia Histochemica et Cytobiologica, 43*(1), 65-67. doi: 10.5603/4631

Klima, A., & Foissner, I. (2008). FM dyes label sterol-rich plasma membrane domains and are internalized independently of the cytoskeleton in Characean internodal cells. *Plant and cell physiology, 49(10),* 1508-1521. doi: 10.1093/pcp/pcn122

Knight, A. E., & Kendrick-Jones, J. (1993). A myosin-like protein from a higher plant. *Journal of Molecular Biology, 231*(1), 148-154. doi: 10.1006/jmbi.1993.1266

Krause, W. (1981). Characeen als Bioindikatoren für den Gewässerzustand. *Limnologica, 13(2),* 399-418.

Kufel, L., & Kufel, I. (2002). *Chara* beds acting as nutrient sinks in shallow lakes—a review. *Aquatic Botany, 72(3),* 249-260. doi: 10.1016/S0304-3770(01)00204-2

Kwiatkowska, M. (2003). Plasmodesmal changes are related to different developmental stages of antheridia of *Chara* species. *Protoplasma, 222*(1), 1-11. doi: 10.1007/s00709-003-0001-y

Lakowicz, J. R. (2013). *Principles of Fluorescence Spectroscopy*. Springer Science & Business Media, New York.

Lang-Pauluzzi, I. (2000). The behaviour of the plasma membrane during plasmolysis: A study by UV microscopy. *Journal of Microscopy, 198(3),* 188-198. doi: 10.1046/j.1365-2818.2000.00677.x

Leitch, A., John, D., & Moore, J. (1990). The oosporangium of the Characeae (Chlorophyta, Charales). *Progress in Phycological Research, 7,* 213-268.

Littlefield, L., & Forsberg, C. (1965). Absorption and translocation of phosphorus-32 by *Chara globularis* Thuill. *Physiologia Plantarum, 18(2),* 291-293. doi: 10.1111/j.1399-3054.1965.tb06891.x

Markham, K., & Porter, L. (1969). Flavonoids in the green algae (Chlorophyta). *Phytochemistry, 8*(9), 1777-1781. doi: 10.1016/S0031-9422(00)85968-3

McMaster, G. K., & Carmichael, G. G. (1977). Analysis of single- and double-stranded nucleic acids on polyacrylamide and agarose gels by using glyoxal and acridine orange. *Proceedings of the National Academy of Sciences of the United States of America, 74(11)*, 4835-4838.

Noordhuis, R., van der Molen, D. T., & van den Berg, M. S. (2002). Response of herbivorous water-birds to the return of *Chara* in Lake Veluwemeer, The Netherlands. *Aquatic Botany, 72(3),* 349-367. doi: 10.1016/S0304-3770(01)00210-8

Oikawa, A., Matsuda, F., Kikuyama, M., Mimura, T., & Saito, K. (2011). Metabolomics of a single vacuole reveals metabolic dynamism in an alga *Chara australis*. *Plant Physiology, 157(2)*, 544-551. doi: 10.1104/pp.111.183772

Oparka, K. J. (1994). Plasmolysis: new insights into an old process. *New Phytologist, 126(4),* 571-591. doi: 10.1111/j.1469-8137.1994.tb02952.x

Pamaploni, F., Chang,B-J., & Stelzer,E.H.K. (2015) Light sheet-based fluorescence microscopy (LSFM) for the quantitative imaging of cells and tissues. *Cell and Tissue Research, 360(1)*, 129-141. doi: 10.1007/s00441-015-2144-5

Pereyra-Ramos, E. (1981). Ecological role of Characeae in the lake littoral. *Polish Journal of Ecology, 29,* 167-209.

Pickett-Heaps, J. (1968a). Ultrastructure and differentiation in *Chara* sp. III. Formation of the antheridium. *Australian Journal of Biological Sciences, 21(2),* 255-274. doi: 10.1071/BI9680255

Pickett-Heaps, J. (1968b). Ultrastructure and differentiation in *Chara* (fibrosa) IV. Spermatogenesis. *Australian Journal of Biological Sciences, 21(4),* 655-690. doi: 10.1071/BI9680655

Proctor, V. W. (1962). Viability of *Chara* oospores taken from migratory water birds. *Ecology, 43(3),* 528-529. doi: 10.2307/1933381

Proctor, V. W. (1999). Charophytivory, playas y papalotes, a local paradigm of global relevance. *Australian Journal of Botany, 47(3),* 399-406. doi: 10.1071/BT97088

Quader, H., & Schnepf, E. (1986). Endoplasmic reticulum and cytoplasmic streaming: fluorescence microscopical observations in adaxial epidermis cells of onion bulb scales. *Protoplasma, 131(3)*, 250-252. doi: 10.1007/BF01282989

Rauf, M. A., Soliman, A. A., & Khattab, M. (2008). Solvent effect on the spectral properties of neutral red. *Chemistry Central Journal, 2*(1), 1-8. doi: 10.1186/1752-153x-2-19

Sakano, K., & Tazawa, M. (1984). Intracellular distribution of free amino acids between the vacuolar and extravacuolar compartments in internodal cells of *Chara australis*. *Plant and Cell Physiology, 25(8),* 1477-1486.

Scheffer, M., van den Berg, M., Breukelaar, A., Breukers, C., Coops, H., Doef, R., & Meijer, M.-L. (1994). Vegetated areas with clear water in turbid shallow lakes. *Aquatic Botany, 49(2-3),* 193-196. doi: 10.1016/0304-3770(94)90038-8

Scheuring, D., Schöller, M., Kleine-Vehn, J., & Löfke, C. (2015). *Vacuolar Staining Methods in Plant Cells.* In M. J. Estevez (Ed.), Plant Cell Expansion: Methods and Protocols (pp. 83-92). New York, NY: Springer, New York.

Semwogerere, D., & Weeks, E. R. (2005). Confocal microscopy. *Encyclopedia of Biomaterials and Biomedical Engineering*, Wnek, G., & Bowlin, G., eds., Taylor and Francis, Abingdon. 1-10. doi: 0.1081/E-EBBE-120024153

Shimmen, T., & MacRobbie, E. (1987). Demonstration of two proton translocating systems in tonoplast of permeabilized *Nitella* cell. *Protoplasma, 136(2)*, 205-207. doi: 10.1007/BF01276370

Sievers, A., Kramer-Fischer, M., Braun, M., & Buchen, B. (1991). The Polar Organization of the Growing Chara Rhizoid and the Transport of Statoliths are Actin-Dependent*. Botanica Acta, 104(2), 103-109. doi: 10.1111/j.1438-8677.1991.tb00204.x

Silverberg, B. A., & Sawa, T. (1974). A cytochemical and ultrastructural study of the echinate cytoplasmic inclusion in *Nitella flexilis* (Characeae). *Canadian Journal of Botany, 52(1),* 159-165. doi: 10.1139/b74-018

Singh, M. K., Pal, H., Bhasikuttan, A. C., & Sapre, A. V. (1998). Dual solvatochromism of neutral red. *Photochemistry and Photobiology, 68*(1), 32-38. doi: 10.1111/j.1751-1097.1998.tb03249.x

Snapp, E. (2005). Design and use of fluorescent fusion proteins in cell biology. *Current Protocols in Cell Biology,* Unit 21. 4. doi: 10.1002/0471143030.cb2104s27. John Wiley & Sons, New York.

Sousa, C., Sá e Melo, T., Gèze, M., Gaullier, J.-M., Mazière, J. C., & Santus, R. (1996). Solvent polarity and pH effects on the spectroscopic properties of neutral eed: Application to lysosomal microenvironment probing in living cells. *Photochemistry and Photobiology, 63*(5), 601-607. doi: 10.1111/j.1751-1097.1996.tb05662.x

Sparks, J. S., Schelly, R. C., Smith, W. L., Davis, M. P., Tchernov, D., Pieribone, V. A., & Gruber, D. F. (2014). The covert world of fish biofluorescence: A phylogenetically widespread and phenotypically variable phenomenon. *PLoS One, 9*(1), e83259. doi: 10.1371/journal.pone.0083259

Stone, B.A., Evans, N.A., Bonig, A., & Clarke, A.E. (1984) The application of Sirofluor, a chemically defined fluorochrome from aniline blue for the histochemical detection of callose. *Protoplasma, 122(3)*, 191-195. doi: 10.1007/BF01281696

Tazawa, M., & Shimmen, T. (2001). How Characean cells have contributed to the progress of plant membrane biophysics. *Functional Plant Biology, 28(7),* 523-539. doi: 10.1071/PP01027

Terasaki, M., Song, J., Wong, J.R., Weiss, M.J., & Chen, L.B. (1984) Localization of endoplasmic reticulum in living and glutaraldehyde-fixed cells with fluorescent dyes. *Cell, 38(1)*, 101-108. doi: 10.1016/0092-8674(84)90530-0

Truong, T.V., Supatto, W., Koos, W.S., Choi, J.M., & Fraser, S.E. (2011) Deep and fast live imaging with two-photon scanned light-sheet microscopy. *Nature Methods, 8(9)*, 757-762. doi: 10.1038/nmeth.1652

Vermeer, C. P., Escher, M., Portielje, R., & de Klein, J. J. (2003). Nitrogen uptake and translocation by *Chara*. *Aquatic Botany, 76(3),* 245-258. doi: 10.1016/S0304-3770(03)00056-1

Verbelen, J-P., & Tao, W. (1998). Mobile arrays of vacuole ripples are common in plant cells. *Plant Cell Reports, 17(12)*, 917-920. doi: 10.1007/s002990050509

Verchot-Lubicz, J., & Goldstein, R. E. (2010). Cytoplasmic streaming enables the distribution of molecules and vesicles in large plant cells. Protoplasma, 240(1-4), 99-107. doi: 10.1007/s00709-009-0088-x

Villalba-Breva, S., & Martín-Closas, C. (2011). A characean thallus with attached gyrogonites and associated fossil Charophytes from the Maastrichtian of the Eastern Pyrenees (Catalonia, Spain). *Journal of Phycology, 47*(1), 131-143. doi: 10.1111/j.1529-8817.2010.00947.x

Virant-Klun, I., Tomazevic, T., & Meden-Vrtovec, H. (2002). Sperm single-stranded DNA, detected by acridine orange staining, reduces fertilization and quality of ICSI-derived embryos. *Journal of Assisted Reproduction and Genetics, 19(7),* 319-328. doi: 10.1023/A:1016006509036

Wang, H., Yu, D., & Xiao, K. (2008). The interactive effects of irradiance and photoperiod on *Chara vulgaris* L.: concerted responses in morphology, physiology, and reproduction. *Hydrobiologia, 610(1),* 33-41. doi: 10.1007/s10750-008-9420-2

Wasteneys, G.O., & Williamson, R.E. (1991) Endoplasmic microtubules and nucleus-associated actin rings in *Nitella* internodal cells. *Protoplasma, 162(1)*, 86-98. doi: 10.1007/BF01281192

Wasteneys, G.O., Collings, D.A., Gunning, B.E.S., Hepler, P.K., Menzel, D. (1996) Actin in living and fixed characean internodal cells: identification of a cortical array of fine actin strands and chloroplast actin rings. *Protoplasma, 190(1*), 29-38. doi: 10.1007/BF01281192

Webb, R.H. (1996). Confocal optical microscopy. *Reports on Progress in Physics, 59*(3), 427-471.

Williamson, R.E. (1974). Actin in the alga, *Chara corallina*. *Nature 248 (5451),* 801-802. doi: 10.1038/248801a0

Williamson, R.E., & Ashley, C.C. (1982) Free Ca^{2+} and cytoplasmic streaming in the alga *Chara*. *Nature 296(5858),* 647–650. doi: 10.1038/296647a0

Williamson, R.E., Hurley, U., & Perkin, J. (1984). Regeneration of actin bundles in *Chara*: polarized growth and orientation by endoplasmic flow. *European Journal of Cell Biology, 34*(2), 221-228.

Wiltshire, E. J., & Collings, D. A. (2009). New dynamics in an old friend: dynamic tubular vacuoles radiate through the cortical cytoplasm of red onion epidermal cells. *Plant and Cell Physiology, 50(10),* 1826-1839. doi: 10.1093/pcp/pcp124

Wodniok, S., Brinkmann, H., Glöckner, G., Heidel, A. J., Philippe, H., Melkonian, M., & Becker, B. (2011). Origin of land plants: Do conjugating green algae hold the key? *BMC Evolutionary Biology, 11*(1), 1-10. doi: 10.1186/1471-2148-11-104

Yilmaz, Ö., Verbeke, P., Lamont, R. J., & Ojcius, D. M. (2006). Intercellular spreading of *Porphyromonas gingivalis* infection in primary gingival epithelial cells. *Infection and Immunity, 74(1),* 703-710. doi: 10.1128/iai.74.1.703-710.2006

Zoccarato, F., Cavallini, L., & Alexandre, A. (1999). The pH-sensitive dye acridine orange as a tool to monitor exocytosis/endocytosis in synaptosomes. *Journal of Neurochemistry, 72(2),* 625-633. doi: 10.1046/j.1471-4159.1999.0720625.x

Appendix - Fluorescent Dyes for Live Cell Imaging

A1.1 Acridine orange

Molecular weight	301.82 g.mol^{-1}
Structure	$C_{17}H_{20}ClN_3$

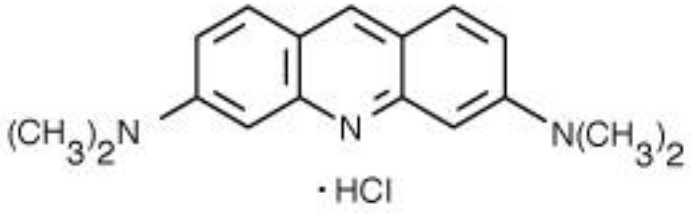

Source	Sigma
Excitation	488/514 nm
Emission range	500-550, 525-575, 600-650, 650-700 nm

Excitation and emission spectrum

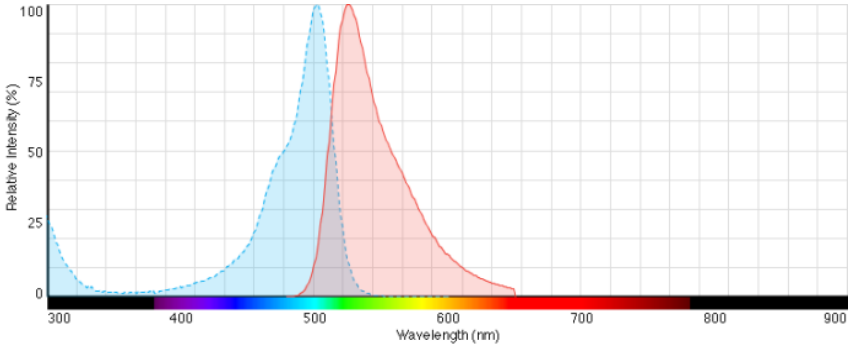

Acridine orange emission spectrum when bound to DNA. Source: ThermoFisher Scientific.

General description

Acridine orange is a weakly-basic dye with a distinctive shift in its spectral properties between staining double-stranded DNA (500⁄526 nm excitation/emission) and RNA (460⁄650 nm in ssDNA/RNA) (McMaster and Carmichael, 1977, Virant-Klun et al., 2002). Acridine orange also demonstrates pH-dependent changes in fluorescence, with highly variable behaviour in terms of absorbance and emission (Han and Burgess, 2010). As it is a weak base, it accumulates in acidic organelles such as lysosomes and vacuoles (Zoccarato et al., 1999). Acridine orange has also been used as a probe for vacuoles in other species, as it accumulates into acidic compartments in a similar fashion to neutral red (Verbelen and Tao, 1998).

A1.2	**Blue-CMAC**
Molecular weight	209.6 g.mol^{-1}
Structure	$C_{10}H_8NO_2Cl$

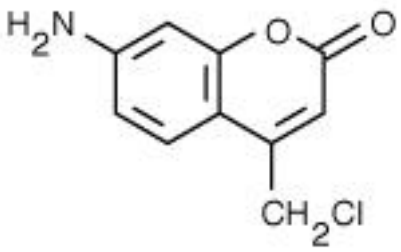

Source	Molecular Probes (Life Technologies)
Excitation	405 nm
Emission range	415 - 465 nm

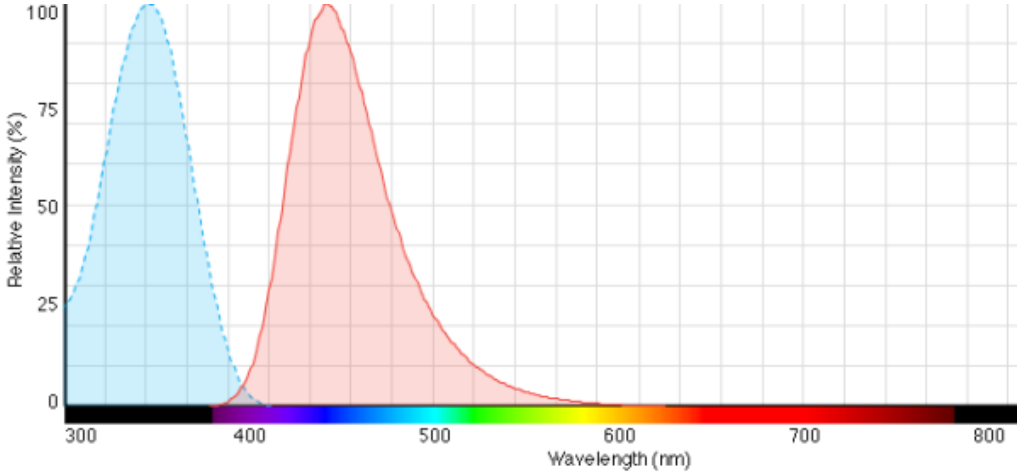

A spectrum is shown for aminomethylcoumarin, the end product of a reaction of Blue CMAC inside the cell. Source: ThermoFisher Scientific.

General description

Blue CMAC (7-amino-4-chloromethylcoumarin) is a low-toxicity dye that loads into the vacuole of yeasts and other fungi, where it can be retained across several generations (Johnson and Spence, 2010). It has also seen usage in assorted animal cells to stain vacuoles, including in gingival epithelial cells (Yilmaz et al., 2006). Its use in Characean algae or plants has not previously been reported, although it can label the higher plant vacuole (D. Collings, *personal communication*).

A1.3 $DIOC_6(3)$

Molecular weight	572.53 $g.mol^{-1}$
Structure	$C_{29}H_{37}IN_2O_2$

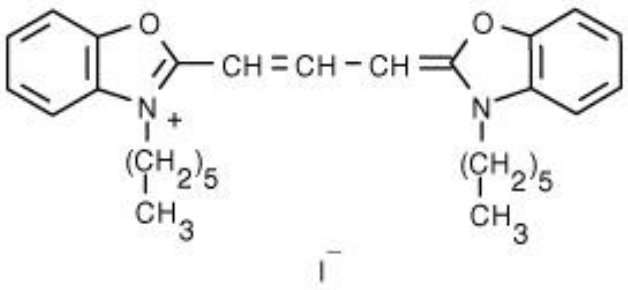

Source	Molecular Probes (Life Technologies)
Excitation	488 nm
Emission range	500 - 550 nm

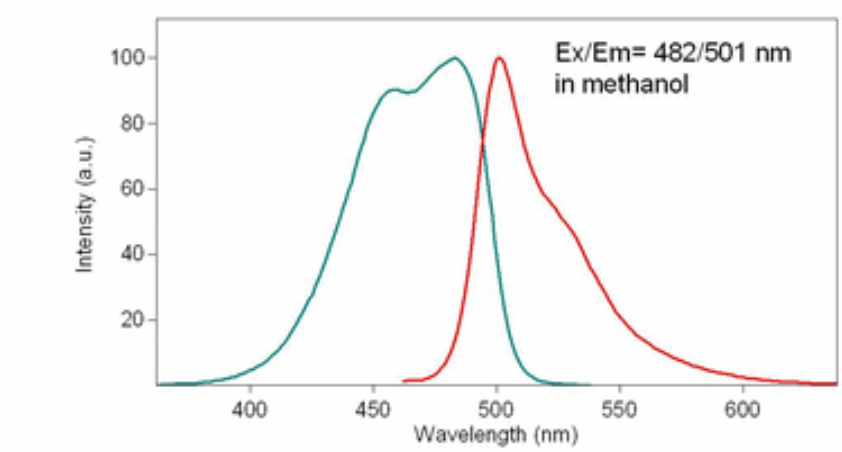

Absorption and emission spectra for $DiOC_6(3)$. Source: Enzo Life Sciences.

Excitation	488 nm excitation
Emission range	500-500 nm emission
General description	$DiOC_6(3)$ is a lipophilic, cationic dye used to stain the mitochondria and, at higher concentrations, the endoplasmic reticulum, although it will eventually cause disruption to both mitochondrial and ER function (Terasaki et al., 1984). $DiOC_6(3)$ has been to stain mitochondria and the ER in Characean algae (Fotopoulos, 2012), and has been extensively used in higher plants (Quader and Schnepf, 1986, Allen and Brown, 1988, Lang-Pauluzzi, 2000, Collings, 2013).

A1.4 MDY-64

Molecular weight	384.5 g.mol^{-1}
Structure	$C_{24}H_{24}N_4O$

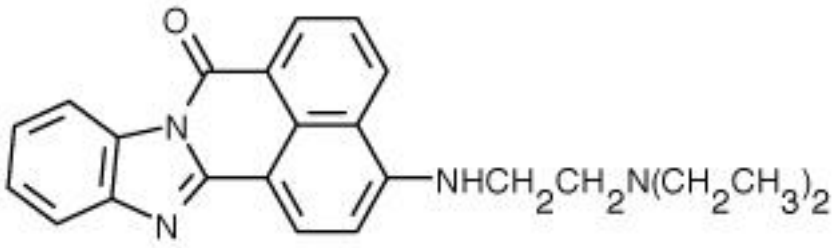

Source	Molecular Probes (Life Technologies)
Excitation	456 nm
Emission range	465 - 515 nm

Excitation and emission spectrum

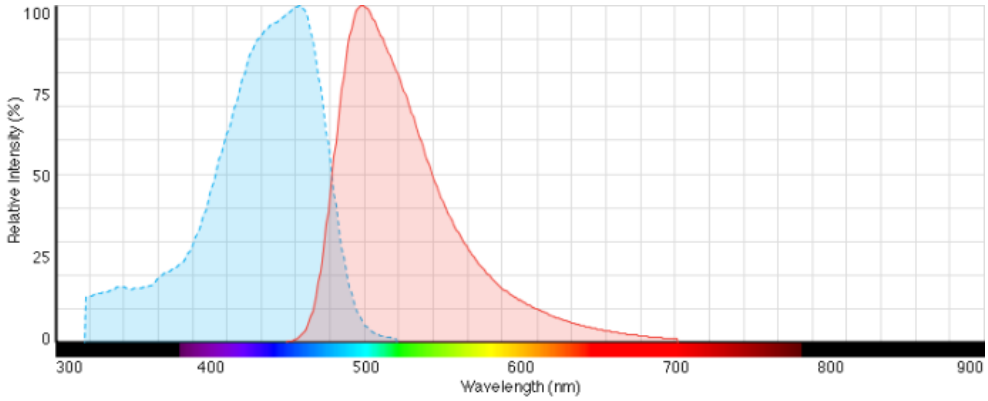

Excitation and emission spectra of MDY-64. Source: ThermoFisher Scientific.

General description

MDY-64 is a lipophilic tonoplast stain developed for use in yeast cells (Johnson and Spence, 2010). Its fluorescent properties are 451/497 nm excitation/emission. Although MDY-64 has been used on occasion in plant cells (Wiltshire and Collings 2009, Collings, 2013, Sheuring et al., 2015), it does not appear that MDY-64 has ever been used in Characean algae, making its usage here novel.

A1.5 Neutral red

Molecular weight	288.78 g.mol^{-1}
Structure	$C_{15}H_{17}ClN_4$

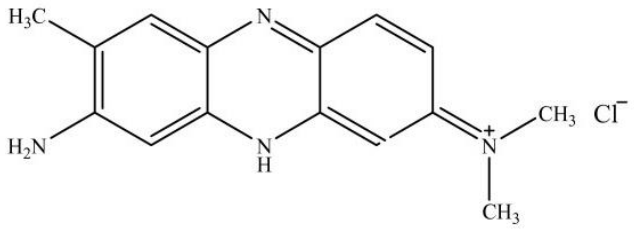

Source	Sigma, Molecular Probes/Life Technologies (high purity)
Excitation	561 nm
Emission range	570 - 620 nm
General description	Neutral red is a popular, non-toxic quinone-imine dye commonly used as a vital stain, lysosomal probe, and biological pH indicator as it changes colour from yellow to red when the pH changes from 5.3 to 8.1. Neutral red can be lipophilic, or can load into acidic organelles (such as lysosomes and acidic vacuoles) through a weak acid-loading effect (Jensen and Bainton, 1973, di Sansebastiano et al., 2001). Neutral red's use with Characean algae goes as far back as 1919, where it was used to stain the central vacuole red (Hitchcock 1919), and its use as a vacuolar label has continued (Shimmen and MacRobbie, 1987, Beilby and Shepherd, 1989). It stains a variety of other objects in both the endoplasm and the vacuole (Hitchcock, 1919), greatly enhancing visualization of the cell contents. These early studies typically used neutral red's colour, rather than its fluorescence, to investigate the cell.

A1.6 Nile red

Molecular weight	318.37 g.mol^{-1}
Structure	$C_{20}H_{18}N_2O_2$

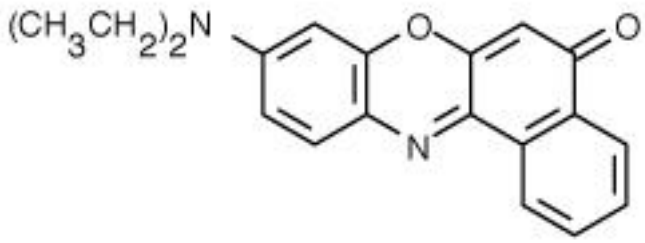

Source	Sigma
Excitation	561 nm
Emission range	525-575 nm

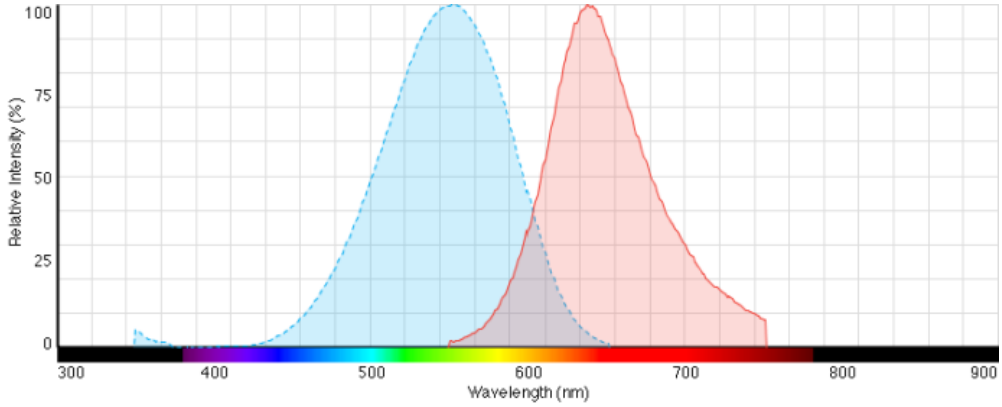

Excitation and emission spectra for Nile red when bound to phospholipid bilayers. Source: ThermoFisher Scientific.

General description

Nile red is a lipophilic dye that stains a variety of membranes inside cells. Nile red's fluorescence properties change depending on the polarity of the substrate, shifting from blue/yellow excitation/emission to yellow/red excitation/emission. It displays little fluorescence in water but bright fluorescence in non-polar environments (Greenspan, 1985). This dye has been used in Characean algae to stain membranes and lipid droplets (F).

A1.7 Syto-13

Molecular weight	unknown
Structure	unknown
Source	Molecular Probes (Life Technologies)
Excitation	488 nm
Emission range	500-550 nm

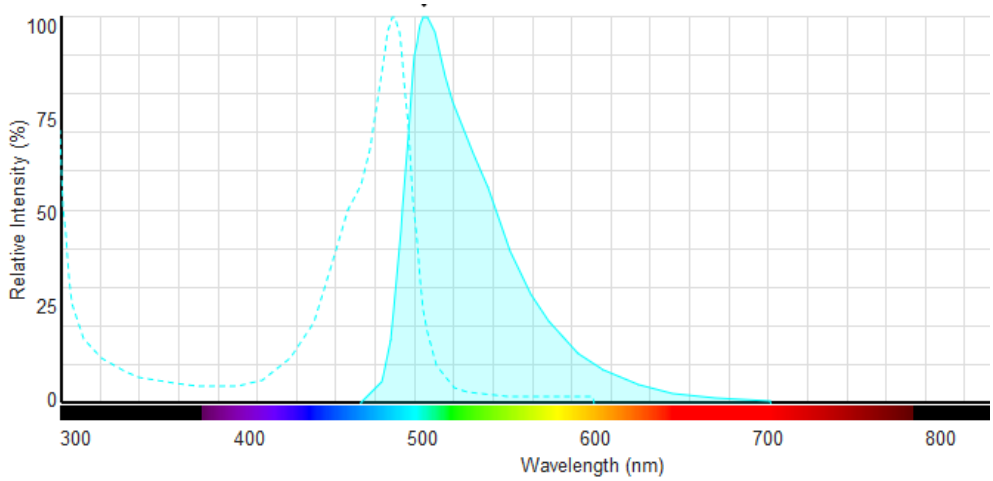

Excitation and emission spectra of Syto-13 when bound to DNA. Source: ThermoFisher Scientific.

General description	Syto-13 is a nucleic stain similar to acridine orange in exhibiting a shift in fluorescent properties, going from 488⁄509 nm excitation/emission when staining DNA, to 491⁄514 nm when staining RNA. In eukaryotic cells, it also shows cytoplasmic and mitochondrial staining. It is low toxicity, and exhibits very little intrinsic fluorescence. Like most dyes in this paper, Syto-13 has no known usage in Characean algae, but it has previously been used in plant cells (Collings, 2013).